Inaugural-Dissertation

zur
Erlangung der Doktorwürde
der
Naturwissenschaftlich-Mathematischen Gesamtfakultät
der
Ruprecht-Karls-Universität
Heidelberg

vorgelegt von
Diplom-Mathematiker Frédéric Weller
aus Stuttgart

Tag der mündlichen Prüfung: 14. Juli 2008

Modeling, Analysis, and Simulation of Thrombosis and Hemostasis

Gutachter: Prof. Dr. Dr. h. c. mult. Willi Jäger

Prof. Dr. Rolf Rannacher

Abstract

This thesis investigates the influences of shear stress, saturation-dependent changes in surface reactivity, and thrombus growth on platelet deposition to reactive materials, which is of paramount interest in bioengineering and clinical practice. For this purpose, two mathematical models based on the Navier-Stokes equations and on particle conservation are developed. The first model is formulated on a fixed domain ("FD-model") and describes the initial phase of platelet adhesion, whereas the second one is a free boundary problem capturing long-term thrombus growth. Several vessel geometries are considered: Stagnation point flow, tubular expansion, and t-junction. Model parameters are optimized to fit the data and their so obtained values are justified on the basis of experimental observations.

The FD-model does not match the experimental data at all, when platelet adhesion is assumed independent of shear stress. In contrast, when adhesion is assumed shear-dependent, at least qualitative agreement is achieved. Solely by consideration of both shear stress and saturation-dependent changes in surface reactivity, good quantitative agreement of FD-model and data is obtainable. Such changes in surface reactivity are taken into account by coupling platelet flux conditions to ordinary differential equations (ODEs) for the evolution of surface-bound platelets. The free boundary problem is simulated by the level set method. Like the FD-model, it shows good qualitative agreement with the experimental evidence when shear stress is taken into account, whereas negligence of shear leads to completely false predictions.

Regarding mathematical well-posedness of the FD-model, existence of weak solutions is shown for generalized parabolic systems having ODE-coupled flux conditions. Uniqueness and positivity of solutions are also investigated. Regarding the free boundary problem, a detailed proof of classical solvability in terms of Hölder spaces is presented.

Zusammenfassung

Diese Arbeit untersucht die Einflüsse von Scherkräften, sättigungsbedingten Änderungen der Oberflächenreaktivität und die Auswirkungen des Thrombenwachstums auf die Adhäsion von Blutplättchen an reaktiven Materialien, was von großem Interesse in Biotechnik und klinischer Praxis ist. Zu diesem Zweck werden zwei mathematische Modelle basierend auf den Navier-Stokes Gleichungen und der Teilchenerhaltung entwickelt. Das erste Modell beschreibt die Anfangsphase der Plättchenadhäsion und nimmt daher ein festes Gebiet an („FD-Modell"), wohingegen das zweite ein freies Randwertproblem zur Beschreibung des längerfristigen Thrombenwachstums darstellt. Es werden mehrere Gefäßgeometrien betrachtet: Staupunkt, Gefäßerweiterung und T-Kreuzung. Die Modellparameter werden anhand der experimentellen Daten gefittet und ihre so erhaltenen Werte mit experimentellen Beobachtungen gerechtfertigt.

Beim FD-Modell stellt sich bei Annahme scherkraftunabhängiger Plättchenadhäsion keine Übereinstimmung mit den experimentellen Daten ein. Bei scherkraftabhängiger Adhäsion wird immerhin qualitative Übereinstimmung erzielt. Gute quantitative Übereinstimmung mit den Daten zeigt das FD-Modell dagegen nur bei gleichzeitiger Berücksichtigung von Scherkräften und sättigungsbedingten Änderungen der Oberflächenreaktivität. Letzteres wird über eine Kopplung des Plättchenflusses mit gewöhnlichen Differenzialgleichungen für die zeitliche Entwicklung der Konzentration gebundener Plättchen realisiert. Das freie Randwertproblem wird mit Hilfe der Level Set Methode numerisch simuliert. Ebenso wie das FD-Modell zeigt es bei Berücksichtigung der Scherkräfte gute qualitative Übereinstimmung mit dem Experiment, wohingegen die Vernachlässigung der Scherkräfte zu völlig falschen Voraussagen führt.

Zur Sicherstellung der mathematischen Wohlgestelltheit des FD-Modells wird die Existenz schwacher Lösungen für allgemeinere parabolische Systeme, die solch gekoppelten Randbedingungen unterworfen sind, gezeigt. Darüberhinaus wird die Eindeutigkeit und Positivität der Lösung untersucht. Für das freie Randwertproblem wird dessen klassische Lösbarkeit in Hölderräumen umfassend bewiesen.

Contents

1 Introduction **1**

2 Biological background **5**
2.1 Primary hemostasis 5
2.2 Secondary hemostasis 6

3 The fixed domain model **13**
3.1 Model development 13
3.2 Numerical methods and optimization of parameters 17
3.3 Numerical results 18
3.3.1 Stagnation point flow 18
3.3.2 Tubular expansion 20
3.3.3 T-junction 24
3.4 Discussion 26
3.5 Mathematical analysis 27
3.5.1 Notation and function spaces 27
3.5.2 Problem statement and assumptions 28
3.5.3 Existence and uniqueness for the linear problem 29
3.5.4 Existence and uniqueness for the nonlinear problem 33
3.5.5 Positivity of solutions 36

4 The free boundary problem **39**
4.1 Model development 39
4.2 The level set method and its implementation 41
4.3 Numerical results 43

5 Classical solvability of the free boundary problem **53**
5.1 Preliminaries 53
5.1.1 Geometry and model equations 53
5.1.2 Notation and function spaces 54
5.1.3 Assumptions and main theorem 55
5.2 Transformation to fixed domain 56
5.3 The linear problem for the platelets; fixed flow 58
5.3.1 Investigation of auxiliary problems in half space 59
5.3.2 Solution of the linear problem in Q_T 79
5.4 Solution of the nonlinear problem for the platelets; fixed flow 86
5.5 Solution of the full nonlinear problem including flow 94

6 Conclusions and outlook **97**

Acknowledgments **99**

List of Figures **101**

List of Tables **103**

Bibliography **105**

1 Introduction

Hemostasis is responsible to stem blood loss after injury by platelet plug formation. Although being life essential, a major part of deaths in the western society is due to thrombotic events provoked by disorders of the hemostatic system. Therefore, a better understanding of the underlying mechanisms is needed. It is known that the overall process is governed by Virchow's triad [94] which comprises composition of blood, surface reactivity, and flow. Nevertheless, previous mathematical models, such as [5, 24, 37, 49, 82, 83], concentrated mainly on kinetics and, if at all, accounted for the in vivo flow situation only in simple terms of transport. But, since the end of the 1970s there is experimental evidence that shear stress strongly influences the activation of platelets and their adhesion to injured tissue [88, 95]—both crucial steps in plug formation. However, there is still confusion about the exact physical quantities that determine spatial platelet distribution and give rise to the well known fact that sites of disturbed flow are prone to platelet deposition [32, 90].

This thesis investigates the influences of shear stress, saturation-dependent changes in surface reactivity, and thrombus growth on the adhesion and aggregation of platelets to reactive materials. For this purpose, two mathematical models based on fluid dynamic and species conservation equations are developed and their ability to match given in vitro experimental data is studied—dependent on whether the above mentioned effects are taken into account or not. The first model describes the initial phase of platelet deposition, when thrombus growth can be neglected. Therefore, this model is formulated on a fixed domain and henceforth referred to as "Fixed Domain model" (FD-model). It accounts for shear stress and changes in surface reactivity. Such changes are due to bound platelets that cover the surface and express platelet-binding sites which are different from those provided by the uncovered surface. The second model captures the long-term behavior of platelet deposition, when changes in surface reactivity can be neglected. Instead, the growth of platelet aggregates (thrombi), which disturb the blood flow and hence alter the shear-field, becomes important. Taking thrombus growth into account results in a free boundary problem with fully coupled fluid dynamic and species conservation equations. Activation of platelets in the bulk flow and subsequent agonist production were suppressed in the below considered experiments and therefore not included in the models derived in this work. However, these effects were subject of previous investigations of the author [97] which allow straightforward extension of the here presented approaches.

The FD-model considers shear stress according to David et al. [20], who showed that the distribution of bound platelets observed by Affeld et al. [1] in stagnation point flow cannot be explained using a shear-independent adhesion rate. However, the use of a shear-dependent adhesion rate at least improved their model predictions in some parts of the flow chamber, whereas notable discrepancies remained in the other parts. That is why the FD-model presented here also accounts for changes in surface reactivity by coupling boundary conditions

on platelet flux to ordinary differential equations (ODEs) describing the evolution of surface-bound platelets, as proposed by Sorensen et al. [82]. The FD-model permits the use of a rather elementary optimization strategy to fit parameters to experimental data. Numerical simulations show that the combination of a shear-dependent adhesion rate with changes in surface reactivity remarkably improves model predictions in stagnation point flow. The FD-model is then applied and optimized to experiments concerned with platelet deposition in other vessel geometries, such as tubular expansion [45] and t-junction [56]. As in stagnation point flow, when adhesion is assumed to depend on both shear stress and surface-bound platelets, the model shows good quantitative agreement with the respective experimental data. In contrast to that, when a shear-independent adhesion rate is used, the numerical results are not at all satisfactory. Differences found between the optimized parameters are explained on the basis of the observations of Brash et al. [13] and the hypothesis is put forward that the impact of changing surface reactivity on platelet adhesion depends on hematocrit. Well-posedness (from a mathematical point of view) of parabolic problems with ODE-coupled flux conditions is investigated: Existence of weak solutions is shown for a generalized class of parabolic systems, whereas uniqueness and positivity of solutions require some tighter conditions which are fulfilled by the presented FD-model.

Using the optimized parameters of the FD-model, numerical simulations of the free boundary problem are performed by the level set method, which has been implemented in the Finite Element toolkit Gascoigne [10]. As in the initial phase of platelet deposition, negligence of shear stress leads to completely false predictions, whereas the inclusion of shear yields good qualitative agreement with the experimental evidence. Finally, a detailed proof of classical solvability of the free boundary problem is presented. The proof consists of several steps: First, the original problem is transformed to an equivalent formulation on the fixed initial domain. Then, the flow field is fixed and the corresponding linear problem for the platelets is investigated. Starting in half space, this coupled linear problem is split up in several auxiliary problems which are treated by Fourier-Laplace transform techniques and pseudodifferential operator theory. After that, the full linear problem is solved in half space by Banach's fixed point theorem. By means of a regularizer, the results for the half space are used to solve the linear problem in the original domain. The theory for the linear case is then applied to the nonlinear problem for the platelets when the flow field is still fixed. Estimates of the nonlinear terms show applicability of Banach's theorem, provided that the time and the initial data for the platelets are sufficiently small. Eventually, the full coupling of flow and platelets is investigated. Based on the here developed theory for fixed flow and on a result of Solonnikov [80], the Schauder theorem yields a classical solution of the free boundary problem.

One purpose of this thesis is to emphasize the need to consider the combined effects of shear stress, changes in surface reactivity, and aggregate growth in modeling approaches addressing hemostasis and thrombosis. These insights shall contribute to minimize thrombus formation in vascular prostheses without the use of strong anticoagulants. This is an important task in bioengineering, which does not only call for materials science to improve surface properties, but also for (mathematical) shape optimization techniques to optimize blood flow conditions with regard to the correlation of platelet deposition and shear. Due to its rather fundamental character, the presented FD-model could be used as starting point for such an optimization problem covering initial platelet adhesion. However, the influence of shear stress, which is further confirmed in this work, demands to include the full coupling of flow and thrombus

growth in models intended to capture the long-term behavior of platelet deposition. By comparison with experimental data and by establishing its classical solvability, the presented free boundary problem is proven to be a valuable approach to this subject, with the potential to enlighten mechanisms in further kinds of adhesion processes.

This work is structured as follows: Chapter 2 provides a biological review of the processes during hemostasis. In Chapter 3, the equations of the FD-model are developed. Then the numerical methods used to simulate this model and to fit its parameters are stated and the considered experiments are described. The numerical results are compared with the experimental data and the optimized parameter values are justified on the basis of experimental evidence. After that, the mathematical well-posedness of the FD-model is investigated. For this purpose, generalized parabolic systems with mixed boundary conditions coupled to ODEs are analyzed and detailed proofs of existence, uniqueness, and positivity of solutions are provided. The results presented in Chapter 3 are subject for publication in [98]. Chapter 4 derives the equations of the free boundary problem. After describing the level set method and its implementation, the numerical results concerning the free boundary model are presented and compared with the above mentioned experiments. Chapter 5 provides a detailed proof of classical solvability of the free boundary problem. Chapter 6 draws conclusions and provides an outlook on future problems.

2 Biological background

2.1 Primary hemostasis

In vivo, the hemostatic system is initiated by disruption of endothelial cells separating blood and reactive tissue in the vessel's wall. Initiation is desired in case of injury, but can also occur in atherosclerotically narrowed vessels, where ruptured plaques and elevated shear rates may induce the formation of platelet-rich thrombi that can become life-threatening occluding the vascular lumen [28, 29]. Platelets—small anucleated blood cells derived from megakaryocytes in the bone marrow—adhere to the reactive tissue and form an aggregate responsible to stem blood loss (primary hemostasis) [73]. In an elevated shear environment this is a multistep process which requires the synergistic interaction of several receptors on the platelets' membrane as well as several ligands [18]. It proceeds from an initial phase mediated by interactions of GPIb receptors and von Willebrand factor (vWf) immobilized onto fibrillar collagen, which slow down the platelet and keep it rolling close to the surface [78]. This permits stable attachment by GPIa/IIa receptors binding to collagen [76] and platelet activation via interactions of collagen and, respectively, GPIa/IIa and GPVI receptors [77]. Upon activation, platelets change their shape from discoid to spherical, release their granule content and increase their stickiness by expression of long pseudopodia (Figure 2.1) and GPIIb/IIIa receptors [31]. These activated GPIIb/IIIa receptors then promote platelet aggregation via fibrinogen and vWf, respectively, dependent on whether shear stress levels are low or increased [39].

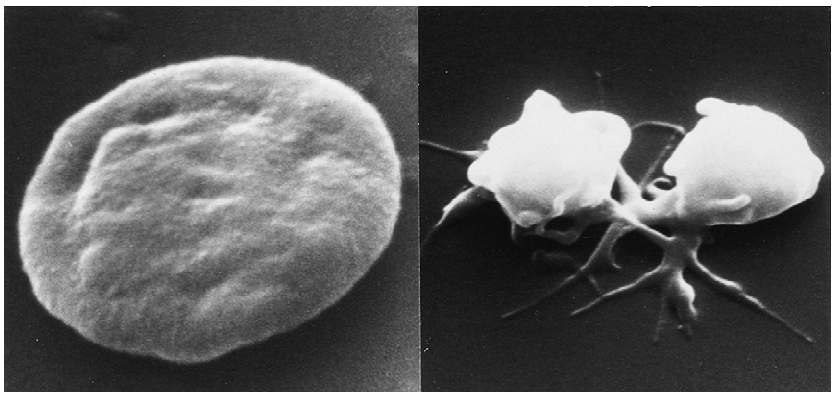

Figure 2.1: Scanning electron micrographs of a resting platelet (*left*, ×20,000) and two activated platelets (*right*, ×10,000). Inactive platelets are disc shaped, whereas the activated ones are more spherical and express long pseudopodia. Electron micrographs taken by J. G. White and M. Krumwiede, University of Minnesota. Reproduced with permission from [30]

When the level of shear exceeds a certain threshold, platelet aggregation occurs even in the absence of any chemical agonist and without any modification of ligands such as vWf [39, 65], whereas in a static suspension mixing vWf with platelets alone does not evoke any response [48]. The reason for this behavior is still unclear. Up for discussion are a shear enhanced exposure or an alteration in structure of GPIb receptors on the platelets' membrane, which increases the efficiency of collisions [48]. In addition, particle migration is known to rise with shear and hematocrit (Ht) up to three orders of magnitude above the Brownian value [34, 89] due to elevated collision frequency, primarily between platelets and red blood cells (RBCs). Furthermore, RBCs are known to potentiate shear-induced platelet adherence not only mechanically, but also chemically by the release of platelet agonist ADP [71]. Besides this, the question whether an uncoiling of bound globular vWf at elevated shear (or related morphologic and conformational changes) is jointly responsible for increased platelet deposition is still controversial. While Siedlecki et al. [79] reported such an uncoiling in the case of vWf bound to an artificial hydrophobic surface, Novak et al. [63] did not observe such an effect in the more physiological situation of vWf bound to collagen.

Upon platelet activation, the release reaction feedback amplifies the hemostatic system. This is due to the fact that platelet granules contain, among others, ADP which activates further platelets in the vicinity, ligands such as vWf and fibrinogen that promote platelet adhesion and aggregation, as well as coagulation factors needed for the processes in secondary hemostasis [31]. The latter refers to a multitude of reactions leading to the production of thrombin, which is a key enzyme in the hemostatic process as well as a strong platelet agonist. In the course of hemostasis, thrombin produces fibrin fibers which surround the platelet aggregate and stabilize it against the shear forces in the flowing blood.

2.2 Secondary hemostasis

Table 2.1 lists the main reactions leading to the conversion of prothrombin (factor II) to thrombin (factor IIa) in vivo (subsequent fibrin production is omitted). A scheme of these processes is provided by Figure 2.2. This review does not consider the possibility to trigger hemostasis via the contact pathway comprising factor XII and XI, since this pathway turned out to be unimportant in trauma-initiated coagulation [19]. The here presented chemical system was investigated by Mann et al.—both by in vitro laboratory experiments [14, 55] and by numerical simulation of two ODE-systems [37, 41]. Based on their results, the cascade of reactions can be subdivided into three phases: initiation via the extrinsic system (green color in Figure 2.2), amplification and propagation by multiple feedback loops in the common pathway (yellow color), and termination (red color) by the stoichiometric inhibitors antithrombin III (ATIII) and tissue factor pathway inhibitor (TFPI).

Initiation Clotting starts upon exposure of (ordinarily hidden) tissue factor (TF) to flowing blood, as a consequence of injury or as a consequence of inflammatory cytokine activation of either vascular cells or monocytes [59]. However, the combined action of TFPI and ATIII prevents initiation of hemostasis unless TF concentration exceeds a certain threshold [37]. By assembly with activated factor VIIa ($\approx$ 1–2 % of factor VII is activated in plasma), the extrinsic tenase complex (TF=VIIa) is formed on the surface of the tissue factor bearing cell

Table 2.1: From the extrinsic system to thrombin generation

Line	Chemical reaction
1	$\mathrm{TF} + \mathrm{VII} \rightleftharpoons \mathrm{TF{=}VII}$
2	$\mathrm{TF} + \mathrm{VIIa} \rightleftharpoons \mathrm{TF{=}VIIa}$
3	$\mathrm{TF{=}VIIa} + \mathrm{VII} \rightarrow \mathrm{TF{=}VIIa} + \mathrm{VIIa}$
4	$\mathrm{Xa} + \mathrm{VII} \rightarrow \mathrm{Xa} + \mathrm{VIIa}$
5	$\mathrm{IIa} + \mathrm{VII} \rightarrow \mathrm{IIa} + \mathrm{VIIa}$
6	$\mathrm{TF{=}VIIa} + \mathrm{X} \rightleftharpoons \mathrm{TF{=}VIIa{=}X} \rightarrow \mathrm{TF{=}VIIa{=}Xa}$
7	$\mathrm{TF{=}VIIa{=}Xa} \rightleftharpoons \mathrm{TF{=}VIIa} + \mathrm{Xa}$
8	$\mathrm{TF{=}VIIa} + \mathrm{IX} \rightleftharpoons \mathrm{TF{=}VIIa{=}IX} \rightarrow \mathrm{TF{=}VIIa} + \mathrm{IXa}$
9	$\mathrm{Xa} + \mathrm{II} \rightarrow \mathrm{Xa} + \mathrm{IIa}$
10	$\mathrm{IIa} + \mathrm{VIII} \rightarrow \mathrm{IIa} + \mathrm{VIIIa}$
11	$\mathrm{VIIIa} + \mathrm{IXa} \rightleftharpoons \mathrm{IXa{=}VIIIa}$
12	$\mathrm{IXa{=}VIIIa} + \mathrm{X} \rightleftharpoons \mathrm{IXa{=}VIIIa{=}X} \rightarrow \mathrm{IXa{=}VIIIa} + \mathrm{Xa}$
13	$\mathrm{VIIIa} \rightleftharpoons \mathrm{VIIIa_1} \cdot L + \mathrm{VIIIa_2}$
14	$\mathrm{IXa{=}VIIIa{=}X} \rightarrow \mathrm{VIIIa_1} \cdot L + \mathrm{VIIIa_2} + \mathrm{X} + \mathrm{IXa}$
15	$\mathrm{IXa{=}VIIIa} \rightarrow \mathrm{VIIIa_1} \cdot L + \mathrm{VIIIa_2} + \mathrm{IXa}$
16	$\mathrm{IIa} + \mathrm{V} \rightarrow \mathrm{IIa} + \mathrm{Va}$
17	$\mathrm{Xa} + \mathrm{Va} \rightleftharpoons \mathrm{Xa{=}Va}$
18	$\mathrm{Xa{=}Va} + \mathrm{II} \rightleftharpoons \mathrm{Xa{=}Va{=}II} \rightarrow \mathrm{Xa{=}Va} + \mathrm{mIIa}$
19	$\mathrm{mIIa} + \mathrm{Xa{=}Va} \rightarrow \mathrm{IIa} + \mathrm{Xa{=}Va}$
20	$\mathrm{TF{=}VIIa{=}Xa} + \mathrm{TFPI} \rightleftharpoons \mathrm{TF{=}VIIa{=}Xa{=}TFPI}$
21	$\mathrm{Xa} + \mathrm{TFPI} \rightleftharpoons \mathrm{Xa{=}TFPI}$
22	$\mathrm{TF{=}VIIa} + \mathrm{Xa{=}TFPI} \rightarrow \mathrm{TF{=}VIIa{=}Xa{=}TFPI}$
23	$\mathrm{Xa} + \mathrm{ATIII} \rightarrow \mathrm{Xa{=}ATIII}$
24	$\mathrm{mIIa} + \mathrm{ATIII} \rightarrow \mathrm{mIIa{=}ATIII}$
25	$\mathrm{IXa} + \mathrm{ATIII} \rightarrow \mathrm{IXa{=}ATIII}$
26	$\mathrm{IIa} + \mathrm{ATIII} \rightarrow \mathrm{IIa{=}ATIII}$
27	$\mathrm{TF{=}VIIa} + \mathrm{ATIII} \rightarrow \mathrm{TF{=}VIIa{=}ATIII}$

(Table 2.1, line 2). The extrinsic tenase activates factor X (Table 2.1, lines 6-7) and factor IX (Table 2.1, line 8). Factor VII was shown to impair thrombin production [93] due to its competition with factor VIIa for TF (Table 2.1, line 1). However, in self-propagating loops, factor VII is activated by TF=VIIa (Table 2.1, line 3) and factor Xa (Table 2.1, line 4). Factor Xa can independently generate thrombin (Table 2.1, line 9), but this reaction is extremely inefficient [37].

Propagation The residual amount of initially produced thrombin amplifies the system through several feedback loops: Besides acting on factor VII (Table 2.1, line 5) and XI (contact pathway; not shown), thrombin activates small quantities of factor V (Table 2.1, line 16) and factor VIII (Table 2.1, line 10), which is crucial for the formation of the membrane bound enzyme-cofactor complexes intrinsic tenase (IXa=VIIIa; Table 2.1, line 11) and prothrombinase (Xa=Va; Table 2.1, line 17). The intrinsic tenase activates factor X (Table 2.1, line 12), which is approximately 50-fold more efficient than factor X activation by the extrinsic tenase. Prothrombinase is responsible for the conversion of prothrombin via meizothrombin (mIIa) to thrombin (Table 2.1, lines 18-19). Thrombin generation ultimately develops once intrinsic tenase and prothrombinase

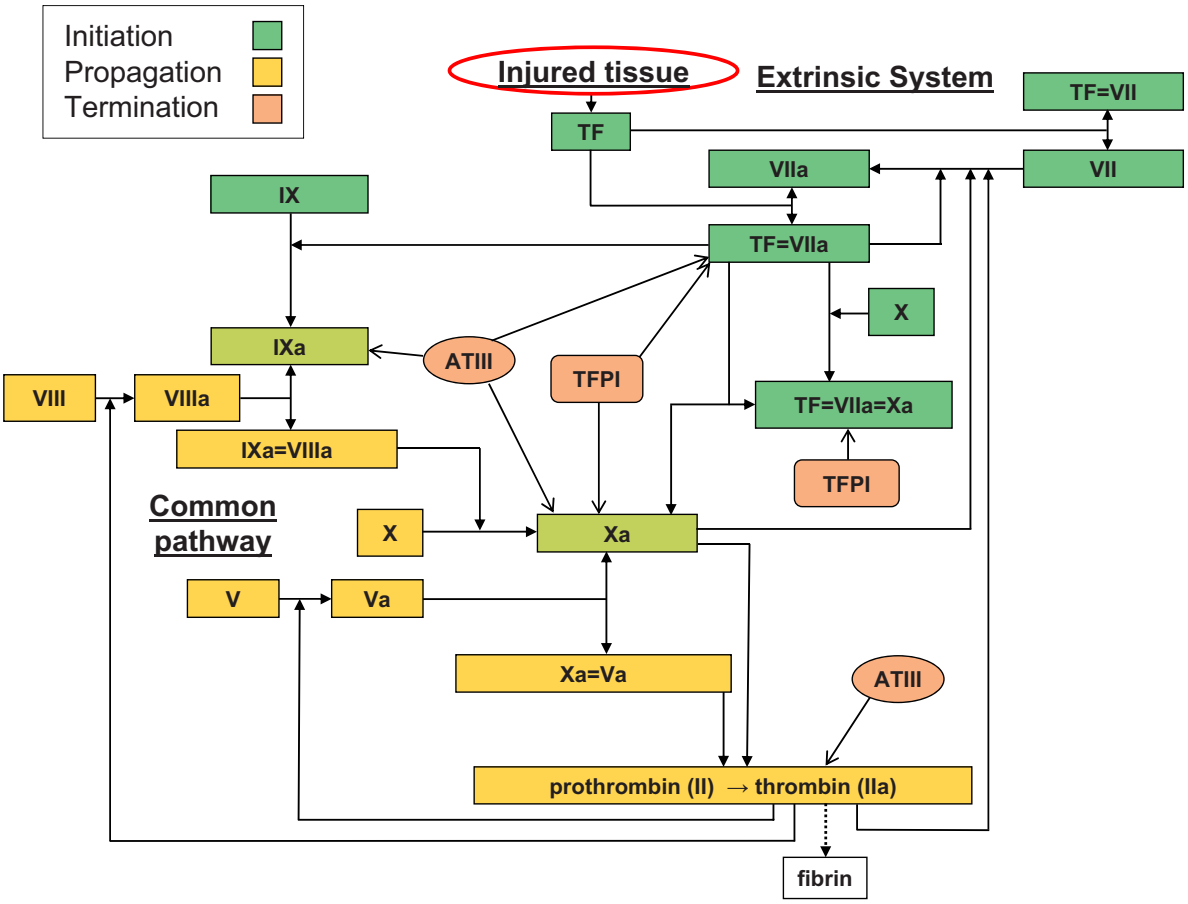

Figure 2.2: The coagulation cascade

have formed on vascular membranes, which is due to the facts that (1) both catalysts are 10^5–10^6-fold more efficient than their components acting independently [59]; (2) factor Xa that is bound in the prothrombinase complex is protected from TFPI [26] and ATIII [72] (in the presence of prothrombin); (3) factor Va that is bound to a platelet's surface is protected from the inhibitor protein C (see below) [46]. The functional structure of these essential enzyme-cofactor complexes is explained in Figure 2.3 on the basis of prothrombinase.

Termination Down-regulation of the reaction cascade is the consequence of three mechanisms: (1) decay of factor VIIIa and of intrinsic tenase due to spontaneous dissociation of the A_2 domain from factor VIIIa (Table 2.1, lines 13-15), according to [22, 23, 58]; (2) inhibition of factor Xa, mIIa, IXa, thrombin, and extrinsic tenase by circulating ATIII (Table 2.1, lines 23-27; see also [17, 43, 54]); (3) the action of the TFPI inhibitor, as described in [6] (Table 2.1, lines 20-22).

Besides ATIII and TFPI, further inhibitors are involved in the regulation of the hemostatic process. The most important of those is the protein C (PC) system, which—in contrast to ATIII and TFPI—dynamically adjusts to the extent of thrombin production. The mechanism is as follows: Thrombin that reaches the intact vascular surface can bind to endothelial throm-

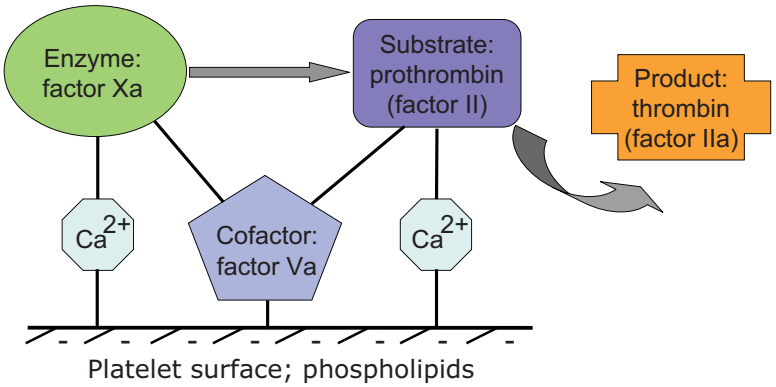

Figure 2.3: The structure of prothrombinase: Calcium ions mediate binding of enzyme (factor Xa) and substrate (II) to the negatively charged, phospholipid coated surface of activated platelets. The close proximity of the bound enzyme and substrate molecules—together with the assistance of the cofactor Va—lead to a burst of thrombin production (see also [67])

bomodulin (Tm); this thrombin-thrombomodulin complex (IIa=Tm) subsequently activates protein C ($\rightarrow$ APC), which inhibits thrombin formation by inactivating factors Va ($\rightarrow$ Va_i) and VIIIa ($\rightarrow$ VIIIa_i) [67]. The efficiency of APC is thereby enhanced by the cofactor protein S (PS). APC is known to exhibit a more antithrombotic than antihemostatic activity, since it permits sufficient thrombin production for hemostatic reactions to proceed [66]. A kinetic in vitro study of protein C is provided in [92]. In summing up, the reactions of the protein C system are

$$\begin{aligned}
\text{IIa} + \text{Tm} &\rightleftharpoons \text{IIa=Tm} \\
\text{IIa=Tm} + \text{PC} &\rightleftharpoons \text{IIa=Tm=PC} \rightarrow \text{IIa=Tm} + \text{APC} \\
\text{APC} + \text{PS} &\rightleftharpoons \text{APC=PS} \\
\text{APC=PS} + \text{VIIIa} &\rightleftharpoons \text{APC=PS=VIIIa} \rightarrow \text{APC=PS} + \text{VIIIa}_i \\
\text{APC=PS} + \text{Va} &\rightleftharpoons \text{APC=PS=Va} \rightarrow \text{APC=PS} + \text{Va}_i\,.
\end{aligned}$$

To confine hemostatic response to the site of injury, the main reactions shown in Figure 2.2 take place primarily on the surface of activated platelets. There, specific receptors are involved in the binding of reactants and the formation of the tenase and prothrombinase complexes, which—as mentioned above—are essential amplifiers of hemostatic reactions [61, 91]. This cell-based view of coagulation (cf. [60]) is explained in the Figures 2.4–2.6, where clotting proceeds in three stages: initiation, priming, and propagation. In contrast to the cascade model presented in Figure 2.2, the cell-based view accounts for platelets as an active means for the propagation and regulation of hemostatic processes. This notion recently replaced the classic theory by which hemostasis was thought to occur in two consecutive steps: First, platelet aggregation and activation; second, the cascade of clotting enzyme complexes leading to fibrin formation on the surface of platelets, the reactions being enhanced by phospholipids from the platelet membrane. Furthermore, the cell-based model provides a satisfying explanation of hemophilia, which could not be derived from the cascade view of coagulation [46, 60].

Therefore, to account for their crucial role in the overall system, platelets should be considered by any future modeling approach attempting to describe the in vivo situation.

In their ODE-models published in [37, 41], Mann et al. neither considered the dynamic inhibitory protein C system, nor did they take into account the platelets. Instead, they concentrated on processes and rate constants which are representative of reaction paths and rates experimentally observed under the condition of saturating phospholipid concentrations [37, p. 18323]. Thus, these models are useful for the simulation of in vitro laboratory tests, such as the prothrombin time [69] and the activated partial thromboplastin time [53], but may fail to explain in vivo mechanisms.

To better capture the in vivo situation, the activation of platelets, the positive feedback induced by thrombin production on the activated platelet membranes, and the negative feedback due to protein C generation along the intact endothelium has been investigated in previous work of the author [97]. In this work, which also takes into account the stoichiometric inhibitor ATIII, the kinetics of platelet activation, subsequent agonist production, and dynamic inhibition were first studied by the use of an ODE-system. This revealed thrombin production to proceed in three phases: initiation during platelet activation, a burst of thrombin generation once sufficient amount of platelet activation is reached, and termination due to the combined action of protein C and ATIII. To investigate the spatial behavior of this coupled reaction system under flow conditions, a model based on reaction-convection-diffusion equations was developed. Numerical simulations confirmed localization of the hemostatic reactions to the site of injury, which is assured by the inhibitors protein C and ATIII, as well as by the restriction of the main reactions to the activated platelet membranes. In addition, protein C was shown to permit sufficient thrombin production to achieve hemostasis, which is consistent with the experience of Pierce et al. [66].

Further biological information concerning hemostasis and thrombosis can be found in [19, 46, 59, 60, 67, 97] and the references cited therein. A publication that reviews thrombus formation from a unique in vivo perspective is provided by [27].

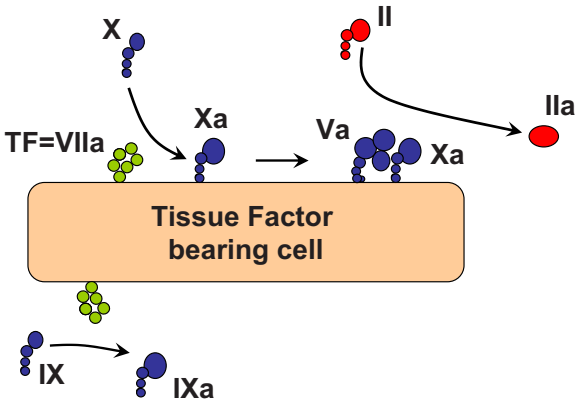

Figure 2.4: *Initiation* Factor VIIa binds to TF and activates factor X and factor IX. Bound to the surface of the TF-bearing cell, factor Xa activates factor V. Both form a complex, which converts small amounts of prothrombin (II) to thrombin (IIa).

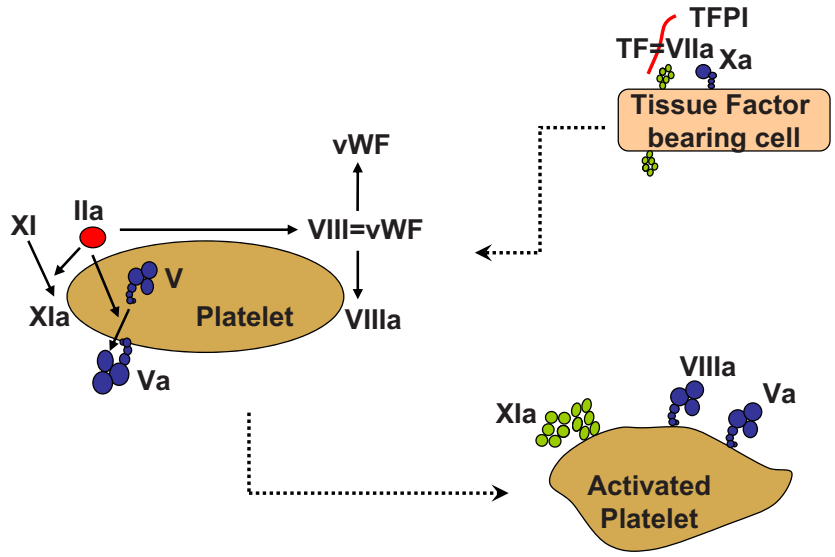

Figure 2.5: *Priming* The initially produced thrombin activates platelets, which release, among others, factor V from their α-granules. Thrombin activates the factors V, XI, and VIII, the latter by cleavage from vWF. These activated factors then bind to the platelet's surface. The TF=VIIa complex on the TF-bearing cell is inhibited by TFPI in complex with factor Xa.

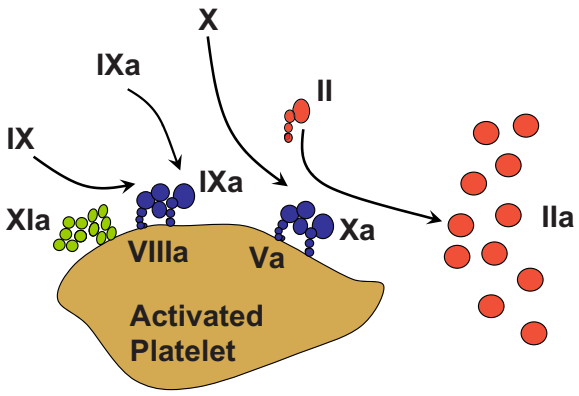

Figure 2.6: *Propagation* Factor IXa generated during initiation binds to the activated platelets. This pool of IXa is supported by factor XIa producing IXa on the platelet's membrane. Factor IXa in complex with factor VIIIa activates factor X, which then moves into the protected prothrombinase complex with factor Va. This eventually results in a burst of thrombin generation.

3 The fixed domain model

To determine the influence of various physical quantities on platelet adhesion, this chapter restricts itself to the initial phase of platelet deposition; that is the period of time when flow disturbances due to thrombus growth are only of secondary importance. Consequently, a fixed fluid domain is assumed. A continuous model of platelet adhesion is developed, henceforth referred to as "Fixed Domain model" (FD-model), which is based on the Navier-Stokes system and on conservation of particles. It is shown by optimization of parameters and by numerical simulation that the FD-model cannot reproduce the spatial distribution of bound platelets observed in three in vitro experiments when platelet adhesion is assumed independent of shear stress. In contrast to that, taking shear stress into account leads to qualitative agreement with the experimental data, although quantitative discrepancies remain. Solely by consideration of both shear stress and saturation-dependent changes in surface reactivity, satisfying quantitative agreement with the data is obtainable. The optimized parameter values are justified on the basis of experimental observations. Moreover, mathematical well-posedness in the sense of weak solutions is established for generalized parabolic systems containing ODE-coupled platelet flux conditions.

3.1 Model development

Despite their enormous concentration in blood ($\approx 250{,}000\,/\mu\mathrm{l}$), platelets constitute only about 0.2% of the blood volume [46]. For computational simulations of millimeter-size geometries it is therefore more appropriate to consider continuous models rather than discrete approaches.

Blood is known to exhibit some shear-thinning non-Newtonian behavior. This relies on the presence of RBCs that form rouleaux at flow stagnation and tend to deform and align with the flow at elevated shear rates. In the latter situation, the viscosity reaches an asymptotic value, so that blood can be regarded as Newtonian once shear rates exceed $200\,\mathrm{s}^{-1}$ [45]. In the tubular expansion experiments considered here, the mean inlet shear rate

$$\overline{g} := \frac{1}{|I|}\int_I g\,dS = \frac{4}{3}\frac{U}{L} \quad \text{(assuming Poiseuille flow)} \tag{3.1}$$

varied from 400 to $1{,}300\,\mathrm{s}^{-1}$ (g: shear rate; I: inlet; U: maximum inlet flow velocity; L: inlet radius). In the stagnation point flow, platelet-rich plasma has been used, which is Newtonian. Therefore, the velocity-field u was calculated from the Navier-Stokes equations (NSE) with constant viscosity. This led to quite accurate results for the t-junction, too, despite a mean inlet shear rate of only $70\,\mathrm{s}^{-1}$. Applicability of NSE was further supported by numerical tests for the tubular expansion case. In these tests, calculation of u was based on the shear-thinning Yasuda model [100], which has recently been applied to blood flow in a bifurcation [15]. However,

this non-Newtonian fluid model did not improve the predictions of the FD-model (data not shown).

The total density w of platelets (both resting and activated) is determined by a species conservation equation. To prevent platelet activation, aggregation, and release reaction, pre-activated platelets have been used in the stagnation point flow experiment and washed platelets in Tyrodes-albumin solution in the tubular expansion. This is why activation of platelets and detailed chemistry does not need to be considered here, but can be included in the FD-model using [37, 81, 97] and the theory presented in Chapter 2. In addition, due to the absence of endothelium in these in vitro experiments, the dynamic inhibitory protein C system does not respond to thrombin production and is therefore not taken into account in this work. However, using [97], the here presented approaches are readily extendable to in vivo considerations.

Adhesion of platelets to reactive material is taken as a first order reaction, with rate k depending on the wall shear stress s and—to account for changes in surface reactivity—on the concentration ψ of bound platelets. Since the focus of the FD-model is on the initial phase of platelet adhesion, long-term flow disturbances due to thrombus growth are neglected: platelets that adhere to the wall are regarded as being completely incorporated into the wall. However, due to the influence of shear stress on platelet adhesion, the coupling of flow and thrombus growth turns out to be important and will therefore be addressed in the next chapter.

Let $\Omega \subset \mathbb{R}^3$ be the vessel geometry under consideration, with boundary $\partial\Omega = \overline{\Gamma} \cup \overline{\Sigma} \cup \overline{I} \cup \overline{O}$, tangent τ and outer unit normal n. Γ denotes reactive material prone to platelet adhesion, Σ non-reactive material, I the inlet and O the outlet of the vessel. The domain and its different parts of the boundary are sketched in Figure 3.1. In cartesian coordinates, the FD-model reads

$$\left.\begin{aligned}
\partial_t u + (u\cdot\nabla)u - \nu\Delta u + \nabla p &= f \quad \text{in } \Omega \\
\nabla\cdot u &= 0 \quad \text{in } \Omega \\
u_{|I} = u_D\ ; \quad u_{|\Gamma\cup\Sigma} = 0\ ; \quad u(t=0) &= u_0 \ \text{ in } \Omega \\
\nu\partial_n u_{|O} = p\cdot n_{|O} \quad &\text{or, in the t-junction case:} \\
u_{|M} = u_{D,M} \quad &\text{for a subset} \quad M \subset O. \\
\partial_t w - D\Delta w + (u\cdot\nabla)w &= 0 \quad \text{in } \Omega \\
-D\partial_n w = \begin{cases} k(\psi,s)w & \text{on } \Gamma \\ 0 & \text{on } \Sigma\cup O \end{cases} & \\
w_{|I} = w_D\ ; \quad w(t=0) &= w_0 \ \text{ in } \Omega \\
\partial_t\psi = k(\psi,s)w\ , \quad \psi(t=0) &= 0 \quad \text{on } \Gamma.
\end{aligned}\right\} \tag{3.2}$$

In this work, ∇ denotes the gradient, Δ the Laplacian, and ν the kinematic viscosity of the fluid. w_0 and u_0 denote the initial concentration of w and u, respectively; w_D and u_D are prescribed values at the inflow.

D denotes the diffusion coefficient of the platelets. In plasma, the Brownian value of D can be estimated from the Stokes-Einstein equation as $D_b = 1.58 \times 10^{-7}\,\mathrm{mm}^2/\mathrm{s}$ [32]. However, the

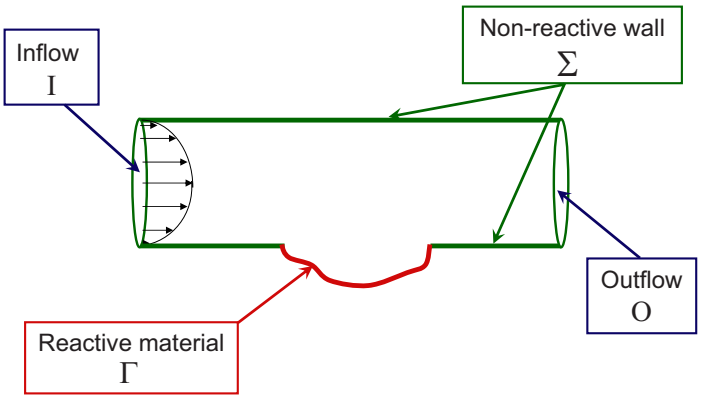

Figure 3.1: The different parts of the boundary

effective diffusion may be increased, dependent on the concentration of RBCs and the level of shear. One common method to take this into account is Keller's model [47], which assumes the augmentation to depend both on the diameter d of RBCs (assumed to be 5.5 µm) and, linearly, on the local shear rate g:

$$D = D_b + 0.045\, d^2 g\,. \tag{3.3}$$

However, as already pointed out by Sorensen [81], application of a shear-proportional enhancement factor in Poiseuille-type flows results in a level of enhancement which is the opposite of what is expected—zero at the centerline, where most of the red cells reside due to the Fahraeus effect, and highest at the wall, where they are excluded. Therefore, following [25, 81], a constant enhancement factor was used for D. Regarding the considered experiments, D was chosen one order of magnitude greater than the Brownian value, and two orders of magnitude greater in cases when RBCs were present, which is in compliance with the range of diffusion predicted by Keller's model.

The adhesion rate k is taken as

$$k(\psi, s) := \underbrace{\left(\lambda^{(1)} + \lambda^{(2)} s\right)\left(1 - \frac{\psi}{\Psi}\right)}_{(I)} + \underbrace{\left(\kappa^{(1)} + \kappa^{(2)} s\right)\frac{\psi}{\Psi}}_{(II)}\,. \tag{3.4}$$

Part (I) accounts for the reactivity of the original surface, whereas part (II) describes ongoing adhesion of platelets to the surface-bound ones. $\lambda^{(i)}$ and $\kappa^{(i)}$ denote reactivities of surface and platelets, respectively, and $\Psi := w_D L$. Wall shear stress s is defined as $s := \nu|g|$, with wall shear rate $g := (\tau \cdot \sigma \cdot n)/\nu$ and stress tensor $\sigma := -pI + \nu(\nabla u + \nabla u^T)$. The exact functional dependence of k on shear stress is unknown. Therefore, in each part of k, the dependence on s has been expanded into a Taylor series up to the linear term. Regarding stagnation point flow, David et al. [20] showed analytically that the use of such a linear dependence is reasonable, since it locates the position of maximum platelet flux within the range reported by Affeld et al. [1].

In order to derive a non-dimensional form of the FD-model, let W be a characteristic platelet concentration (here: $W := w_D$), take L/U as characteristic time, set $\tilde{x} := x/L$, $\tilde{t} := Ut/L$,

and define the following normalizations:

$$\begin{aligned} \tilde{u}(\tilde{x},\tilde{t}) &:= \frac{u(x,t)}{U}\,, \quad \tilde{p}(\tilde{x},\tilde{t}) := \frac{p}{U^2}\,, \quad \tilde{w}(\tilde{x},\tilde{t}) := \frac{w(x,t)}{W}\,, \quad \tilde{\psi}(\tilde{x},\tilde{t}) := \frac{\psi(x,t)}{\Psi} \\ \tilde{s}(\tilde{x},\tilde{t}) &:= \frac{s(x,t)L}{U\nu}\,, \quad \mathrm{Re} := \frac{LU}{\nu}\,, \quad \mathrm{Pe} := \frac{LU}{D}\,, \quad \lambda_1 := \frac{\lambda^{(1)}}{U}\,, \quad \lambda_2 := \frac{\lambda^{(2)}\nu}{L}\,. \end{aligned} \tag{3.5}$$

κ_1 and κ_2 are defined similar to λ_1 and λ_2, respectively. Note that λ_1 and κ_1 implicitly depend on U and therefore need to be adjusted upon changes in inflow velocity, whereas λ_2 and κ_2 are independent of flow, but depend on viscosity.

Except the t-junction, the setup of all considered experiments exhibits cylindrical symmetry (geometry, boundary conditions, etc.). In these cases, we switch from cartesian coordinates (x, y, z) to cylindrical coordinates (r, θ, z) and may assume $u_\theta = \partial_\theta u = 0$, $\partial_\theta w = 0$, which reduces dimension. The reasonability of using cylindrical coordinates is further confirmed by the below presented comparison of numerical and experimental results. Leaving out the tilde, we obtain

$$\left.\begin{aligned} \partial_t u_r + (u\cdot\nabla)u_r - \mathrm{Re}^{-1}(\Delta u_r - r^{-2}u_r) + \partial_r p = 0 \quad &\text{in } \Omega_c \\ \partial_t u_z + (u\cdot\nabla)u_z - \mathrm{Re}^{-1}\Delta u_z + \partial_z p = 0 \quad &\text{in } \Omega_c \\ r^{-1}\partial_r(ru_r) + \partial_z u_z = 0 \quad &\text{in } \Omega_c \\ u_{|I_c} = u_D/U\ ; \quad u_{|\Gamma_c\cup\Sigma_c} = 0\ ; \quad u(t=0) = u_0/U \quad &\text{in } \Omega_c \\ \mathrm{Re}^{-1}\partial_n u_{|O_c} = p\cdot n_{|O_c} \quad &\text{or, in the t-junction case:} \\ u_{|M_c} = u_{D,M_c}/U \quad &\text{for a subset} \quad M_c \subset O_c. \\ \partial_t w - \mathrm{Pe}^{-1}\Delta w + (u\cdot\nabla)w = 0 \quad &\text{in } \Omega_c \\ -\mathrm{Pe}^{-1}\partial_n w = \begin{cases} k(\psi,s)w & \text{on } \Gamma_c \\ 0 & \text{on } \Sigma_c\cup O_c \end{cases} & \\ w_{|I_c} = w_D/W\ ; \quad w(t=0) = w_0/W \quad &\text{in } \Omega_c \\ \partial_t\psi = k(\psi,s)w\,, \quad \psi(t=0) = 0 \quad &\text{on } \Gamma_c, \end{aligned}\right\} \tag{3.6}$$

where

$$k(\psi,s) := (\lambda_1 + \lambda_2 s)(1-\psi) + (\kappa_1 + \kappa_2 s)\psi\,. \tag{3.7}$$

Here, $u := (u_r, u_z)$, $\nabla := (\partial_r, \partial_z)^T$, $\Delta := \partial_r^2 + \partial_z^2$. Pe and Re are Peclet and Reynolds number, respectively, which are known from the experiment. In contrast to that, λ_i and κ_i are unknown and have to be fitted to experimental results. Ω_c denotes the two-dimensional computational domain, with Γ_c, Σ_c, I_c, $O_c \subset \partial\Omega_c$.

However, in order to perform numerical simulations based on the Finite Element (FE) method, the three-dimensional cartesian model (3.2) was first written in variational form, then transformed to cylindrical coordinates, and finally reduced to a two-dimensional system. This procedure avoids the necessity of introducing artificial boundary conditions on the artificial boundary $\Lambda_c := \{r = 0\}$ of Ω_c, which would arise when starting from the strong formulation (3.6).

3.2 Numerical methods and optimization of parameters

The numerical solution of (3.6) was performed using the FE library GASCOIGNE [10]. The Peclet number being rather large, steep gradients in platelet density have to be expected along the reactive wall. Therefore, a locally refined quadrilateral mesh was used, consisting of a total of cells ranging from 18,656 (stagnation point) to 47,104 (tubular expansion). Spatial Discretization was achieved using bilinear finite elements, together with a local projection stabilization of transport and pressure [9, 12]. The linear systems were solved by the Generalized Minimal Residual (GMRES) algorithm [74], which was preconditioned by a geometric multigrid method with block-ILU smoothing. A second order Crank-Nicolson scheme was applied for time-stepping. However, this scheme being prone to oscillations, four implicit Euler steps were used in the beginning to damp high frequency error components. This strategy—proposed by [70]—combines the smoothing property of the Euler scheme and, at the same time, preserves the higher order of Crank-Nicolson. Further information on these methods can be found in [68]. The implementational details of using the multigrid on locally refined meshes are provided in [8].

The equations of the FD-model permit the use of an elementary, well working, and easily implementable optimization strategy to fit the parameters λ_i, κ_i. To sketch the procedure, the special case $\lambda_1 \equiv \kappa_1 \equiv 0$ is sufficient. Set $\delta := \kappa_2 - \lambda_2$ and $\lambda := \lambda_2$. The aim to minimize the Euclidean distance of the predicted bound platelet concentration to the experimentally determined values $\tilde{\psi}_i$ (measured in $x_i \in \Gamma$), i.e.,

$$J(\psi) := \sum_{i=1}^{N} (\psi_i - \tilde{\psi}_i)^2 \longrightarrow \min!\,, \quad \psi_i := \psi(x_i, T)\,, \tag{3.8}$$

was followed by consideration of the necessary conditions

$$\partial_\lambda J = 0\,, \quad \partial_\delta J = 0\,. \tag{3.9}$$

Starting from $\partial_t \psi = k(\psi, s)w$, the ψ_i permit the representation

$$\psi_i = \frac{\lambda}{\delta} e^{\delta m_i} - \frac{\lambda}{\delta}\,, \quad m_i := \int_0^T s(x_i, \tau) w(x_i, \tau) d\tau \tag{3.10}$$

which is inserted in (3.8). The key idea that simplifies (3.9) is to neglect the dependence of w on δ and λ by the use of a fixed approximation $\hat{w}$ to w with corresponding weights $\hat{m}_i := \int_0^T s(x_i, \tau)\hat{w}(x_i, \tau)d\tau$. The equations (3.9) then reduce to

$$\sum_{i=1}^{N} \left(\frac{\lambda}{\delta} e^{\delta \hat{m}_i} - \frac{\lambda}{\delta} - \tilde{\psi}_i \right) \left(e^{\delta \hat{m}_i} - 1 \right) = 0, \quad \sum_{i=1}^{N} \left(\frac{\lambda}{\delta} e^{\delta \hat{m}_i} - \frac{\lambda}{\delta} - \tilde{\psi}_i \right) e^{\delta \hat{m}_i} \hat{m}_i = 0 \tag{3.11}$$

which can be solved by a damped Newton's method. The solution (λ, δ) is then inserted in (3.6) and the so modified system is solved again. The whole process is repeated several times until no further reduction of J is obtained.

3.3 Numerical results

3.3.1 Stagnation point flow

Affeld et al. [1] used platelet-rich plasma (PRP) of pre-activated platelets to study their deposition onto glass in a rotationally symmetric stagnation point flow environment. Steady inflow in form of a laminar jet was directed onto a glass plane that was positioned perpendicular to the jet axis. Figure 3.2 shows the computational domain with locally refined mesh and the computed streamlines of flow.

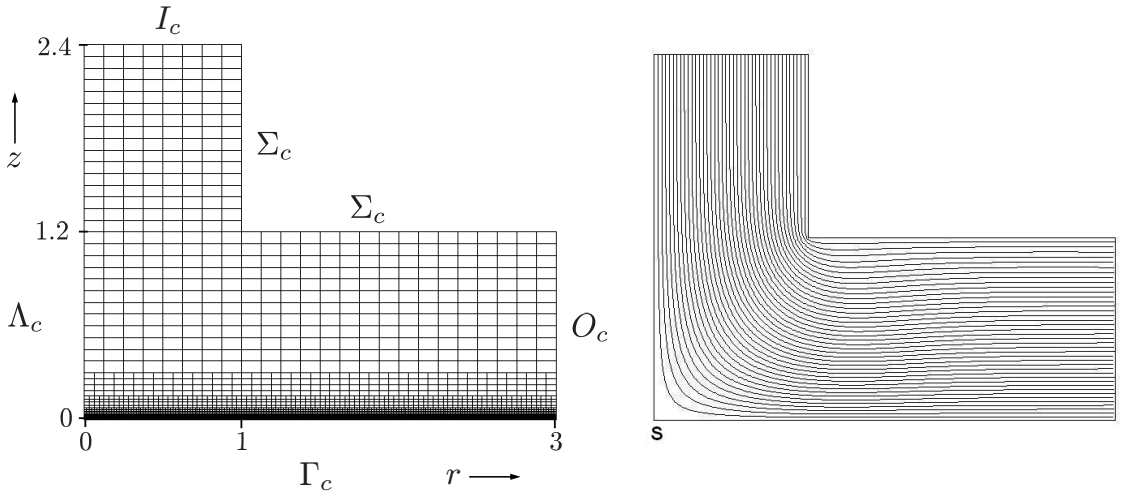

Figure 3.2: *Left* Computational domain; locally refined mesh. *Right* Computed streamlines

At the intersection of the jet axis with the surface a stagnation point (S) is generated. Platelet deposition has been evaluated in three runs over a period of 160, 170, and 180 s, respectively. As their main result, the researchers reported platelet deposition to be minimal at the stagnation point, where shear rate is lowest. Maximum deposition was found downstream of the stagnation point, at a location of elevated shear rate (Figure 3.3).

Following the presentation in [20], the data was normalized by time, yielding the mean platelet flux over a period of $160-180$ s. This is displayed in Figure 3.4, together with 68.26% confidence intervals and the optimized solutions of: (1) FD-model with purely shear-dependent platelet adhesion ($\lambda_1 = \kappa_1 = 0$); (2) FD-model with shear-independent platelet adhesion ($\lambda_2 = \kappa_2 = 0$); (3) FD-model with purely shear-dependent platelet adhesion, but without changes in surface reactivity: $k(\psi, s) := \lambda_2 s$. The respective parameters are provided by Table 3.1 on page 20.

FD-model number 2 and 3 are similar to those examined by David et al. [20] (except the ODEs in no. 2). As in their work, the FD-model with shear-independent platelet adhesion predicts maximum deposition at the stagnation point, which does not match the experimental data at all. Better compliance is obtained in the third case, when adhesion is assumed shear-dependent. However, there remains a relatively large overprediction around the stagnation point and downstream of the maximum.

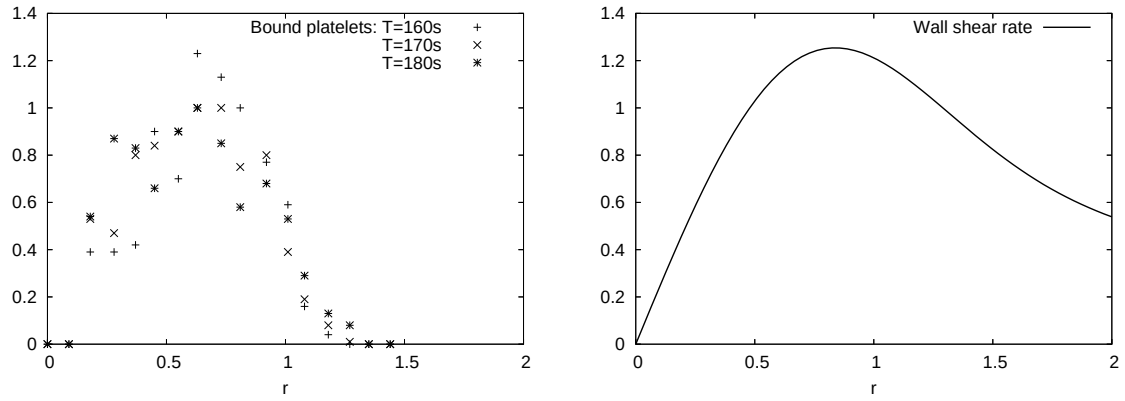

Figure 3.3: *Left* Normalized density of bound platelets. *Right* Computed normalized wall-shear rate

The best fit is achieved when both shear stress and changes in surface reactivity (due to platelet adhesion) are taken into account. In that case, the predicted curve passes well both through the area of negligible deposition around the stagnation point and the following maximum. In addition, overprediction further downstream is significantly reduced.

However, the question remains why there is such a remarkable decrease in experimentally measured platelet flux distal to the maximum. Comparison of wall-shear rate and adhesion proximal and distal to the maximum reveals that this decrease cannot be explained by a threshold behavior in the dependency on shear—which would actually be a first guess. It can rather be explained by upstream thrombus growth—an observation that has also been made by Sakariassen and Baumgartner [75] studying flow of citrated blood over collagen in a parallel-plate perfusion chamber. Platelets that would by-pass these growing aggregates on adjacent streamlines and then hit the glass plane further downstream might be entrapped by the already bound ones. Depletion of the boundary layer distal to the thrombus is the consequence, provided that shear rates are not high enough for replenishment. This effect exceeds the decrement in steady state platelet flux with axial distance l predicted by the classical theory of Lévêque and Levich [57] for convective diffusion in Poiseuille flow through a circular tube,

$$-D\left(\frac{\partial w}{\partial n}\right)_{|\Gamma} = 0.67 w_D \left(\frac{gD^2}{2l}\right)^{1/3},$$

and is remarkably reduced when aggregate growth is partially inhibited, for example in the presence of aspirin [75]. These conclusions also explain the experimentally observed "tendency for the platelets to deposit in the close vicinity of others already adhering (...)" which results in the formation of "extensive blots" [1] and is well reflected in the differences in magnitude of the parameters λ_2 and κ_2 of FD-model number 1. (see Table 3.1).

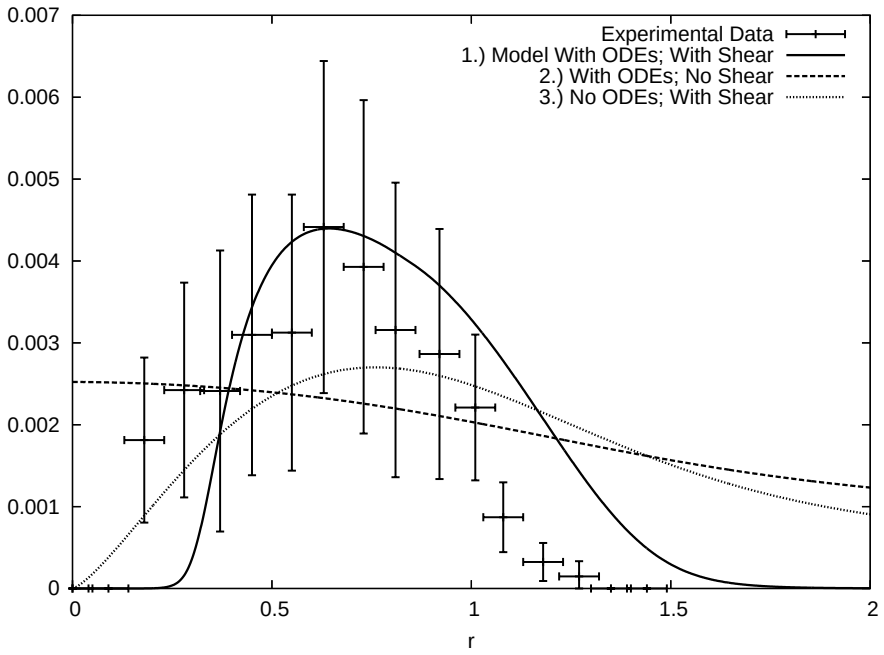

Figure 3.4: Normalized platelet flux. Optimized solutions of: *1* FD-model with changes in surface reactivity and shear-dependent platelet adhesion; *2* FD-model with changes in surface reactivity and shear-independent platelet adhesion; *3* FD-model without changes in surface reactivity, but with shear-dependent platelet adhesion

Table 3.1: Optimized parameters for platelet deposition from PRP onto glass in stagnation point flow. Mean inlet velocity $\overline{U} = 15.8\,\mathrm{mm/s}$; $L = 0.335\,\mathrm{mm}$; $\mathrm{Re} := 2\overline{U}L/\nu = 9.5$; $W = 1.9 \times 10^6\,/\mu\mathrm{l}$ (PRP)

FD-model	λ_1	λ_2	κ_1	κ_2
1	0	4.79×10^{-12}	0	1.15×10^{-3}
2	1.25×10^{-11}	0	1.38×10^{-3}	0
3	–	3.62×10^{-5}	–	–

3.3.2 Tubular expansion

Karino and Goldsmith [45] investigated adhesion of human platelets from reconstituted blood to collagen fibers on glass in a concentric tubular expansion geometry, both in steady and in pulsatile flow as well as under various Ht. The numerical simulations presented here consider the case of steady flow over a period of 60 s, Ht= 20%, and various Reynolds numbers. A magnification of the streamlines and the computational domain are shown in Figure 3.5.

In all considered cases, the experimentally determined number of attached platelets had a pronounced peak in the area of the vortex, followed by a minimum at the reattachement point

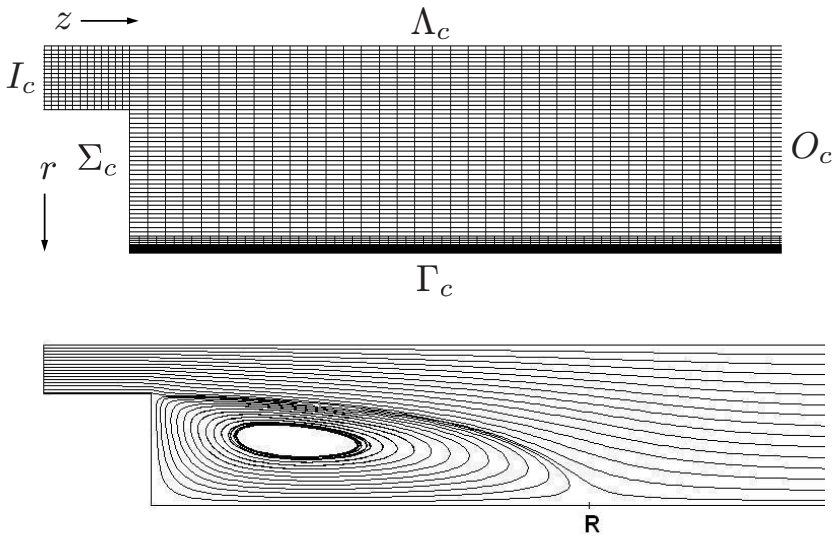

Figure 3.5: *Top* Computational domain; locally refined mesh. *Bottom* Computed streamlines

(R) and a smaller secondary maximum downstream, after which a steady value was reached (see figures 3.7, 3.8, and 3.9).

Jordan et al. [42] investigated computationally the effect of hematocrit and of RBC augmented platelet diffusivity on platelet adhesion in the tubular expansion. For this purpose, they employed the diffusion model proposed by Zydney and Colton [102],

$$D = D_b + 0.15\, d^2 g\, c\, (1-c)^{0.8}.$$

This model can be regarded as an extension of Keller's model (3.3), since, besides shear, it also takes into account the mass fraction c of RBCs. By fitting their parameters to the experimental data corresponding to the $\mathrm{Re} = 37.7$ situation, Jordan et al. obtained reasonable qualitative agreement. However, notable quantitative discrepancies remained, since agreement with the in vitro data could only be achieved either in the vortex area or around the reattachement point and the secondary peak, but not along the whole boundary. These results confirm, to some extent, the influence of shear enhanced diffusion on platelet adhesion. However, the authors neglected the influence of shear stress on surface reactivity. Furthermore, instead of using the local RBC concentration, Jordan et al. employed the averaged hematocrit to calculate the enhanced diffusion. But, as discussed on page 15, there are situations (e.g., Poiseuille flow) where the use of such an approximation may be misleading. Therefore, the following investigations concentrate on the effect of shear enhanced surface reactivity. It is shown that by the use of a time-dependent model which also accounts for changes in surface reactivity, good quantitative agreement is obtainable along the whole boundary (Figure 3.7).

To determine fluid viscosities, Karino and Goldsmith extrapolated stress-shear rate plots to a characteristic value for the mean inlet shear rate, which they chose to be U/L. This value being smaller than the mathematical expression (3.1) for the mean inlet shear rate, the viscosities were a little overestimated. Compared to the experimental data, the so obtained numerical

results were shifted slightly to the left. However, good agreement was achieved when the viscosities were determined by the use of (3.1). Therefore, the numerical results presented below are based on these corrected viscosities. The considered Reynolds numbers are: 40.9 (which corresponds to 37.7 in [45]), 30.1 (28.5) and 56.7 (50.6). The computed normalized wall-shear rates that prevail at the different Reynolds numbers are shown in Figure 3.6.

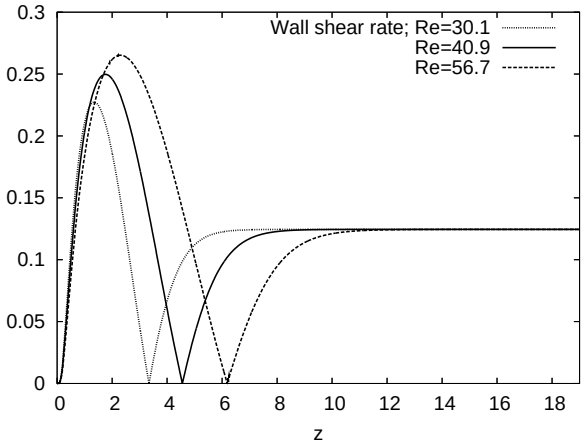

Figure 3.6: Computed normalized wall-shear rates

In order to test the behavior of the FD-model under different flow conditions, the parameters have been optimized for the case Re = 40.9 and then been applied to the cases of different Reynolds number. The adhesion rate k was chosen according to (3.7), with $\kappa_1 \equiv 0$ in the shear-dependent case (referred to as FD-model no. 1 in Table 3.2). In the shear-independent case (FD-model no. 2) the best fit was achieved for $\lambda_1 = \kappa_1$. In all cases, comparison of measured platelet number with wall-shear rate reveals platelet adhesion to be shear-dependent. This is further supported by the fact that the FD-model neglecting shear shows only poor agreement with the experimental data, as it predicts only one maximum in platelet deposition instead of two. In contrast to that, predictions of the shear-dependent FD-model show good agreement in the optimized Re = 40.9 case (Figure 3.7).

However, some overprediction occurs in the case of elevated Reynolds number (Figure 3.8), whereas for Re = 30.1 there is a remarkable underprediction in the vortex area (Figure 3.9).
Hence, with increasing Reynolds number, the behavior of the FD-model is contrary to the experimentally observed flattening of adhesion peaks. A reason for this could be that Karino and Goldsmith used Tyrodes-albumin (containing apyrase) as solvent that does neither contain vWf, nor fibrinogen. The effects of such lack of ligands (or associated receptors) on primary hemostasis are reflected in the corresponding bleeding disorders, such as von Willebrand disease (quantitative or qualitative defects in vWf), Bernard-Soulier syndrome (deficiency in GPIb receptors), or Glanzmann's thrombasthenia (deficiency in GPIIb/IIIa receptors), where platelet adhesion or aggregation is known to be impaired [96]. Indeed, for the considered range of shear rate, the FD-model trends agree with the following experimental findings on whole blood which demonstrate platelet adhesion to be favored at elevated shear. For example, using non-anticoagulated human blood flowing over type III collagen in a stenoses for 1 minute, Barstad et al. [4] observed an increase in % surface coverage at the stenosis apex by a factor of

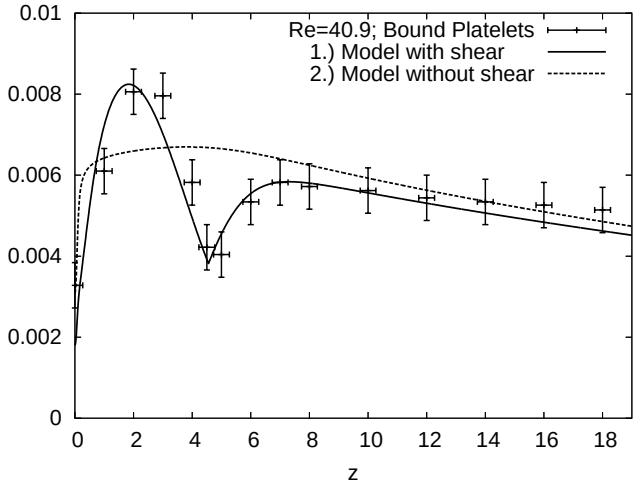

Figure 3.7: Normalized densities of bound platelets. Optimized solutions of: *1* FD-model with shear- and saturation-dependent platelet adhesion; *2* FD-model with shear-independent platelet adhesion; Re = 40.9

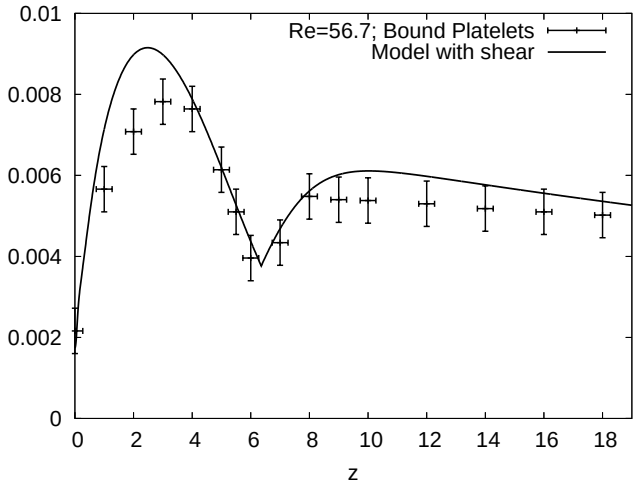

Figure 3.8: Re = 56.7: normalized densities of bound platelets; FD-model with shear- and saturation-dependent platelet adhesion.

1.5 when wall shear rate was increased from $420\,s^{-1}$ to $2{,}600\,s^{-1}$. Studying platelet adhesion from citrated whole blood to confluent spread platelet monolayers in an in vitro flow-based platelet-aggregation assay, Kulkarni et al [50] observed even a quadruplication of the number of tethered platelets upon an increase of shear rate from $150\,s^{-1}$ to $1{,}800\,s^{-1}$. Finally, using anticoagulated whole blood (with PPACK and PGE_1) in a parallel plate flow chamber, Savage et al. [78] reported a triplication of platelets attached to immobilized vWf when wall shear rate increased from $50\,s^{-1}$ to $1{,}500\,s^{-1}$. However, caution is advised, since platelet adhesion to immobilized fibrinogen behaves contrary to the case of immobilized vWf [78].

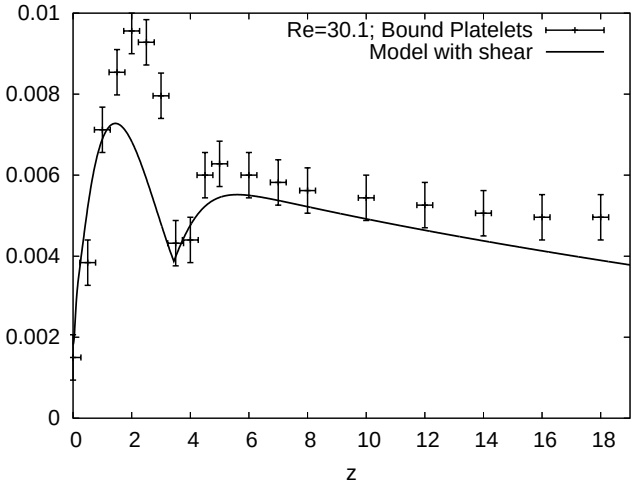

Figure 3.9: Re = 30.1: normalized densities of bound platelets; FD-model with shear- and saturation-dependent platelet adhesion.

Table 3.2: Optimized parameters for the deposition of washed platelets to collagen fibers on glass in a tubular expansion. Diameter of inlet tube: $d := 0.917\,\text{mm}$; outlet tube: $3.0\,\text{mm}$. $L := 1.0\,\text{mm}$; $\overline{U}$: mean inlet velocity; $\text{Re} := \overline{U}d/\nu$; $W = 5 \times 10^5\,/\mu\text{l}$. *Note that λ_1, κ_1 have to be adjusted upon changes in inflow velocity, and λ_2, κ_2 upon changes in viscosity

Re	FD-model	$\lambda_1{}^*$	$\lambda_2{}^*$	$\kappa_1{}^*$	$\kappa_2{}^*$	$\overline{U}\,(\text{mm}\,s^{-1})$
40.9	1	5.16×10^{-7}	2.59×10^{-6}	0	3.31×10^{-6}	90.1
40.9	2	8.7×10^{-7}	–	8.7×10^{-7}	–	90.1
30.1	1	6.55×10^{-7}	2.69×10^{-6}	0	3.44×10^{-6}	71.0
56.7	1	4.06×10^{-7}	2.37×10^{-6}	0	3.03×10^{-6}	114.4

3.3.3 T-junction

Lee et al. [56] used citrated human blood to study platelet deposition to polypropylene in a t-junction geometry. Several runs with steady flow were conducted, of which each had a period of 60 s. Peak adhesion was found to occur around the apex (A) of the flow divider. Although the t-junction is actually a three-dimensional problem, deposition at the top sides of the tubes and deposition at the bottom sides were virtually the same. Therefore, the two-dimensional version of (3.2) was used to simplify numerical calculations. Figure 3.10(a) shows the computational domain; a magnification of the fluid streamlines is provided in Figure 3.10(b).

The predictions of the FD-model were investigated for the long side of the main tube (referred to as Side(I)) and for the right side of the branching tube (Side(II)). Optimization of parameters showed that changes in surface reactivity due to platelet adhesion were only of secondary

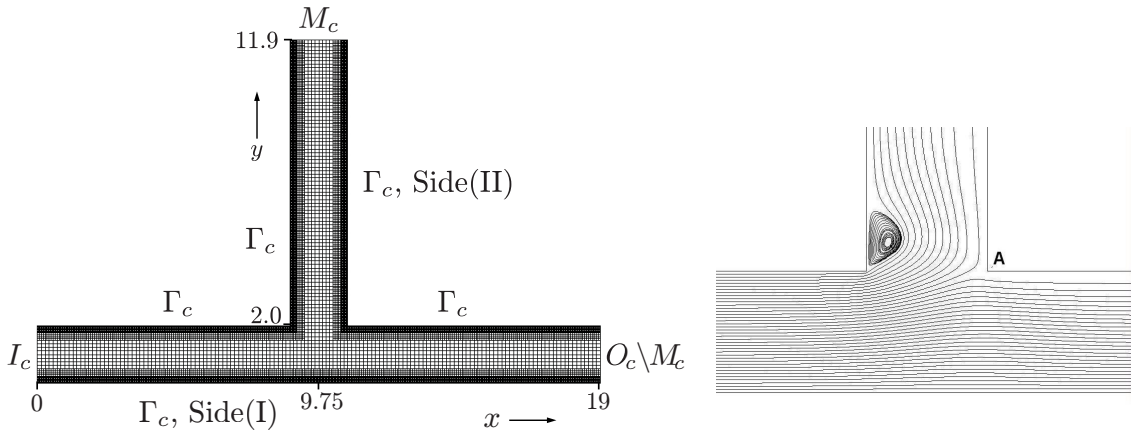

(a) Computational domain; locally refined mesh

(b) Computed streamlines of flow

Figure 3.10: T-junction

importance (i.e., $\lambda_i = \kappa_i$). Therefore, the henceforth considered cases are: (1) shear-dependent adhesion, that is $k(\psi, s) := \lambda_2 s$; (2) shear-independent adhesion, that is $k(\psi, s) := \lambda_1$. Comparison of experimentally measured deposition with computed wall-shear rate shows that platelet adhesion is strongly determined by wall-shear rate both in the main tube (Figure 3.11) and in the branching tube (Figure 3.12). This is the reason why the shear-independent FD-model shows only poor agreement with the experimental data. In contrast, the shear-dependent version accurately captures the minimum adhesion in the branching area of the main tube (Figure 3.11) as well as the peak adhesion around the flow divider of the side tube (Figure 3.12).

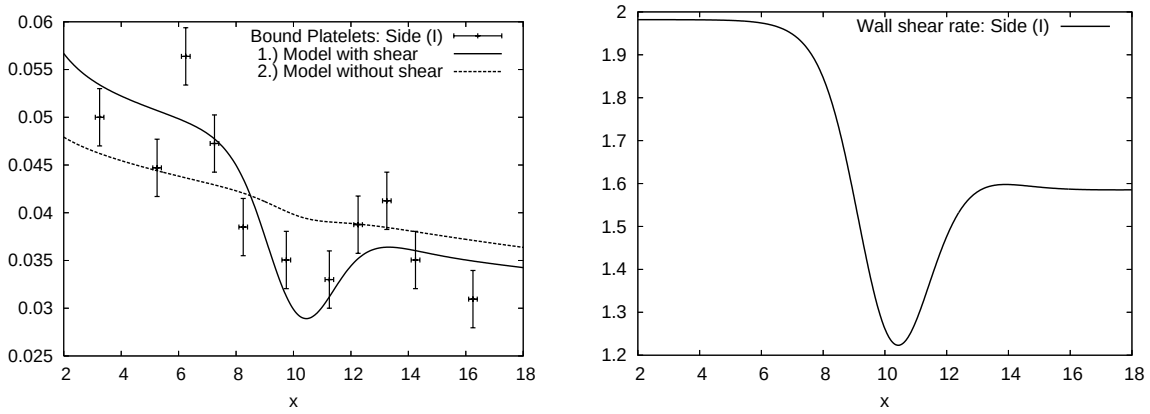

Figure 3.11: *Left* Normalized density of bound platelets, Side (I); Optimized solutions of: *1* FD-model with shear-dependent platelet adhesion; *2* FD-model with shear-independent platelet adhesion. *Right* Computed normalized wall-shear rate

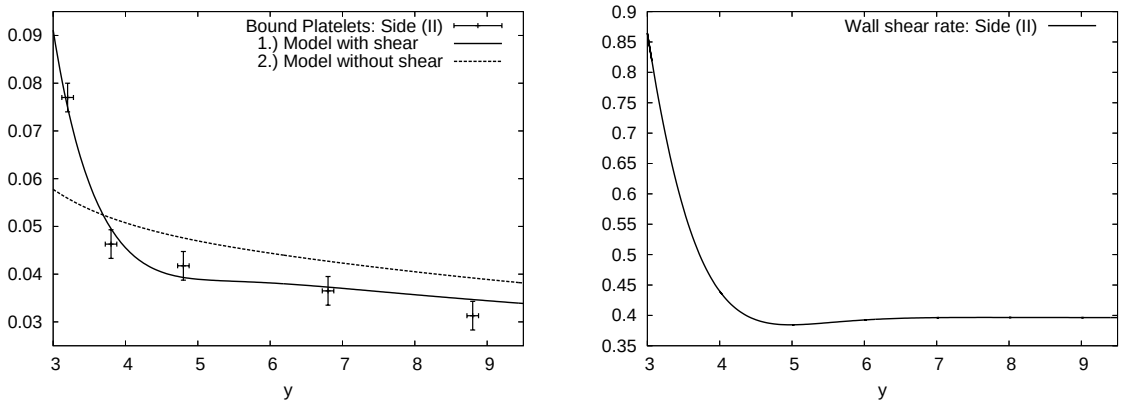

Figure 3.12: *Left* Normalized density of bound platelets, Side (II); Optimized solutions of: *1* FD-model with shear-dependent platelet adhesion; *2* FD-model with shear-independent platelet adhesion. *Right* Computed normalized wall-shear rate

Table 3.3: Optimized parameters for platelet deposition from citrated blood onto polypropylene in a t-junction. Mean inlet velocity $\overline{U} = 25.0\,\mathrm{mm/s}$; $L = 1.0\,\mathrm{mm}$; $\mathrm{Re} := 2\overline{U}L/\nu = 15.7$; $W = 2 \times 10^5\,/\mu\mathrm{l}$

Side	FD-model	λ_1	λ_2
(I)	1	0	0.86×10^{-5}
(I)	2	1.87×10^{-5}	0
(II)	1	0	4.08×10^{-5}
(II)	2	2.35×10^{-5}	0

3.4 Discussion

The aim of this section is to explain the differences among the optimized parameters. In the stagnation point, initial platelet flux to the surface is low due to the small value of λ_2 (cf. Table 3.1, FD-model no. l), whereas adhesion of platelets to already bound ones is high (cf. κ_2). In contrast to that, in the tubular expansion, adhesion to collagen coated glass and adhesion to bound platelets seem to be more balanced (cf. the magnitudes of λ_i and κ_2 in Table 3.2, FD-model no. 1). In the t-junction, changes in surface reactivity could even be neglected in the considered time-frame of 1 min (Table 3.3).

By means of the experimental data of Brash et al. [13], these effects are related to differences in surface material, solvent, hematocrit, and to more or less pronounced expression of pseudopodia by the bound platelets. Using rotating cylindrical probes, this group investigated adhesion of washed pig platelets to glass, to various polymer surfaces, and to collagen coated glass—both from citrated plasma and from Tyrodes-albumin. The effects of various hematocrits were studied by adding washed RBCs. Shear rate was $19\,\mathrm{s}^{-1}$. ADP-induced aggregation was

inhibited and almost all platelets were found to adhere singly and directly to the surface.

Firstly, Brash et al. report hematocrit to increase adhesion. However, the augmentation strongly depends on the surface material and therefore cannot be explained solely by increased diffusion. At 0% Ht (corresponding to the stagnation point) adhesion is small and almost the same over the whole range of considered materials. An increase of Ht to 20% (corresponding to the tubular expansion) greatly increases adhesion to collagen coated glass (tubular expansion), but has only minor effect on adhesion to glass (stagnation point) and to polymers. Secondly, Tyrode-solution (used in the tubular expansion) is found to better support platelet adhesion than plasma (stagnation point). Both effects explain the differences in initial platelet flux predicted for the stagnation point flow and for the tubular expansion. The differences in platelet-platelet adhesion can be explained by the fact that Brash et al. observed expression of pseudopodia only when the platelets were bound to glass (stagnation point).

Finally, a rise of Ht to 45% (corresponding to the t-junction) led to a remarkable increase in platelet adhesion to the glass and polymer surfaces (t-junction). In addition, Brash et al. reported adhesion to reach equilibrium within two minutes, which exceeds well the duration of the runs performed in the t-junction. This partially explains why changes in surface reactivity turned out to be negligible there (although they certainly come into play in longer runs).

Altogether, it seems that in the described range of Ht changes in surface reactivity have a stronger impact on initial platelet adhesion at lower Ht than at elevated Ht. However, it should be noted that further mechanisms could be important, too, and that more experiments under comparable conditions are needed to confirm this hypothesis.

3.5 Mathematical analysis

This section deals with the mathematical well-posedness of (3.2). Existence, uniqueness, and positivity of solutions are proven. In (3.2), the fluid dynamic equations and the species equations are only coupled in one way: u can be calculated independently of w and then be inserted into the species equation. Since the NSE have already been extensively studied, for example in [86], it remains to investigate the coupling of ODEs along the boundary to a parabolic equation in the interior of the domain via a Robin-type boundary condition. Although this kind of problem arises in mathematical models concerned with changes in surface reactivity, for example in [82, 83], its mathematical investigation is still missing. Regarding existence of solutions, it is not more elaborate to consider the generalized situation of a parabolic system with a nonlinear right hand side—provided that certain growth conditions are fulfilled. This accounts for possible extensions of the FD-model involving chemistry.

3.5.1 Notation and function spaces

Let Ω be a bounded open subset of $\mathbb{R}^n$, with Lipschitz boundary $\partial\Omega$ (i.e., $\partial\Omega \in C^{0,1}$ in the sense of [99, p. 48]) consisting of two relatively open parts Λ and Ξ. Regarding (3.2), Ξ stands for reactive and non-reactive wall, whereas Λ comprises inflow and outflow. Here, for simplicity, the case of Dirichlet boundary conditions on w at the outflow is considered. However, if

there is no backflow into the domain, only slight modifications are needed for the original Neumann case. The following theory makes use of Lebesgue spaces L^p and Sobolev spaces W_2^s ($s \geq 0$) which are defined, for example, in [21, 99]. Norms, such as $\|.\|_{L^2(0,T;L^2(\Omega))}$, are intuitively abbreviated with $\|.\|_{L^2L^2}$. We also write $W_2^1(\Omega)$ instead of $W_2^1(\Omega, \mathbb{R}^m)$, and so forth. In addition, let $X := \{w \in W_2^1(\Omega) : \ w_{|\Lambda} = 0\}$ with norm $\|w\|_X := \|\nabla w\|_{L^2(\Omega)}$ and associated dual space X'. Define $\Omega_T := \Omega \times (0,T]$, $\Xi_T := \Xi \times (0,T]$, $\Lambda_T := \Lambda \times (0,T]$, and let $|.|$ denote the euclidean norm of $\mathbb{R}^m$ and $\mathbb{R}^r$, respectively.

3.5.2 Problem statement and assumptions

The following boundary value problem is investigated, which contains the equations for w in (3.2) as special case.

$$\begin{cases} \partial_t w_i + L_i w_i = f_i(w,x,t) & \text{in } \Omega_T\,,\ i = 1,...,m \\ -\sum_{l,j=1}^{n} a_i^{lj} w_{ix_l} n^j = k_i(w,\psi,x,t) & \text{on } \Xi_T\,,\ i = 1,...,m \\ w = g(x,t) & \text{on } \Lambda_T \\ w(.\,,0) = w_0 & \text{in } \Omega \\ \partial_t \psi = q(w,\psi,x,t) & \text{on } \Xi_T \\ \psi(.\,,0) = \psi_0 & \text{on } \Xi\,. \end{cases} \tag{3.12}$$

Here, $w := (w_i)_{i=1}^m$, $\psi := (\psi_i)_{i=1}^r$, $g := (g_i)_{i=1}^m$, $q := (q_i)_{i=1}^r$. The L_i are linear elliptic operators with bounded coefficients $a_i^{lj}, b_i^l, c_i \in L^\infty(\Omega_T)$,

$$L_i w_i := -\sum_{l,j=1}^{n} \left(a_i^{lj}(x,t) w_{ix_l}\right)_{x_j} + \sum_{l=1}^{n} b_i^l(x,t) w_{ix_l} + c_i(x,t) w_i\,. \tag{3.13}$$

In the following, $f := (f_i)_{i=1}^m$, $k := (k_i)_{i=1}^m$, and q are assumed measurable. Furthermore,

$$\begin{gathered} g \in L^2(0,T;W_2^1(\Omega)) \cap W_2^1(0,T;W_2^1(\Omega)') \quad , \quad q(0,0,.\,,.\,) \in L^2(0,T;L^2(\Xi)) \\ w_0 \in L^2(\Omega) \quad , \quad \psi_0 \in L^2(\Xi)\,. \end{gathered} \tag{3.14}$$

f and k are required to satisfy $\forall h, s \in \mathbb{R}^m$ and $\forall \varphi \in \mathbb{R}^r$ the growth conditions

$$|f(h,x,t)| \leq \Theta_1^{(1)} + \Theta_1^{(2)}|h|\,, \quad |k(s,\varphi,x,t)| \leq \Theta_2^{(1)} + \Theta_2^{(2)}|s| + \Theta_2^{(3)}|\varphi|\,, \tag{3.15}$$

and to be continuous in h, s, and φ. q is assumed Lipschitz continuous:

$$|q(s,\varphi,x,t) - q(\tilde{s},\tilde{\varphi},x,t)| \leq \Theta_3^{(1)}|s-\tilde{s}| + \Theta_3^{(2)}|\varphi - \tilde{\varphi}| \quad \forall s,\tilde{s} \in \mathbb{R}^m \ \ \forall \varphi,\tilde{\varphi} \in \mathbb{R}^r. \tag{3.16}$$

3.5.3 Existence and uniqueness for the linear problem

To solve the nonlinear system (3.12) we first consider the corresponding linear problem

$$\begin{cases} \partial_t w + Lw = h & \text{in } \Omega_T \\ -\sum_{l,j=1}^{n} a^{lj} w_{x_l} n^j = kw + l & \text{on } \Xi_T \\ w = g & \text{on } \Lambda_T \\ w(.,0) = w_0 & \text{in } \Omega\,, \end{cases} \tag{3.17}$$

where $h \in L^2(0,T;X')$, $k \in L^\infty(0,T;L^\infty(\Xi,\mathbb{R}_+))$, and $l \in L^2(0,T;L^2(\Xi))$. We define the bilinear form

$$B[w,v;t] := \int_\Omega \sum_{l,j=1}^{n} a^{lj}(x,t) w_{x_l} v_{x_j} + \sum_{l=1}^{n} b^l(x,t) w_{x_l} v + c(x,t) wv \, dx + \int_\Xi k(x,t) wv \, d\sigma$$

and say that w is a weak solution of (3.17) if and only if (1) $w - g \in L^2(0,T;X) \cap W_2^1(0,T;X')$, (2) w fulfills the equation

$$\langle w'(t), v\rangle + B[w(t),v;t] = \langle h(t), v\rangle - (l(t),v)_{L^2(\Xi)} \quad \forall v \in X \tag{3.18}$$

for almost every $t \in [0,T]$, and (3) $w(t=0) = w_0$.

The aim is to solve (3.18) by Galerkin's method. For this purpose, we choose a system of functions $\{u_k\}_{k=1}^\infty$ that constitutes an orthonormal basis of $L^2(\Omega)$ as well as an orthogonal basis of X and look for functions $w_m(t) := \sum_{k=1}^{m} d_m^k(t) u_k$ that satisfy the system of ordinary differential equations

$$(w_m'(t), u_k)_{L^2} + B[w_m(t), u_k; t] = \langle h(t), u_k\rangle - (l(t), u_k)_{L^2(\Xi)} \quad (k = 1, ..., m), \tag{3.19}$$

subject to the initial conditions $d_m^k(0) = (w_0, u_k)_{L^2}$ $(k = 1, ..., m)$. Application of Banach's fixed point theorem reveals (3.19) to have a unique solution w_m for each $m \in \mathbb{N}$. We further note that one can employ the eigenfunctions of the Laplacian subject to mixed boundary conditions as basis functions u_k, i.e.

$$\begin{cases} -\Delta u_k = \lambda_k u_k & \text{in } \Omega \\ \partial_n u_k = 0 & \text{on } \Xi \\ u_k = 0 & \text{on } \Lambda\,. \end{cases}$$

Lemma 3.5.1 (A priori estimates for the approximate solutions)**.** *The following estimates hold uniformly for all $m \in \mathbb{N}$:*

$$\begin{aligned} \max_{0\le t\le T} \|w_m(t)\|_{L^2} + \|w_m\|_{L^2X} &\le C_1 \left(\|h\|_{L^2X'} + \|l\|_{L^2L^2(\Xi)} + \|w_0\|_{L^2} \right) \\ \|w_m'\|_{L^2X'} &\le C_2 \left(\|h\|_{L^2X'} + \|l\|_{L^2L^2(\Xi)} + \|w_0\|_{L^2} \right). \end{aligned} \tag{3.20}$$

Here, $C_1 = C_1(\Omega, T, L)$ and $C_2 = C_2(k, \Omega, T, L)$.

Proof. 1. We multiply (3.19) by $d_m^k(t)$ and sum over $k = 1, ..., m$. This yields

$$(w_m'(t), w_m(t))_{L^2} + B[w_m(t), w_m(t); t] = \langle h(t), w_m(t)\rangle - (l(t), w_m(t))_{L^2(\Xi)} \tag{3.21}$$

for almost every $t \in [0, T]$. Ellipticity of the operator L implies

$$\beta\|w_m(t)\|_X^2 \leq B[w_m(t), w_m(t); t] + \gamma\|w_m(t)\|_{L^2}^2 \tag{3.22}$$

for some constants $\beta > 0$ and $\gamma \geq 0$. Combining (3.21) and (3.22) we obtain

$$\frac{d}{dt}\left(\|w_m(t)\|_{L^2}^2\right) + \beta\|w_m(t)\|_X^2 \leq C_1\|w_m(t)\|_{L^2}^2 + C_2\left(\|h(t)\|_{X'}^2 + \|l(t)\|_{L^2(\Xi)}^2\right). \tag{3.23}$$

Application of Gronwall's inequality (see [21, p. 624]) yields

$$\max_{0\leq t\leq T}\|w_m(t)\|_{L^2}^2 \leq C\left(\|h\|_{L^2X'}^2 + \|l\|_{L^2L^2(\Xi)}^2 + \|w_0\|_{L^2}^2\right). \tag{3.24}$$

Integrating (3.23) over time and making use of (3.24) we end up with

$$\|w_m(T)\|_{L^2}^2 - \|w_m(0)\|_{L^2}^2 + \beta\|w_m\|_{L^2X}^2 \leq C\left(\|h\|_{L^2X'}^2 + \|l\|_{L^2L^2(\Xi)}^2 + \|w_0\|_{L^2}^2\right).$$

2. To prove the estimate of $\|w_m'\|_{L^2X'}$ we choose $v \in X$ with $\|v\|_X \leq 1$. Furthermore, we define $V_m := \text{span}\{u_k : k = 1, ..., m\}$ and observe that $L^2(\Omega) = V_m \oplus V_m^\perp$, i.e. each $v \in L^2(\Omega)$ has a unique decomposition $v = v_1 + v_2$ with $v_1 \in V_m$ and $v_2 \in V_m^\perp$. Clearly, $1 \geq \|v\|_X^2 \geq \|v_1\|_X^2$. Since $w_m'(t) \in V_m$, we obtain using (3.19)

$$\langle w_m'(t), v\rangle = (w_m'(t), v)_{L^2} = (w_m'(t), v_1)_{L^2} = \langle h(t), v_1\rangle - (l(t), v_1)_{L^2(\Xi)} - B[w_m(t), v_1; t]\,. \tag{3.25}$$

The assumptions on the coefficients of L ensure continuity of the bilinear form B, i.e.

$$|B[w_m(t), v_1; t]| \leq C\|w_m(t)\|_X\|v_1\|_X\,.$$

Hence, (3.25) implies

$$\|w_m'(t)\|_{X'}^2 \leq C\left(\|h(t)\|_{X'}^2 + \|l(t)\|_{L^2(\Xi)}^2 + \|w_m(t)\|_X^2\right).$$

Integrating over time and employing the above derived estimate for $\|w_m\|_{L^2X}^2$ yields the assertion for $\|w_m'\|_{L^2X'}$. □

Theorem 3.5.1 (Existence and uniqueness in the case of zero boundary values)**.** *Suppose that $g \equiv 0$. Then there exists a unique weak solution $w \in L^2(0, T; X) \cap W_2^1(0, T; X')$ of* (3.17)*. This solution fulfills the estimates*

$$\begin{aligned}\max_{0\leq t\leq T}\|w(t)\|_{L^2} + \|w\|_{L^2X} &\leq C_1\left(\|h\|_{L^2X'} + \|l\|_{L^2L^2(\Xi)} + \|w_0\|_{L^2}\right)\\ \|w'\|_{L^2X'} &\leq C_2\left(\|h\|_{L^2X'} + \|l\|_{L^2L^2(\Xi)} + \|w_0\|_{L^2}\right),\end{aligned} \tag{3.26}$$

where $C_1 = C_1(\Omega, T, L)$ and $C_2 = C_2(k, \Omega, T, L)$.

Proof. 1. As a consequence of (3.20) there exist a subsequence $m_l \to \infty$ and two functions $w \in L^2(0,T;X)$ and $v \in L^2(0,T;X')$, such that

$$\begin{cases} w_{m_l} \rightharpoonup w & \text{weakly in } L^2(0,T;X) \\ w'_{m_l} \rightharpoonup v & \text{weakly in } L^2(0,T;X'). \end{cases} \tag{3.27}$$

Consequently, we deduce $v = w'$ and prove (3.26) to be fulfilled by the weak limits w and w'.

We further note that each weak solution w of (3.17) with $g \equiv 0$ necessarily fulfills the first estimate of (3.26) and therefore must be unique. This follows by testing (3.18) with $w(t)$ and making use of the fact that $w \in L^2(0,T;X) \cap W_2^1(0,T;X')$ implies absolute continuity of the mapping $t \mapsto \|w(t)\|^2_{L^2(\Omega)}$ as well as $\partial_t \|w(t)\|^2_{L^2(\Omega)} = 2\langle w'(t), w(t)\rangle$ to hold almost everywhere on $[0,T]$ (see [101, p. 446-447]), which allows us to use arguments similar to those given in the proof of Lemma 3.5.1.

2. Next, we demonstrate the weak limit w to be a solution of (3.18). For this purpose, we fix $N \in \mathbb{N}$ and choose a function $v(t) = \sum_{k=1}^{N} d^k(t) u_k \in C^1([0,T];X)$. Furthermore, we choose a measurable subset $E \subset [0,T]$. From (3.19) it follows that

$$\int_E \langle w'_m(t), v(t)\rangle + B[w_m(t), v(t); t]\, dt = \int_E \langle h(t), v(t)\rangle - (l(t), v(t))_{L^2(\Xi)} dt\,. \tag{3.28}$$

We observe that the left hand side of (3.28) fulfills

$$\begin{aligned} A_v^E(w'_m) &:= \int_E \langle w'_m(t), v(t)\rangle dt \Rightarrow A_v^E \in \left(L^2(0,T;X')\right)', \\ B_v^E(w_m) &:= \int_E B[w_m(t), v(t); t] dt \Rightarrow B_v^E \in \left(L^2(0,T;X)\right)', \end{aligned}$$

which implies (3.28) to hold in the limit $m_l \to \infty$:

$$\int_E \langle w'(t), v(t)\rangle + B[w(t), v(t); t]\, dt = \int_E \langle h(t), v(t)\rangle - (l(t), v(t))_{L^2(\Xi)} dt\,. \tag{3.29}$$

Since E was arbitrary, for fixed v there exists a subset $N_v \subset [0,T]$ of measure zero, such that

$$\langle w'(t), v(t)\rangle + B[w(t), v(t); t] = \langle h(t), v(t)\rangle - (l(t), v(t))_{L^2(\Xi)} \tag{3.30}$$

holds for all $t \in [0,T]\backslash N_v$. Since $\{u_k\}_{k=1}^{\infty}$ constitutes a countable basis of X we obtain the validity of (3.18) for all $t \in [0,T]\backslash N$, where $N := \bigcup_{k=1}^{\infty} N_{u_k}$ has measure zero.

3. It remains to show that $w(t=0) = w_0$. Performing partial integration in (3.29) we deduce

$$\begin{aligned} \int_0^T -\langle w(t), v'(t)\rangle + B[w(t), v(t); t]\, dt = \int_0^T \langle h(t), v(t)\rangle - (l(t), v(t))_{L^2(\Xi)} dt \\ + (w(0), v(0))_{L^2} \end{aligned} \tag{3.31}$$

for a function $v(t) = \sum_{k=1}^{N} d^k(t)u_k \in C^1([0,T];X)$ with $v(T) = 0$. Furthermore, equation (3.28) implies

$$\int_0^T -\langle w_{m_l}(t), v'(t)\rangle + B[w_{m_l}(t), v(t); t]\, dt = \int_0^T \langle h(t), v(t)\rangle - (l(t), v(t))_{L^2(\Xi)} dt + (w_{m_l}(0), v(0))_{L^2}\,. \tag{3.32}$$

We take the limit $m_l \to \infty$ in (3.32) and thereby employ (3.27) and the fact that $w_{m_l}(0) \to w_0$ in $L^2(\Omega)$. Subtracting the so obtained result from (3.31) yields

$$(w(0) - w_0, v(0))_{L^2} = 0\,.$$

□

Corollary 3.5.1 (Existence and uniqueness for nonzero boundary values)**.** *There exists a unique weak solution $w \in L^2(0,T;W_2^1(\Omega)) \cap W_2^1(0,T;X')$ of the linear problem* (3.17)*. Furthermore, this solution satisfies the estimate*

$$\begin{aligned}&\max_{0\le t\le T} \|w(t)\|_{L^2} + \|w\|_{L^2W_2^1(\Omega)} + \|w'\|_{L^2X'} \\ &\quad\le C\left(\|h\|_{L^2X'} + \|l\|_{L^2L^2(\Xi)} + \|g\|_{L^2W_2^1(\Omega)} + \|g'\|_{L^2W_2^1(\Omega)'} + \|w_0\|_{L^2}\right),\end{aligned} \tag{3.33}$$

where $C = C(k, \Omega, T, L)$.

Proof. Due to Theorem 3.5.1 there exists a unique solution $\tilde{w} \in L^2(0,T;X) \cap W_2^1(0,T;X')$ of

$$\begin{aligned}\langle \tilde{w}'(t), v\rangle + B[\tilde{w}(t), v; t] &= \langle \tilde{h}(t), v\rangle - (l(t), v)_{L^2(\Xi)} \\ &:= \langle h(t), v\rangle - \langle g'(t), v\rangle - B[g(t), v; t] - (l(t), v)_{L^2(\Xi)} \quad \forall v \in X,\end{aligned}$$

subject to the initial condition $\tilde{w}(0) = w_0 - g(0)$. Hence, defining $w := \tilde{w} + g$ yields a weak solution of the original problem (3.18). Uniqueness follows immediately from Theorem 3.5.1 applied to the difference of two weak solutions of (3.18).

To prove the estimate (3.33) we observe that

$$\|\tilde{h}\|_{L^2X'} \le C\left(\|h\|_{L^2X'} + \|g'\|_{L^2W_2^1(\Omega)'} + \|g\|_{L^2W_2^1(\Omega)}\right).$$

Together with (3.26), this implies

$$\begin{aligned}\|\tilde{w}\|_{L^2X} &\le C\left(\|\tilde{h}\|_{L^2X'} + \|l\|_{L^2L^2(\Xi)} + \|w_0 - g(0)\|_{L^2}\right) \\ &\le C\left(\|h\|_{L^2X'} + \|l\|_{L^2L^2(\Xi)} + \|g\|_{L^2W_2^1(\Omega)} + \|g'\|_{L^2W_2^1(\Omega)'} + \|w_0\|_{L^2} + \|g(0)\|_{L^2}\right).\end{aligned}$$

Since $\|g(0)\|_{L^2} \le C\left(\|g\|_{L^2W_2^1(\Omega)} + \|g'\|_{L^2W_2^1(\Omega)'}\right)$ (see [101, p. 446-447]) we obtain the desired result for $\|w\|_{L^2W_2^1(\Omega)}$. The estimates of $\|w'\|_{L^2X'}$ and $\max_{0\le t\le T} \|w(t)\|_{L^2}$ can be derived similarly.

□

3.5.4 Existence and uniqueness for the nonlinear problem

The nonlinear system (3.12) is solved by an appropriate fixed point argument. Define the Banach space $Y := L^2(0,T;L^2(\Omega))\times L^2(0,T;L^2(\Xi))\times L^2(0,T;L^2(\Xi))$ with norm $\|(h,s,\varphi)\|_Y := \|h\|_{L^2L^2(\Omega)} + \|s\|_{L^2L^2(\Xi)} + \|\varphi\|_{L^2L^2(\Xi)}$ and consider the operator

$$K: \begin{array}{ccc} Y & \to & Y \\ (h,s,\varphi) & \mapsto & (w, w_{|\Xi}, \psi) \end{array}$$

which maps (h,s) onto the unique weak solution $(w, w_{|\Xi})$ of the linear system

$$\begin{cases} \partial_t w_i + L_i w_i = f_i(h,x,t) & \text{in } \Omega_T\,,\ i=1,...,m \\ -\sum\limits_{l,j=1}^{n} a_i^{lj} w_{ix_l} n^j = k_i(s,\varphi,x,t) & \text{on } \Xi_T\,,\ i=1,...,m \\ w = g & \text{on } \Lambda_T \\ w(.\,,0) = w_0 & \text{in } \Omega\,. \end{cases} \tag{3.34}$$

φ shall be mapped onto the unique solution ψ of the corresponding system of integral equations

$$\psi(.\,,t) = \psi_0(.) + \int_0^t q(w,\psi,.\,,\tau)d\tau\,. \tag{3.35}$$

By definition, a fixed point of K is a weak solution of (3.12). K has the following properties:

Lemma 3.5.2. *The operator K is well-defined. Furthermore, K is compact.*

Proof. 1. Using Corollary 3.5.1, the assumptions (3.13), (3.14), and (3.15) yield the existence of a unique weak solution $w \in L^2(0,T;W_2^1(\Omega)) \cap W_2^1(0,T;X')$ of the linear problem (3.34). Furthermore, this solution satisfies

$$\begin{aligned} &\max_{0\le t\le T} \|w(t)\|_{L^2} + \|w\|_{L^2W_2^1(\Omega)} + \|w'\|_{L^2X'} \\ &\quad \le C\left(\|f^h\|_{L^2X'} + \|k^{s,\varphi}\|_{L^2L^2(\Xi)} + \|g\|_{L^2W_2^1(\Omega)} + \|g'\|_{L^2W_2^1(\Omega)'} + \|w_0\|_{L^2}\right), \end{aligned} \tag{3.36}$$

where $f^h := f(h(.\,,.),.\,,.)$ and $k^{s,\varphi} := k(s(.\,,.),\varphi(.\,,.),.\,,.)$. Since q is Lipschitz continuous, repeated application of Banach's theorem on the operator

$$S:\ L^2(0,\tilde T;L^2(\Xi)) \to L^2(0,\tilde T;L^2(\Xi))\,,\quad S\varphi := \left[t \mapsto \psi(.\,,t) := \psi_0(.) + \int_0^t q(w,\varphi,.\,,\tau)d\tau\right]$$

for small enough $\tilde T$ shows unique solvability of (3.35). Hence, K is well-defined.

2. To demonstrate continuity, let $(h_n,s_n,\varphi_n) \to (h,s,\varphi)$ in Y as $n\to\infty$. Choose an arbitrary subsequence $n_k \to \infty$. We can then extract a sub-subsequence (termed n_k again), such that for almost every (x,t): $h_{n_k} \to h$, $s_{n_k} \to s$, $\varphi_{n_k} \to \varphi$. According to continuity

$$f^{h_{n_k}} \to f^h\,,\quad k^{s_{n_k},\varphi_{n_k}} \to k^{s,\varphi}\,.$$

This—together with the above growth conditions—allows application of Lebesgue's theorem, which then provides convergence in $L^2(\Omega_T)$ and $L^2(\Xi_T)$, respectively. By the use of (3.36) we obtain

$$\|w_{n_k} - w\|_{L^2W_2^1(\Omega)} \leq C \left(\|f^{h_{n_k}} - f^h\|_{L^2L^2(\Omega)} + \|k^{s_{n_k},\varphi_{n_k}} - k^{s,\varphi}\|_{L^2L^2(\Xi)} \right) \to 0. \tag{3.37}$$

It remains to be shown that $\psi_{n_k} \to \psi$ in $L^2(\Xi_T)$. Once more, using Lipschitz continuity of q,

$$|\psi_{n_k}(x,t) - \psi(x,t)| \leq C \left(\int_0^t |w_{n_k}(x,\tau) - w(x,\tau)| d\tau + \int_0^t |\psi_{n_k}(x,\tau) - \psi(x,\tau)| d\tau \right).$$

We take the square, apply Hölder's inequality, and integrate with respect to x

$$\|\psi_{n_k}(t) - \psi(t)\|^2_{L^2(\Xi)} \leq C \left(\|w_{n_k} - w\|^2_{L^2L^2(\Xi)} + \int_0^t \|\psi_{n_k}(\tau) - \psi(\tau)\|^2_{L^2(\Xi)} d\tau \right).$$

Gronwall's inequality (see [21, p. 624]) provides

$$\int_0^t \|\psi_{n_k}(\tau) - \psi(\tau)\|^2_{L^2(\Xi)} d\tau \leq CTe^{CT} \|w_{n_k} - w\|^2_{L^2L^2(\Xi)},$$

and hence, due to (3.37),

$$\|\psi_{n_k} - \psi\|_{L^2L^2(\Xi)} \leq C \|w_{n_k} - w\|_{L^2L^2(\Xi)} \to 0. \tag{3.38}$$

3. In order to show compactness, let $(h_n, s_n, \varphi_n)_{n=1}^\infty$ be a bounded sequence in Y. First, we prove that the corresponding sequence $(w_n)_{n=1}^\infty$ is relative compact in $L^2(0,T;W_2^{3/4}(\Omega))$ and hence in $L^2(0,T;L^2(\Omega))$: According to the estimate (3.36) and with the growth conditions (3.15), the corresponding sequence $(w_n)_{n=1}^\infty$ is bounded in $L^2(0,T;W_2^1(\Omega))$ as well as in $W_2^1(0,T;X')$. The embedding

$$W_2^1(0,T;X') \cap L^2(0,T;W_2^1(\Omega)) \hookrightarrow L^2(0,T;W_2^{3/4}(\Omega))$$

is compact (Lions–Aubin). Thus, we can extract a subsequence $(w_{n_k})_{k=1}^\infty$ that converges in $L^2(0,T;W_2^{3/4}(\Omega))$.

Since the trace operator is continuous, the sequence $(w_{n_k|\Xi})_{k=1}^\infty$ converges in $L^2(0,T;L^2(\Xi))$. Furthermore, by the use of (3.38) we obtain for $k_1, k_2 \to \infty$

$$\|\psi_{n_{k_1}} - \psi_{n_{k_2}}\|_{L^2L^2(\Xi)} \leq C \|w_{n_{k_1}} - w_{n_{k_2}}\|_{L^2L^2(\Xi)} \to 0,$$

which shows that $(\psi_{n_k})_{k=1}^\infty$ is a Cauchy-Sequence in $L^2(0,T;L^2(\Xi))$. This completes the proof. □

Lemma 3.5.2 allows application of Schauder's fixed point theorem, which yields the existence of a weak solution of (3.12).

Theorem 3.5.2 (Existence of weak solutions)**.** *Provided that the constants $\Theta_1^{(2)}$, $\Theta_2^{(2)}$, and $\Theta_2^{(3)}$ are small enough (dependent on Ω, T, L_i, and the remaining constants $\Theta_j^{(k)}$), there exists at least one weak solution (w, ψ) of* (3.12)*.*

Proof. We want to apply Schauder's fixed point theorem. Since the operator K is compact, it is enough to prove the existence of a closed Ball $\overline{B}_R(0) \subset Y$, such that $K : \overline{B}_R(0) \to \overline{B}_R(0)$. First, we calculate using (3.16)

$$|\psi(x,t)| \leq |\psi_0(x)| + C \int_0^t \left(|w(x,\tau)| + |\psi(x,\tau)| + |q(0,0,x,\tau)|\right) d\tau \,.$$

We take the square, use Hölder's inequality, integrate with respect to x, and apply (3.14)

$$\|\psi(t)\|^2_{L^2(\Xi)} \leq C \left(1 + \|\psi_0\|^2_{L^2(\Xi)} + \|w\|^2_{L^2 W^1_2(\Omega)} + \int_0^t \|\psi(\tau)\|^2_{L^2(\Xi)} d\tau\right).$$

Application of Gronwall's inequality (in integral form; see [21, p. 625]) yields

$$\|\psi(t)\|^2_{L^2(\Xi)} \leq C \left(1 + CTe^{CT}\right) \left(1 + \|\psi_0\|^2_{L^2(\Xi)} + \|w\|^2_{L^2 W^1_2(\Omega)}\right). \tag{3.39}$$

$K(h,s,\varphi)$ can now be estimated as follows, using (3.36), (3.39), and (3.15):

$$\begin{aligned}
\|K(h,s,\varphi)\|_Y &\leq C \left(\|w\|_{L^2 H^1(\Omega)} + \|\psi\|_{L^2 L^2(\Xi)}\right) \\
&\leq C\Big(\|f^h\|_{L^2 L^2(\Omega)} + \|k^{s,\varphi}\|_{L^2 L^2(\Xi)} + \|g\|_{L^2 H^1(\Omega)} + \|g'\|_{L^2 H^1(\Omega)'} \\
&\qquad + \|w_0\|_{L^2(\Omega)} + \|\psi_0\|_{L^2(\Xi)} + 1\Big) \\
&\leq C \left(1 + D + \Theta_1^{(2)} \|h\|_{L^2 L^2(\Omega)} + \Theta_2^{(2)} \|s\|_{L^2 L^2(\Xi)} + \Theta_2^{(3)} \|\varphi\|_{L^2 L^2(\Xi)}\right) \\
&=: \alpha + \beta \|h\|_{L^2 L^2(\Omega)} + \gamma \|s\|_{L^2 L^2(\Xi)} + \delta \|\varphi\|_{L^2 L^2(\Xi)} \,,
\end{aligned} \tag{3.40}$$

where $C = C(\Omega, T, L, \Theta_k^{(1)}, \Theta_3^{(2)})$, $D := \|g\|_{L^2 W^1_2(\Omega)} + \|g'\|_{L^2 W^1_2(\Omega)'} + \|w_0\|_{L^2(\Omega)} + \|\psi_0\|_{L^2(\Xi)}$ and $\alpha := C(1+D)$, $\beta := C\Theta_1^{(2)}$, $\gamma := C\Theta_2^{(2)}$, $\delta := C\Theta_2^{(3)}$.

We want the right hand side of (3.40) to be smaller than R, which requires conditions on the constants $\Theta_1^{(2)}$, $\Theta_2^{(2)}$, and $\Theta_2^{(3)}$. Observe that $\|(h,s,\varphi)\|_Y \leq R$ implies $\|h\|_{L^2 L^2(\Omega)} \leq R - \|s\|_{L^2 L^2(\Xi)} - \|\varphi\|_{L^2 L^2(\Xi)}$, and hence

$$\|K(h,s,\varphi)\|_Y \leq \alpha + \beta R + (\gamma - \beta)\|s\|_{L^2 L^2(\Xi)} + (\delta - \beta)\|\varphi\|_{L^2 L^2(\Xi)}$$

due to (3.40). We assume that $\beta < 1$, $\gamma < 1$, and $\delta < 1$. We distinguish the following cases:

1. If $\beta \geq \gamma$ and $\beta \geq \delta$ let $R := \frac{\alpha}{1-\beta}$.
2. If $\beta < \gamma$ and $\beta \geq \delta$ let $R := \frac{\alpha}{1-\gamma}$.
3. If $\beta \geq \gamma$ and $\beta < \delta$ let $R := \frac{\alpha}{1-\delta}$.

In the remaining case, $\beta < \gamma$ and $\beta < \delta$, we observe that $\|s\|_{L^2 L^2(\Xi)} \leq R - \|h\|_{L^2 L^2(\Omega)} - \|\varphi\|_{L^2 L^2(\Xi)}$, and hence

$$\|K(h,s,\varphi)\|_Y \leq \alpha + \gamma R + (\beta - \gamma)\|h\|_{L^2 L^2(\Omega)} + (\delta - \gamma)\|\varphi\|_{L^2 L^2(\Xi)} \,.$$

Thus, we can choose $R := \frac{\alpha}{1-\delta}$. In all cases, K maps $\overline{B}_R(0)$ onto itself. Hence, the existence of a weak solution of (3.12) follows from Schauder's theorem. □

However, Schauder does not guarantee uniqueness. This requires some tighter conditions.

Remark 3.5.1. *If f and k are even Lipschitz continuous, i.e., $\forall h, \tilde{h}, s, \tilde{s} \in \mathbb{R}^m$, $\forall \varphi, \tilde{\varphi} \in \mathbb{R}^r$*

$$\begin{aligned} |f(h,x,t) - f(\tilde{h},x,t)| &\leq \Theta_1 |h - \tilde{h}| \\ |k(s,\varphi,x,t) - k(\tilde{s},\tilde{\varphi},x,t)| &\leq \Theta_2^{(1)} |s - \tilde{s}| + \Theta_2^{(2)} |\varphi - \tilde{\varphi}| \,, \end{aligned} \tag{3.41}$$

and provided that $\Theta_2^{(1)}$ is small enough, then a weak solution of (3.12) is unique, too.

In contrast to Theorem 3.5.2, no smallness of the growth constants of f is needed.

Proof. 1. To demonstrate uniqueness, suppose (w, ψ) and $(\tilde{w}, \tilde{\psi})$ are two weak solutions of (3.12). Due to (3.36), (3.41), and (3.16)

$$\begin{aligned} &\max_{0\leq\tau\leq t} \|w(\tau) - \tilde{w}(\tau)\|_{L^2(\Omega)} + \|w_{|\Xi} - \tilde{w}_{|\Xi}\|_{L^2(0,t;L^2(\Xi))} + \max_{0\leq\tau\leq t} \|\psi(\tau) - \tilde{\psi}(\tau)\|_{L^2(\Xi)} \\ &\quad \leq C \left(\|w - \tilde{w}\|_{L^2(0,t;L^2(\Omega))} + \Theta_2^{(1)} \|w_{|\Xi} - \tilde{w}_{|\Xi}\|_{L^2(0,t;L^2(\Xi))} + \|\psi - \tilde{\psi}\|_{L^2(0,t;L^2(\Xi))} \right). \end{aligned}$$

If $\Theta_2^{(1)} C < 1$, then Gronwall's inequality yields $w \equiv \tilde{w}$ and $\psi \equiv \tilde{\psi}$.

2. Existence is obtained by consideration of $Y := C^0([0,T_1], L^2(\Omega)) \times L^2(0,T_1; L^2(\Xi)) \times C^0([0,T_1], L^2(\Xi))$ with norm $\|(h,s,\varphi)\|_Y := \|h\|_{C^0L^2(\Omega)} + \|s\|_{L^2L^2(\Xi)} + \|\varphi\|_{C^0L^2(\Xi)}$ and repeated application of Banach's theorem on

$$K: \begin{array}{ccc} Y & \to & Y \\ (h,s,\varphi) & \mapsto & (w, w_{|\Xi}, \psi) \end{array}$$

for small enough T_1, where $(w, w_{|\Xi})$ denotes the weak solution of (3.34) and φ is mapped onto $\psi(.\,,t) := \psi_0(.) + \int_0^t q(w,\varphi,.\,,\tau) d\tau$. □

3.5.5 Positivity of solutions

To demonstrate positivity, we restrict ourselves to the special case of the FD-model—slightly generalized by a nonnegative right hand side. Furthermore, the original Neumann outflow condition is imposed on w.

Theorem 3.5.3. *Let w be solution of (3.2) and (3.4) (with right hand side $h(w,x,t) \geq 0$ in the species equation in (3.2)). Suppose that $u \in C^1$ and that w_0, w_D, $\lambda^{(i)}$, and $\kappa^{(i)}$ are continuous. Furthermore, let $D \equiv$ const. and let Ω fulfill the interior ball condition in each point of Ξ (specified in [21, p. 330]), where $\Xi := \Gamma \cup \Sigma \cup O$. Assume that*

$$w \in C_1^2(\Omega_T) \cap C^1\big((\Omega \cup \Xi)_T\big) \cap C^0\big(\overline{\Omega_T}\big)$$

and set

$$\alpha := \frac{\lambda - \kappa}{\Psi}\,, \quad \lambda := \lambda^{(1)} + \lambda^{(2)} s\,, \quad \kappa := \kappa^{(1)} + \kappa^{(2)} s\,.$$

If w_0, w_D are nonnegative and $\lambda \geq \alpha\psi_0$, then w also stays nonnegative.

Proof. 1. Let w attain its minimum in $(x_0, t_0) \in \overline{\Omega_T}$. Assume $w(x_0, t_0) < 0$. The maximum principle ([21, p. 368]) together with nonnegativity of initial and boundary data implies $x_0 \in \Xi$. An extension of the elliptic Hopf's Lemma ([21, p. 330]) to the parabolic situation then yields $\partial_n w(x_0, t_0) < 0$, which implies $x_0 \in \Gamma$. There we have $-D\partial_n w(x_0, t_0) = \big(k(\psi, s)w\big)(x_0, t_0)$, so that it suffices to show $\xi := k(\psi, s)(x_0, t_0) \geq 0$ to obtain a contradiction.

2. Since ψ is the unique solution of $\partial_t \psi = k(\psi, s)w,\ \psi(t = 0) = \psi_0$, it permits the representation

$$\psi(t) = \lambda \int_0^t w(\tau) \exp\left(-\alpha \int_\tau^t w(s)ds\right) d\tau + \psi_0 \exp\left(-\alpha \int_0^t w(s)ds\right). \tag{3.42}$$

Observe that $\xi = -\alpha\psi(x_0, t_0) + \lambda$. We insert (3.42) and obtain

$$\begin{aligned}
\xi &= \lambda \left(1 - \alpha \int_0^{t_0} w(\tau) \exp\left(-\alpha \int_\tau^{t_0} w(s)ds\right) d\tau\right) - \alpha\psi_0 \exp\left(-\alpha \int_0^{t_0} w(s)ds\right) \\
&= \lambda \left(1 - \int_0^{t_0} \frac{d}{d\tau} \exp\left(\alpha \int_{t_0}^{\tau} w(s)ds\right) d\tau\right) - \alpha\psi_0 \exp\left(-\alpha \int_0^{t_0} w(s)ds\right) \\
&= \lambda \left(1 - \left(\exp(0) - \exp\left(-\alpha \int_0^{t_0} w(s)ds\right)\right)\right) - \alpha\psi_0 \exp\left(-\alpha \int_0^{t_0} w(s)ds\right).
\end{aligned}$$

Hence, $\lambda \geq \alpha\psi_0$ implies $\xi \geq 0$. □

4 The free boundary problem

Chapter 3 showed that the above proposed continuous, particle conservation-based FD-model cannot reproduce experimentally observed spatial platelet distribution without consideration of shear stress. Thus, there is a strong coupling between flow and platelet deposition, since the growth of platelet aggregates not only changes the flow field and hence the transport processes at the surface, but it also alters the shear stress. Indeed, in stagnation point flow, the development of thrombi was identified as the most likely cause for the remaining discrepancies between experimental data and the predictions of the FD-model (see page 19). Therefore, the present chapter derives a free boundary problem of long-term thrombus growth. Numerical simulations in stagnation point flow and in the tubular expansion are carried out by the level set method. Comparison of the so obtained results with the experimental data further confirms the importance of shear stress in the process of platelet deposition.

4.1 Model development

Figure 4.1 sketches the situation that arises when thrombus growth is taken into account. In that case, the reactive boundary Γ separating flow and platelet aggregates evolves in time: $\Gamma = \Gamma_t$.

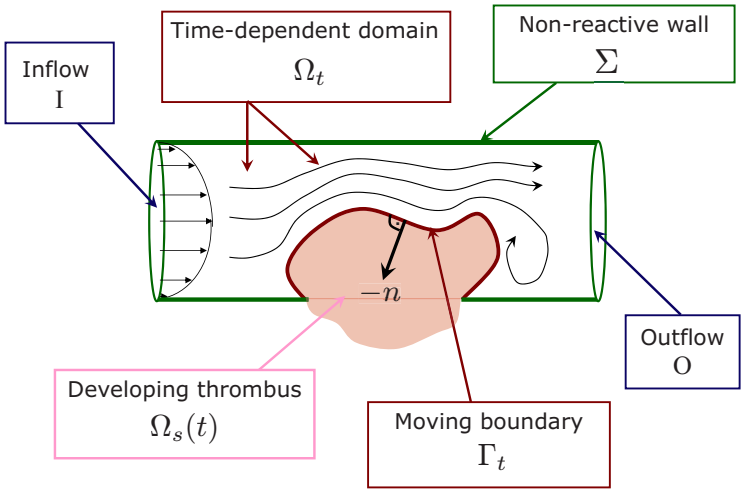

Figure 4.1: The time-dependent domain

The evolution of Γ_t depends on the flux of platelets $J := -D\nabla w$ attaching to the thrombus. We denote the velocity of this free boundary by v. To derive an equation for v, we consider its

Taylor expansion in platelet flux up to first order: $v(J) = v(0) + v'(0)J + O(|J|^2)$. Clearly, $v(0) = 0$. We assume v to be antiparallel to J. This implies that $v'(0)$ is a diagonal matrix, that is $v'(0) = -\mathrm{diag}(\alpha)$ with an appropriate constant $\alpha > 0$. Hence, in the first approximation v fulfills

$$v = \alpha D \nabla w \,.$$

Since this chapter focuses on the long-term, growth-induced flow disturbances, changes in surface reactivity due to saturation of the original surface with bound platelets are not considered here. Instead, at the beginning of the calculations, the original surface is assumed to be completely covered by a layer of bound platelets.

As in the FD-model, the flow field is based on the NSE and conservation of particles is assumed for the platelets. At the moving interface, the flow velocity u equals the velocity v of Γ_t: $u = v$. However, switching to non-dimensional quantities as in (3.5) yields $\tilde{u} = \tilde{v}V/U$, where U and V denote characteristic velocities of fluid and interface, respectively. Since $U \gg V$ holds in all considered experiments, this model assumes zero flow velocity along the interface. In vivo, the prerequisite $U \gg V$ is fulfilled, for example, in the arterial circulation (see, e.g., [48]).

We define $\tilde{\alpha} := \alpha DW/(VL)$ and $\tilde{k}(\tilde{s}) := \kappa_1 + \kappa_2 \tilde{s}$, with the parameters κ_1 and κ_2 of equation (3.7). Furthermore, we set $I_T := I \times (0,T]\,, \quad O_T := O \times (0,T]\,,$

$$\Sigma_T := \Sigma \times (0,T]\,, \qquad \Gamma_T := \bigcup_{0<t\le T} \Gamma_t \times \{t\}\,, \qquad \Omega_T := \bigcup_{0<t\le T} \Omega_t \times \{t\}\,. \tag{4.1}$$

Let $n = n_t$ denote the inward unit normal to $\partial\Omega_t$. For the sake of brevity, ν is written instead of Re^{-1}, D is used instead of Pe^{-1}, and the tilde is omitted. In cartesian coordinates, the free boundary model reads

$$\begin{cases} \partial_t u - \nu\Delta u + (u\cdot\nabla)u + \nabla p = f & \text{in } \Omega_T \\ \nabla \cdot u = 0 & \text{in } \Omega_T \\ u = 0 & \text{on } \Gamma_T \cup \Sigma_T \\ u = u_D/U & \text{on } I_T \\ \nu\partial_n u = p\cdot n & \text{on } O_T \\ u(t=0) = u_0/U & \text{in } \Omega_0\,, \end{cases} \tag{4.2}$$

$$\begin{cases} \partial_t w - D\Delta w + (u\cdot\nabla)w = 0 & \text{in } \Omega_T \\ D\partial_n w = kw & \text{on } \Gamma_T \\ \partial_n w = 0 & \text{on } \Sigma_T \cup O_T \\ w = w_D/W & \text{on } I_T \\ w(t=0) = w_0/W & \text{in } \Omega_0 \\ v = \alpha\nabla w & \text{on } \Gamma_T\,. \end{cases} \tag{4.3}$$

4.2 The level set method and its implementation

An apparent strategy to treat the moving boundary problem (4.2)-(4.3) would be to discretize the initial interface Γ_0 by finitely many, connected points $x_i^0 \;\; (i = 1, ..., N)$ and then to move these marker points according to the system of ordinary differential equations

$$\frac{dx_i}{dt} = v(x_i)\,, \qquad x_i(0) = x_i^0 \qquad (i = 1, ..., N)\,.$$

This front-tracking approach has been employed to solve numerous problems, such as multiphase flows [87] and dendritic solidification [44]. However, the explicit tracking of the interface and the identification of the phase to which a point belongs to is quite complex. This requires notable technical efforts, particularly in 3D, where the connectivity of the interface is not as apparent as in 2D, and in cases when topological changes occur.

Compared to front-tracking, the level set method described in [64] provides a convenient alternative, which allows to perform all calculations on a fixed configuration $\Omega^* \supset \Omega_0$ using a fixed mesh. Furthermore, this approach has been successfully applied to the solution of the classical two-phase Stefan problem and to dendritic solidification [16], to the classical single-phase Stefan problem [40], as well as to two-phase flows [85]. It avoids complicated interface-tracking and is even able to easily handle changes in topology. The idea behind the level set method is that the moving wall Γ_t can be represented implicitly as the zero level set of a function ϕ, whose sign can serve to distinguish the "phases" fluid domain $\Omega_f(t) := \Omega_t$ and emerging thrombus $\Omega_s(t)$. To be more specific, the different parts of the domain are constituted by

$$\Omega_f(t) = \{x \in \Omega^* : \phi(x,t) > 0\}, \quad \Gamma_t = \{x \in \Omega^* : \phi(x,t) = 0\}, \quad \Omega_s(t) = \{x \in \Omega^* : \phi(x,t) < 0\},$$

and $\Omega^* = \Omega_f(t) \cup \Gamma_t \cup \Omega_s(t)$. From the definition of ϕ it follows that the transport equation

$$\partial_t \phi + v\nabla\phi = \partial_t \phi + \alpha k D^{-1} w |\nabla\phi| = 0 \tag{4.4}$$

has to be fulfilled along the moving interface. The second equation provides a continuous extension of v to the whole domain Ω^*, which is used in the numerical calculations.

At time $t = 0$, the level set function is initialized as signed distance function (SDF), that is

$$\phi(x,0) := \begin{cases} \;\;\mathrm{dist}(x,\Gamma_0) & x \in \Omega_0 \cup \Gamma_0 \\ -\mathrm{dist}(x,\Gamma_0) & x \in \Omega_s(0)\,. \end{cases}$$

The use of SDF is advantageous compared to the normal distance function for two reasons: First, the SDF facilitates the identification of the phase to which a point belongs to. Second, the SDF is monotone over the interface, whereas the gradient of the normal distance function has jump. Thus, the approximation of $\nabla\phi$ is numerically more stable when ϕ is a SDF.

To realize vanishing fluid velocities along the a priori unknown interface Γ_t, the term

$$\int_{\Gamma_t} (-\nu\partial_n u + pn)\psi \, dS$$

that arises upon multiplication of the NSE with a test function ψ followed by partial integration is replaced by

$$\beta(h) \int_{\Gamma_t} u\psi \, dS \,,$$

where β depends on the local cell size h such that $\beta(h) \to \infty$ as $h \to 0$. This strategy to approximate solutions corresponding to prescribed Dirichlet data by switching to appropriate natural boundary conditions was proposed by Babuska [3] to solve the Dirichlet problem. Regarding the Dirichlet problem, this method yields an approximation of order $3/4 - \epsilon$ ($\epsilon > 0$) with respect to the W_2^1-norm, provided that the exact solution of the Dirichlet problem is in $W_2^2(\Omega)$ (see also [62]).

Next, the flow field is appropriately extended to the solid region Ω_s: The flow velocity shall fulfill $u = 0$ in Ω_s, which yields an additional term $\int_{\Omega_s} u\psi \, \mathrm{dx}$. A homogeneous Dirichlet condition is prescribed on u along $\partial\Omega_s(t) \setminus \Gamma_t$ and a harmonic extension into the solid is used for the pressure. Volume and surface integrals are represented by the use of ϕ as

$$\int_{\Omega_f} g \, dx = \int_{\Omega^*} gH(\phi) dx \,, \qquad \int_{\Omega_s} g \, dx = \int_{\Omega^*} g(1 - H(\phi)) dx \,, \qquad \int_{\Gamma_t} g \, dS = \int_{\Omega^*} g\delta(\phi) \, dx \,,$$

where δ denotes the delta function and H denotes the Heavyside function

$$H(\phi) := \begin{cases} 1 & \phi \geq 0 \\ 0 & \phi < 0 \,. \end{cases}$$

Furthermore, the tangent and the normal vectors to Γ_t needed to determine the shear stress are also readily available from ϕ:

$$n = \frac{\nabla\phi}{|\nabla\phi|} \,, \qquad \tau = \begin{pmatrix} -n_2 \\ n_1 \end{pmatrix} .$$

H and δ are approximated by the smeared out functions

$$\begin{aligned} H_{kh}(\phi) &:= \begin{cases} 0 & \phi < -kh \\ \frac{1}{2} + \frac{\phi}{2kh} + \frac{1}{2\pi} \sin\left(\frac{\pi\phi}{kh}\right) & -kh \leq \phi \leq kh \\ 1 & kh < \phi \,, \end{cases} \\ \delta_{kh}(\phi) &:= \begin{cases} 0 & \phi < -kh \\ \frac{1}{2kh} + \frac{1}{2kh} \cos\left(\frac{\pi\phi}{kh}\right) & -kh \leq \phi \leq kh \\ 0 & \phi > kh \,, \end{cases} \end{aligned} \tag{4.5}$$

where $k > 0$ is fixed. This yields an approximation of first order (see [64, p. 15]) and hence provides an accuracy which is comparable to that of Babuska's method. The choice $k = 1/2$, together with an adaptive quadrature rule increasing the accuracy around the interface, turned out to be best working. The mesh was adaptively refined, dependent on the distance to the interface. Coarsening of cells was omitted in the stagnation point, since calculation of the pressure was observed to be more stable in that case.

All equations were solved simultaneously. The numerical methods were the same as for the fixed domain model: Spatial discretization was achieved with bilinear finite elements on a

quadrilateral mesh, together with a local projection stabilization of transport and pressure. GMRES with multigrid as preconditioner was used to solve the linear systems. Time-stepping was done with Crank-Nicolson. However, in contrast to the the fixed domain model, some implicit Euler steps to damp high frequency error components were used not only at the beginning of the calculation, but also repeated times throughout the simulation. Furthermore, an adaptive time-step size was used. The adjustment of the step size was based on a heuristic criterion: If the number of Newton steps needed to decrease the nonlinear residual below a prescribed tolerance exceeded a certain value, say 7 or 10, then the step size was halved. In contrast, if only few steps were needed, say one or two, then the step size was doubled.

4.3 Numerical results

This section presents the results of the numerical simulation of the free boundary problem (4.2)-(4.3) (transformed to cylindrical coordinates) by the level set method, as obtained in stagnation point flow and in the tubular expansion. All pictures were made with the visualization toolkit VisuSimple [11].

The figures 4.2, 4.3, and 4.4 on page 45-47 show the location of the interface (black line) separating thrombus and fluid in stagnation point flow, as well as the radial component of the flow velocity (color). The results at different points in time are presented, as obtained on various meshes having different levels of refinement. Platelet adhesion is assumed shear-dependent. In the beginning of the calculation, the interface is parallel to the lower boundary of the domain, in a distance of approximately one coarse cell (Figure 4.2(a), 4.3(a), and 4.4(a)). After, respectively, 190 and 215 time units a platelet aggregate has formed downstream of the stagnation point (the interface has moved upwards there), at a location of elevated shear stress (Figure 4.2(b), 4.2(c), 4.3(b), and 4.4(b); Figure 4.3(c) and 4.4(c)). This is in good accordance with the data of Affeld et al. [1] and with the predictions of the FD-model assuming shear-dependent platelet adhesion (see Section 3.3.1). Comparison of the relatively rough shape of the thrombus in Figure 4.2(b) with the smooth ones in Figure 4.3(b) and Figure 4.4(b) reveals the necessity of a certain mesh refinement to accurately resolve the interface. However, once a certain level of refinement is reached, almost no difference is observed neither in the location of the interface nor in the flow velocity (Figure 4.3(b) and 4.4(b); Figure 4.3(c) and 4.4(c)).

In addition, the figures 4.2, 4.3, and 4.4 report an increase in radial flow velocity $\tilde{u}_r$ due to the narrowing of the vessel associated with thrombus growth. Since the latter is located downstream of the stagnation point, the axial component $\tilde{u}_z$ of the velocity, which possesses only non-positive values at the beginning of the simulation (the flow is directed downwards), becomes positive once the fluid has to flow around the developing platelet aggregate. This increase in axial velocity is also confirmed by the presented results.

Figure 4.5 on page 48 shows how thrombus growth affects the radial component of the velocity and the pressure in stagnation point flow. The increase of the velocities' maximum is evident, as well as the emerging bump in the velocity field a little downstream of the stagnation point, which corresponds to vanishing flow velocities inside the evolving thrombus. Figure 4.6 on page 49 shows the flowfield in the vicinity of the thrombus (Figure 4.6(a)) and a magnification of

the flow around the thrombus' tip (Figure 4.6(b)). Both of these pictures confirm that the flow field adjusts instantaneously to the growth of the platelet aggregate and that the streamlines pass well around the obstacle. In addition, both Figure 4.5 and Figure 4.6 prove that the flow velocity drops to zero inside the thrombus after a bandwith of approximately one grid cell. Actually, this guarantee of flow coming to rest within a sharp layer around the interface is crucial to ensure an accurate approximation of the free boundary problem (4.2)-(4.3) by the level set method. Furthermore, it confirms the efficiency of the above described strategy to impose zero flow velocities along the interface and inside the thrombus.

Figure 4.7 on page 50 shows the results obtained in stagnation point flow, when platelet adhesion is assumed independent of shear stress. In that case, it is unnecessary to precisely evaluate the stress tensor (and hence the derivatives of the velocity field) along the moving boundary. For this reason, accurate results could already be obtained on grids that were noticeably coarser than those employed in the shear-dependent case. Again, the calculation starts with the interface being located parallel to the lower boundary of the domain, in a distance of approximately one coarse cell (Figure 4.7(a)). As in the shear-dependent case, the radial velocity component increases in time, due to the narrowing of the vessel. However, in contrast to shear-dependent platelet adhesion, the maximum thrombotic mass forms directly at the stagnation point and the axial velocity component therefore stays non-positive. The location of the interface after 190 time units is shown in Figure 4.7(b) and 4.7(c). Thus, the behavior of the shear-independent free boundary problem is similar to the behavior of the shear-independent FD-model (see Section 3.3.1). Both of these models show absolutely no agreement with the experimental data reported by Affeld et al. [1].

Figure 4.8 and 4.9 on page 51 and 52 display the location of the interface separating thrombus and fluid in the tubular expansion. The results obtained at different points in time by the use of various meshes having a different level of refinement are shown. Figure 4.8 is the shear-dependent case. Compared to the simulation of the stagnation point, satisfying results were already available on coarser grids. However, in the tubular expansion geometry the so achieved saving of computational time was consumed by an observed necessity of choosing smaller time-steps in order to decrease the nonlinear residual below a prescribed tolerance, which was handled by the above described adaptive time-stepping strategy. Like the FD-model assuming shear-dependent platelet adhesion (Section 3.3.2), the shear-dependent free boundary problem predicts minimal platelet deposition at the reattachement point and maximal deposition in the vortex area, which is in good accordance with the data of Karino and Goldsmith [45]. In contrast to that, when shear stress is neglected, the maximal deposition is found at the reattachement point (Figure 4.9), which is similar to the behavior of the corresponding FD-model and completely contradicts the experimental observations.

In summing up, it should first be noted that the above presented strategies to approximate the free boundary problem (4.2)-(4.3) by the level set method have proven successful, since they were capable to satisfyingly handle the full coupling of flow and thrombus growth. Furthermore, similar to the observations made in Chapter 3 for the FD-model, the predictions of the free boundary problem turned out to be incompatible with the experimental data when shear stress was neglected, whereas consideration of shear stress in the above proposed way led to good agreement with the experimental evidence.

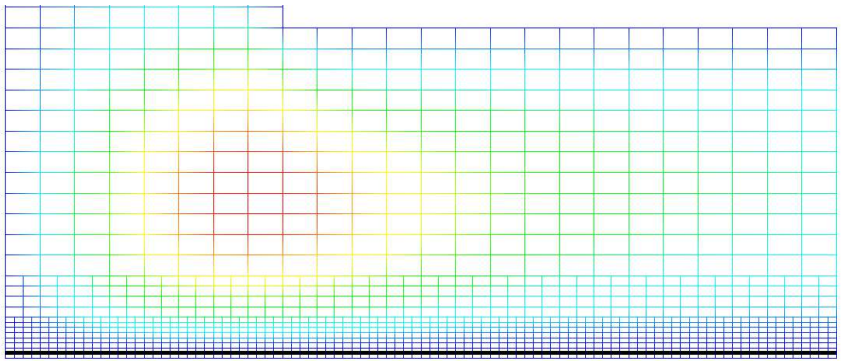

(a) Location of the interface at $\tilde{t} = 0$; cell size: $h_{\max} = 12.5 \times 10^{-2}$, $h_{\min} = 3.125 \times 10^{-2}$; #cells = 1,376, #nodes = 1,513; $\max \tilde{u}_r = 0.310$, $\max \tilde{u}_z = 0$

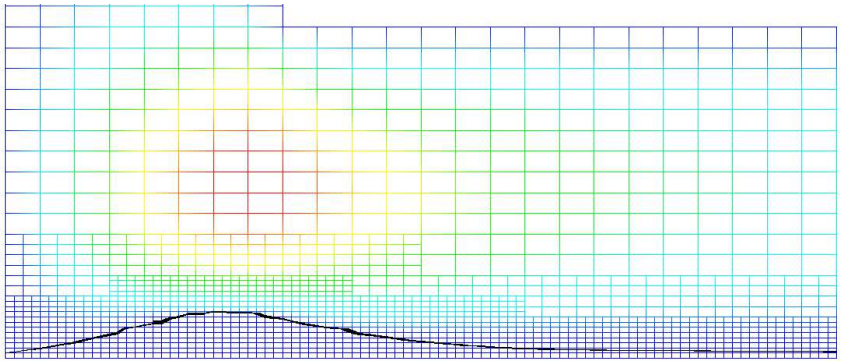

(b) Location of the interface at $\tilde{t} = 190$; cell size: $h_{\max} = 12.5 \times 10^{-2}$, $h_{\min} = 3.125 \times 10^{-2}$; #cells = 1,712, #nodes = 1,855; $\max \tilde{u}_r = 0.339$, $\max \tilde{u}_z = 0.008$

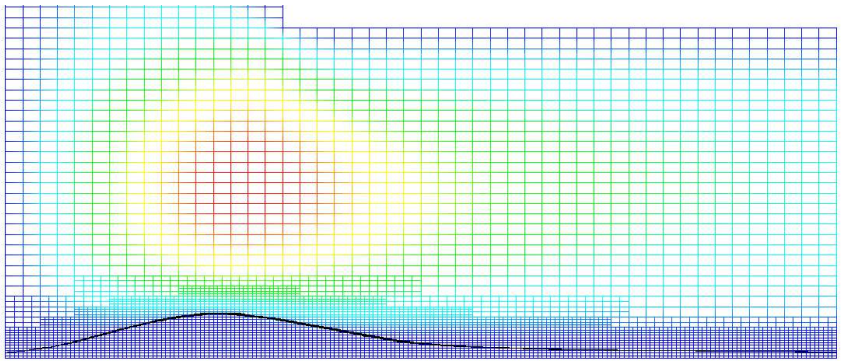

(c) Location of the interface at $\tilde{t} = 190$; cell size: $h_{\max} = 6.25 \times 10^{-2}$, $h_{\min} = 1.5625 \times 10^{-2}$; #cells = 6,128, #nodes = 6,413; $\max \tilde{u}_r = 0.336$, $\max \tilde{u}_z = 0.007$

Figure 4.2: Stagnation point flow with shear-dependent platelet adhesion calculated on a coarse grid (*top and middle*) and on a once refined grid (*bottom*). Red color indicates elevated radial velocity, whereas dark blue color denotes vanishing radial velocity.

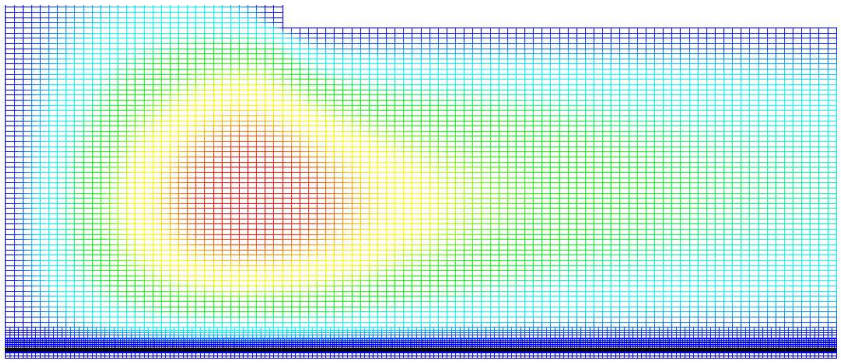

(a) Location of the interface at $\tilde{t} = 0$; #cells = 13,376, #nodes = 13,901; $\max \tilde{u}_r = 0.312$, $\max \tilde{u}_z = 0$

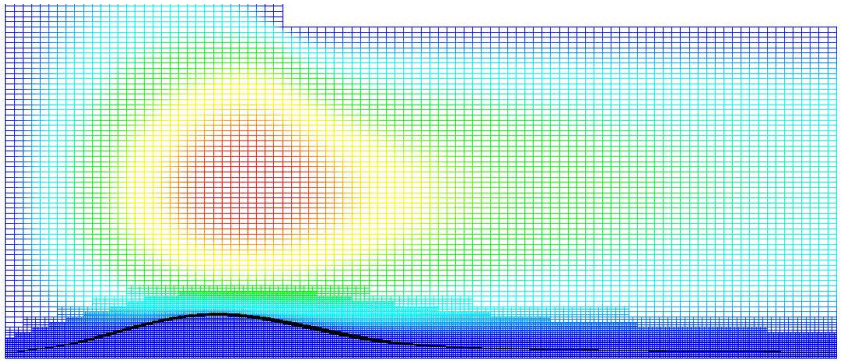

(b) Location of the interface at $\tilde{t} = 190$; #cells = 21,440, #nodes = 21,993; $\max \tilde{u}_r = 0.335$, $\max \tilde{u}_z = 0.007$

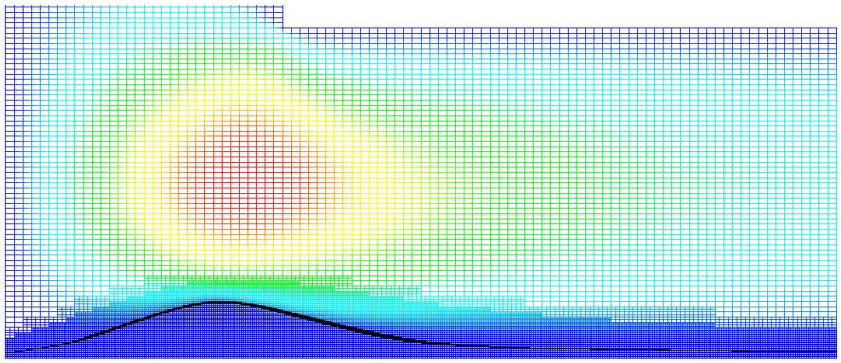

(c) Location of the interface at $\tilde{t} = 215$; #cells = 22,904, #nodes = 23,463; $\max \tilde{u}_r = 0.350$, $\max \tilde{u}_z = 0.010$

Figure 4.3: Stagnation point flow with shear-dependent platelet adhesion calculated on a fine grid. Cell size ranges from $h_{\max} = 3.125 \times 10^{-2}$ to $h_{\min} = 0.78125 \times 10^{-2}$ around the interface. Red color indicates elevated radial velocity, whereas dark blue color denotes vanishing radial velocity.

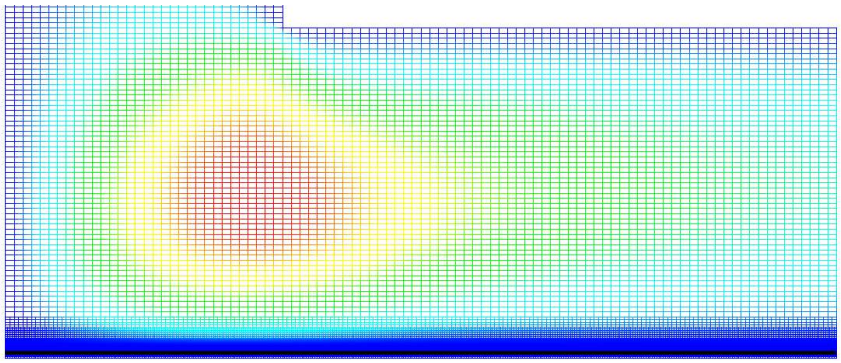

(a) Location of the interface at $\tilde{t} = 0$; #cells = 33,536, #nodes = 34,467; $\max \tilde{u}_r = 0.312$, $\max \tilde{u}_z = 0$

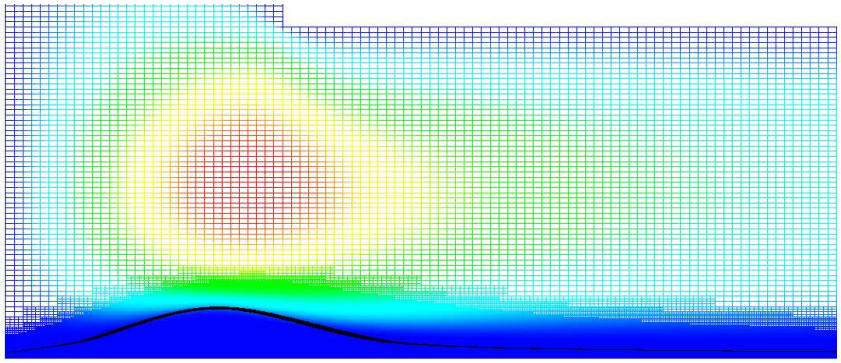

(b) Location of the interface at $\tilde{t} = 190$; #cells = 70,688, #nodes = 71,697; $\max \tilde{u}_r = 0.335$, $\max \tilde{u}_z = 0.006$

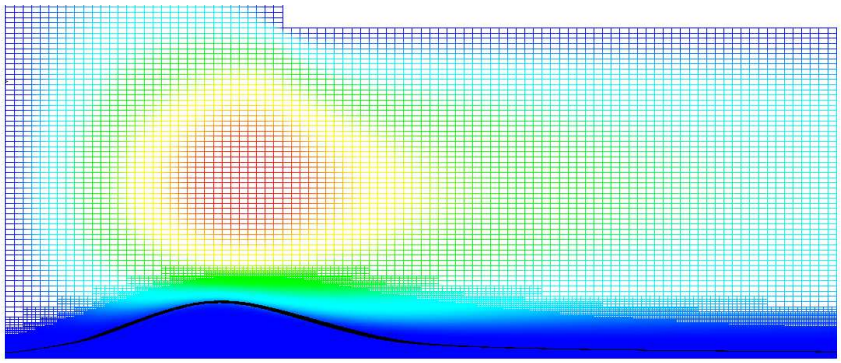

(c) Location of the interface at $\tilde{t} = 215$; #cells = 73,592, #nodes = 74,605; $\max \tilde{u}_r = 0.348$, $\max \tilde{u}_z = 0.009$

Figure 4.4: Stagnation point flow with shear-dependent platelet adhesion calculated on a very fine grid. Cell size ranges from $h_{\max} = 3.125 \times 10^{-2}$ to $h_{\min} = 0.390625 \times 10^{-2}$ around the interface. Red color indicates elevated radial velocity, whereas dark blue color denotes vanishing radial velocity.

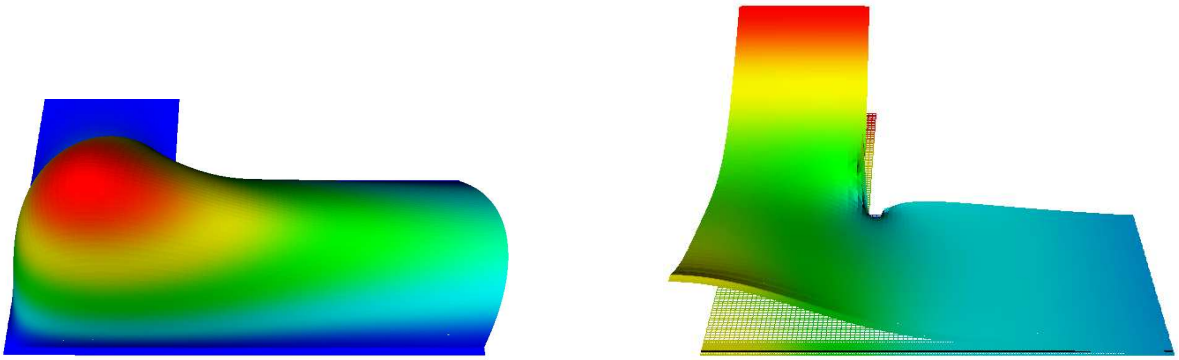

(a) $\tilde{t} = 0$; #cells = 13,376, #nodes = 13,901; $\max \tilde{u}_r = 0.312$

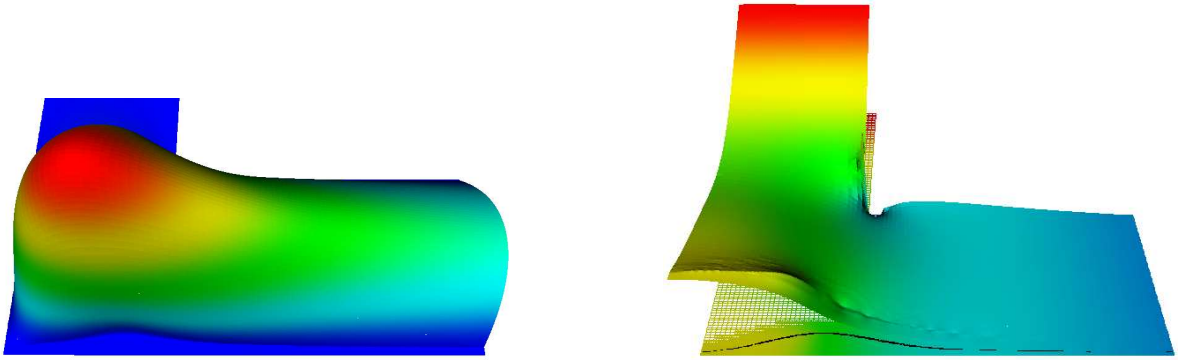

(b) $\tilde{t} = 190$; #cells = 21,440, #nodes = 21,993; $\max \tilde{u}_r = 0.335$

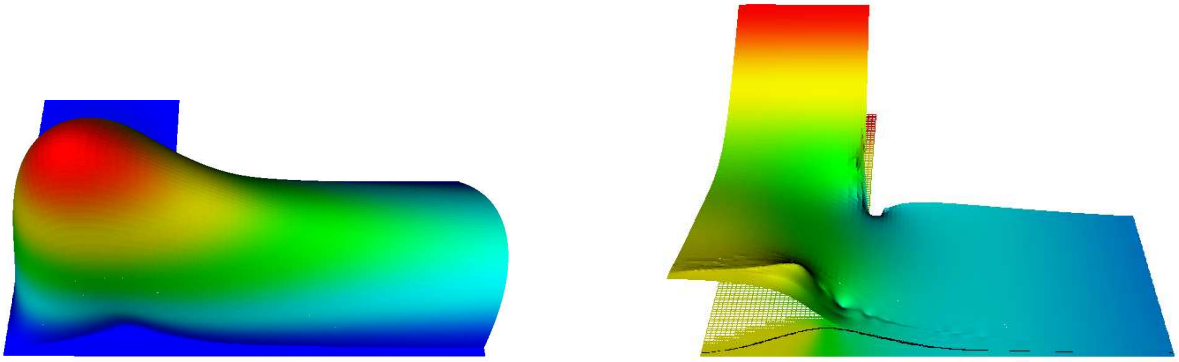

(c) $\tilde{t} = 215$; #cells = 22,904, #nodes = 23,463; $\max \tilde{u}_r = 0.350$

Figure 4.5: Thrombus growth affecting radial flow velocity $\tilde{u}_r$ (*left column*) and pressure $\tilde{p}$ (*right column*) in stagnation point flow, assuming shear-dependent platelet adhesion. The values of $\tilde{u}_r$ and $\tilde{p}$ are drawn in the direction perpendicular to the mesh. The locally refined mesh and the interface separating fluid and thrombus are also contained in the pictures on the right. Cell size ranges from $h_{\max} = 3.125 \times 10^{-2}$ to $h_{\min} = 0.78125 \times 10^{-2}$ around the interface.

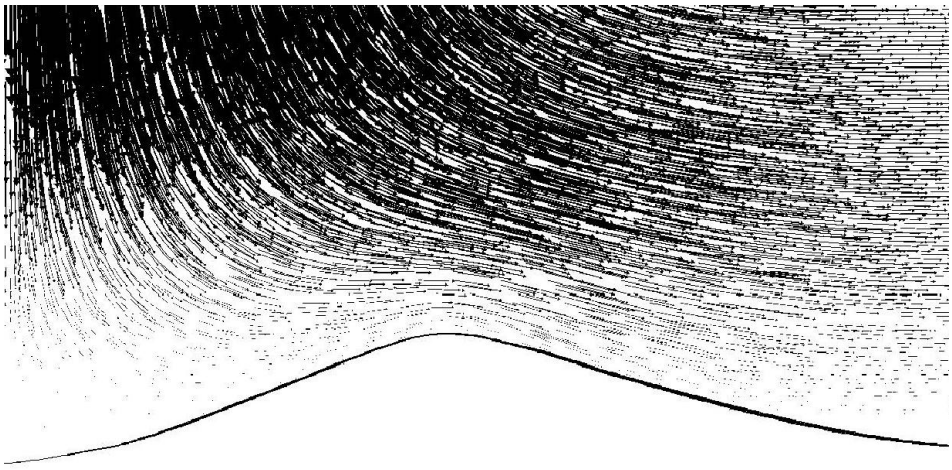

(a) Flowfield in the vicinity of the thrombus

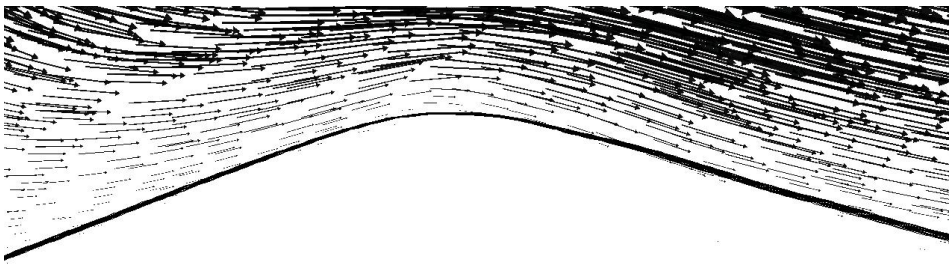

(b) Magnification of the flowfield around the thrombus' tip

Figure 4.6: Thrombus growth affecting the flow field in stagnation point flow at $\tilde{t} = 215$, assuming shear-dependent platelet adhesion. The requirement that the flow velocity vanishes inside the thrombus is fulfilled after a bandwith of approximately one cell size around the interface (see Figure (b)). Calculations were performed on a grid consisting of 22,904 cells and 23,463 nodes (not shown). Cell size ranges from $h_{\max} = 3.125 \times 10^{-2}$ to $h_{\min} = 0.78125 \times 10^{-2}$ around the interface.

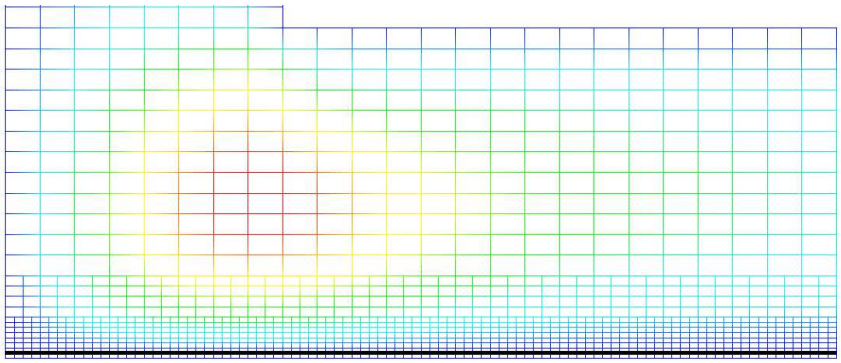

(a) Location of the interface at $\tilde{t} = 0$; cell size: $h_{\max} = 12.5 \times 10^{-2}$, $h_{\min} = 3.125 \times 10^{-2}$; #cells = 1,376, #nodes = 1,513; $\max \tilde{u}_r = 0.310$

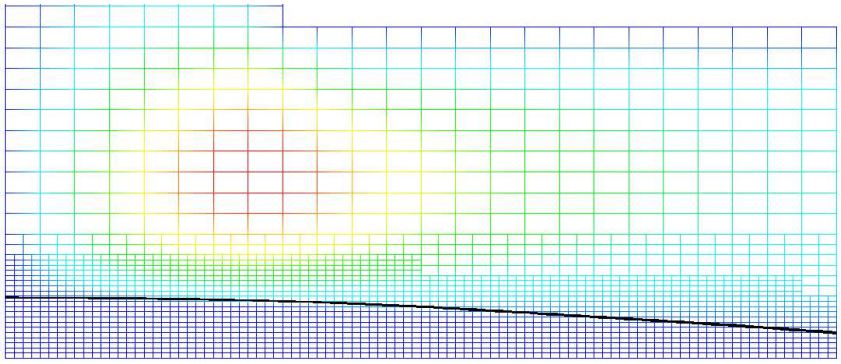

(b) Location of the interface at $\tilde{t} = 190$; cell size: $h_{\max} = 12.5 \times 10^{-2}$, $h_{\min} = 3.125 \times 10^{-2}$; #cells = 2,228, #nodes = 2,373; $\max \tilde{u}_r = 0.352$

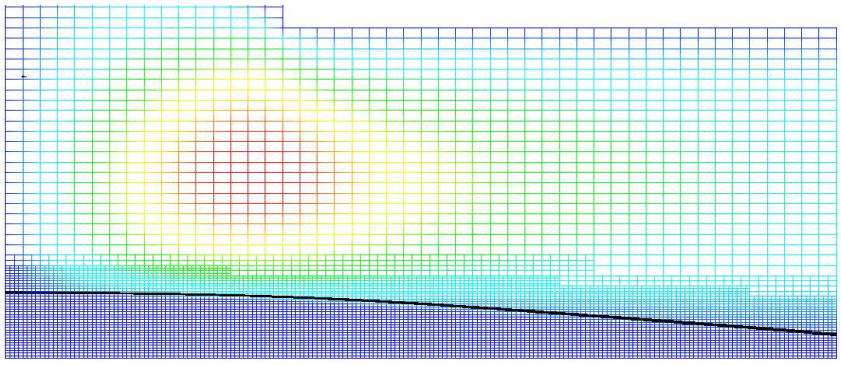

(c) Location of the interface at $\tilde{t} = 190$; cell size: $h_{\max} = 6.25 \times 10^{-2}$, $h_{\min} = 1.5625 \times 10^{-2}$; #cells = 7,916, #nodes = 8,201; $\max \tilde{u}_r = 0.359$

Figure 4.7: Stagnation point flow with shear-independent platelet adhesion calculated on various grids. Red color indicates elevated radial velocity, whereas dark blue color denotes vanishing radial velocity.

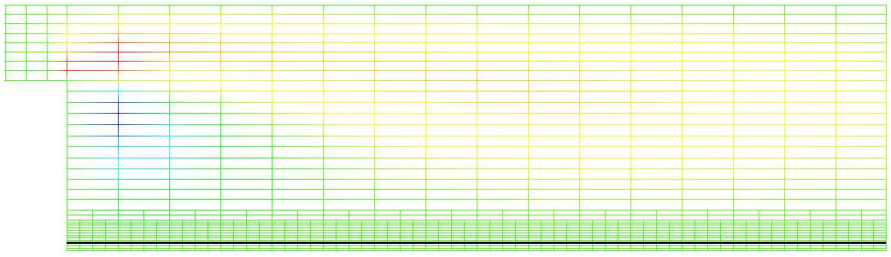

(a) Location of the interface at $\tilde{t} = 0$; cell size: $h_{\max} = 5.73 \times 10^{-2}$, $h_{\min} = 1.4325 \times 10^{-2}$; #cells = 1,216, #nodes = 1,323

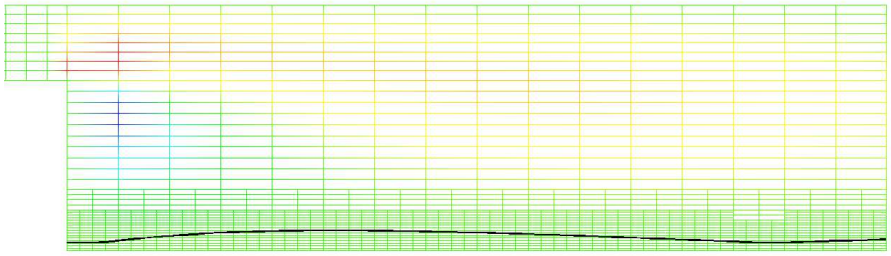

(b) Location of the interface at $\tilde{t} = 110$; cell size: $h_{\max} = 5.73 \times 10^{-2}$, $h_{\min} = 1.4325 \times 10^{-2}$; #cells = 1,492, #nodes = 1,605

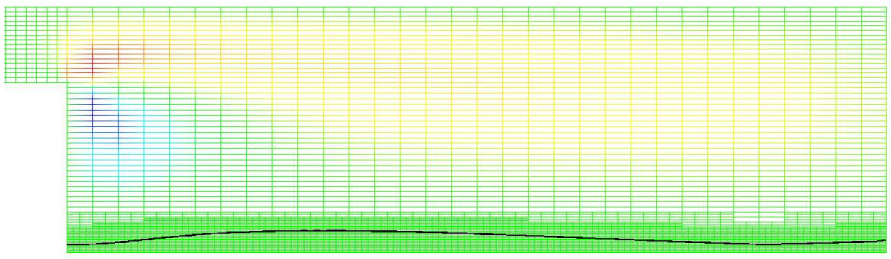

(c) Location of the interface at $\tilde{t} = 110$; cell size: $h_{\max} = 2.865 \times 10^{-2}$, $h_{\min} = 0.71625 \times 10^{-2}$; #cells = 4,948, #nodes = 5,167

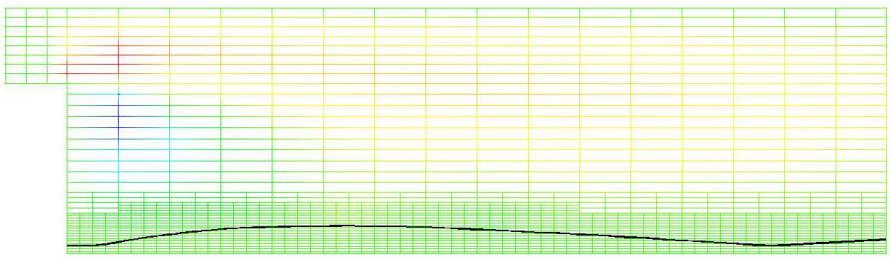

(d) Location of the interface at $\tilde{t} = 190$; cell size: $h_{\max} = 5.73 \times 10^{-2}$, $h_{\min} = 1.4325 \times 10^{-2}$; #cells = 1,612, #nodes = 1,725

Figure 4.8: Tubular expansion with shear-dependent platelet adhesion calculated on various grids. Red color indicates elevated radial velocity, green color corresponds to zero radial velocity, and dark blue color denotes elevated negative radial velocity.

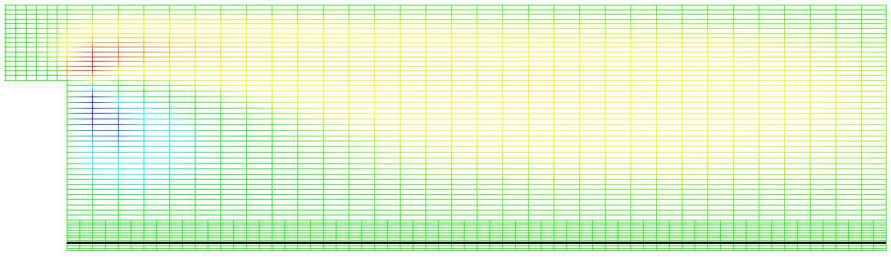

(a) Location of the interface at $\tilde{t} = 0$; cell size: $h_{\max} = 2.865 \times 10^{-2}$, $h_{\min} = 1.4325 \times 10^{-2}$; #cells = 2,368, #nodes = 2,503

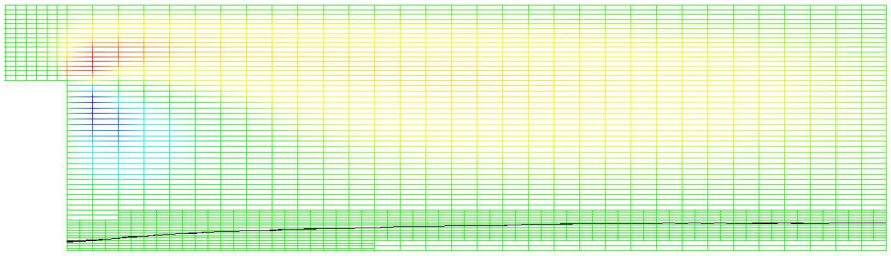

(b) Location of the interface at $\tilde{t} = 130$; cell size: $h_{\max} = 2.865 \times 10^{-2}$, $h_{\min} = 1.4325 \times 10^{-2}$; #cells = 2,428, #nodes = 2,565

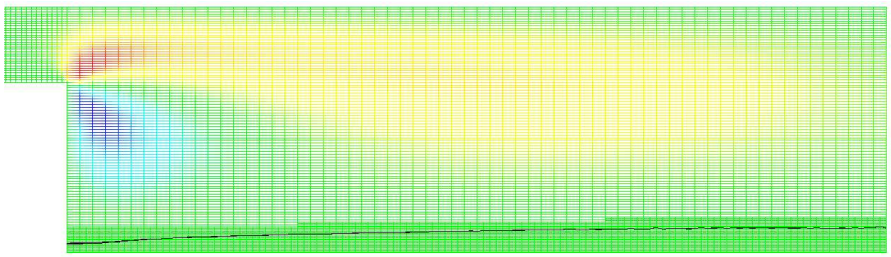

(c) Location of the interface at $\tilde{t} = 130$; cell size: $h_{\max} = 1.4325 \times 10^{-2}$, $h_{\min} = 0.71625 \times 10^{-2}$; #cells = 9,496, #nodes = 9,767

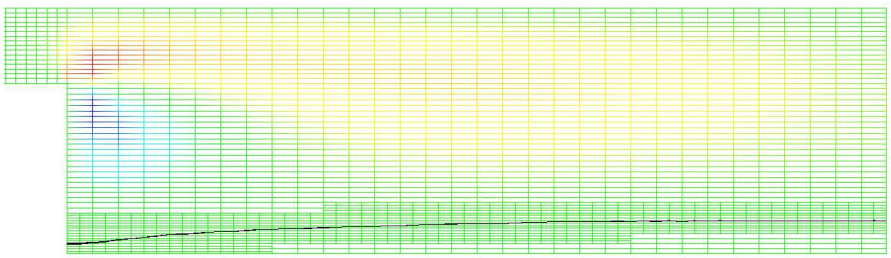

(d) Location of the interface at $\tilde{t} = 155$; cell size: $h_{\max} = 2.865 \times 10^{-2}$, $h_{\min} = 1.4325 \times 10^{-2}$; #cells = 2,488, #nodes = 2,627

Figure 4.9: Tubular expansion with shear-independent platelet adhesion calculated on various grids. Red color indicates elevated radial velocity, green color corresponds to zero radial velocity, and dark blue color denotes elevated negative radial velocity.

5 Classical solvability of the free boundary problem

This chapter proves classical solvability of (5.1)-(5.2) under the assumptions specified below. The proof consists of several steps, which are presented in the following sections. First, the original moving boundary problem is transformed to an equivalent formulation on the fixed initial domain Ω_0. This is presented in Section 5.2, making use of a transformation that was originally employed by Hanzawa [36] to prove classical solvability of the single phase Stefan problem. Then, in Section 5.3, the flow field is fixed and the corresponding linear problem for the platelets is investigated. Starting in half space, this coupled linear problem is split up in several auxiliary problems, which are treated by Fourier-Laplace transform techniques. One of these auxiliary problems has been investigated by Kusaka and Tani, who also derived an explicit representation formula of its solution (see [51, p. 594]). The remaining ones are treated here by similar techniques. Besides this, some results on pseudodifferential operators are employed to derive a priori estimates (see the proof of Lemma 5.3.3). After that, the full linear problem is solved in half space by Banach's fixed point theorem, which requires a thorough investigation of the representation formula reported by Kusaka and Tani. Then, by means of a regularizer, the results for the half space are used to solve the linear problem in the original domain Ω_0. Relying on the linear theory, Section 5.4 is devoted to the solution of the nonlinear problem for the platelets, when the flow field is still fixed. After quite technical estimates of the nonlinear terms it turns out that Banach's theorem is applicable—provided that time and the initial data for the platelets are sufficiently small. Finally, in Section 5.5, the full coupling of flow and platelets is investigated. The transformed Navier-Stokes system has been studied by Solonnikov [80] and his results even yield compactness of a thoroughly defined operator solving the full problem. Furthermore, it is shown here that this operator maps a ball into itself—provided that time is sufficiently small. Thus, Schauder's theorem yields a classical solution of the whole system.

5.1 Preliminaries

5.1.1 Geometry and model equations

Consider a domain as displayed in Figure 5.1, where $k > 0$ on the reactive (free) boundary and $k, l = 0$ on the non-reactive (fixed) wall.

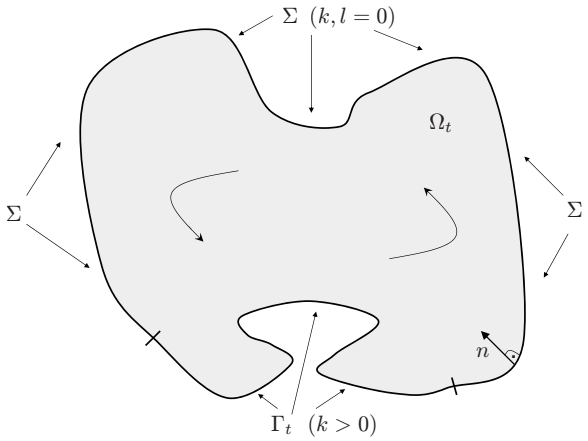

Figure 5.1: Considered domain

In this situation, the free boundary problem (4.2)-(4.3) reads

$$\begin{cases} \partial_t u - \nu\Delta u + (u\cdot\nabla)u + \nabla p = f & \text{in } \Omega_T \\ \nabla\cdot u = 0 & \text{in } \Omega_T \\ u = 0 & \text{on } \Gamma_T \cup \Sigma_T \\ u(t=0) = u_0 & \text{in } \Omega_0 \end{cases} \tag{5.1}$$

$$\begin{cases} \partial_t w - D\Delta w + (u\cdot\nabla)w = 0 & \text{in } \Omega_T \\ D\partial_n w = kw + l & \text{on } \Gamma_T \cup \Sigma_T \\ w(t=0) = w_0 & \text{in } \Omega_0 \\ v = \nabla w & \text{on } \Gamma_T\,. \end{cases} \tag{5.2}$$

Ω_T, Γ_T, and Σ_T are defined as in (4.1). Furthermore, the factor α in (4.3) has been set to one, which is possible after an obvious redefinition of w, w_0, and l.

5.1.2 Notation and function spaces

Let $l > 0$ be nonintegral and let ρ_0 be a fixed positive number. According to Ladyzenskaja et al. [52], we define the Hölder spaces $H^l(\overline{\Omega})$ as Banach spaces of functions $w(x)$ that are continuous in $\overline{\Omega}$, together with all derivatives up to order $[l]$ inclusively, and have a finite norm

$$\|w\|_\Omega^{(l)} := \langle w\rangle_\Omega^{(l)} + \sum_{j=0}^{[l]} \langle w\rangle_\Omega^{(j)}\ , \quad \langle w\rangle_\Omega^{(0)} := \|w\|_\Omega^{(0)} := \max_{\overline{\Omega}} |w|\ , \quad \langle w\rangle_\Omega^{(j)} := \sum_{|s|=j} \|D_x^s w\|_\Omega^{(0)},$$

$$\langle w\rangle_\Omega^{(l)} := \sum_{|s|=[l]} \langle D_x^s w\rangle_\Omega^{(l-[l])}\ ; \qquad \langle w\rangle_\Omega^{(\alpha)} := \sup_{\substack{x,\,y\,\in\,\Omega \\ |x-y|\,\le\,\rho_0}} \frac{|w(x)-w(y)|}{|x-y|^\alpha} \quad (0<\alpha<1)\,.$$

In addition, we set $Q_T := \Omega_0 \times (0,T]$, $S_T := \partial\Omega_0 \times (0,T]$, and define the Hölder spaces $H^{l,l/2}(\overline{Q_T})$ as Banach spaces of functions $w(x,t)$ that are continuous in $\overline{Q_T}$, together with all derivatives of the form $D_t^r D_x^s w$ for $2r+|s| < l$, and have a finite norm

$$\|w\|_{Q_T}^{(l)} := \langle w\rangle_{Q_T}^{(l)} + \sum_{j=0}^{[l]} \langle w\rangle_{Q_T}^{(j)}\,, \qquad \langle w\rangle_{Q_T}^{(0)} := \|w\|_{Q_T}^{(0)} := \max_{\overline{Q_T}} |w|,$$

$$\langle w\rangle_{Q_T}^{(j)} := \sum_{2r+|s|=j} \|D_t^r D_x^s w\|_{Q_T}^{(0)}, \qquad \langle w\rangle_{Q_T}^{(l)} := \langle w\rangle_{x,Q_T}^{(l)} + \langle w\rangle_{t,Q_T}^{(l/2)}\,,$$

$$\langle w\rangle_{x,Q_T}^{(l)} := \sum_{2r+|s|=[l]} \langle D_t^r D_x^s w\rangle_{x,Q_T}^{(l-[l])}\,, \qquad \langle w\rangle_{t,Q_T}^{(l/2)} := \sum_{0<l-2r-|s|<2} \langle D_t^r D_x^s w\rangle_{t,Q_T}^{\left(\frac{l-2r-s}{2}\right)}\,.$$

Here, for $0<\alpha<1$,

$$\langle w\rangle_{x,Q_T}^{(\alpha)} := \sup_{\substack{(x,t),(y,t)\in\overline{Q_T}\\ |x-y|\le\rho_0}} \frac{|w(x,t)-w(y,t)|}{|x-y|^\alpha}\,, \quad \langle w\rangle_{t,Q_T}^{(\alpha)} := \sup_{\substack{(x,t),(x,s)\in\overline{Q_T}\\ |t-s|\le\rho_0}} \frac{|w(x,t)-w(x,s)|}{|t-s|^\alpha}\,.$$

Let $H_0^{l,l/2}(\overline{Q_T})$ be the Hölder spaces corresponding to zero initial conditions, that is $w \in H_0^{l,l/2}(\overline{Q_T})$ satisfies $\partial_t^k w(t=0)=0\ \forall k \in \{0,...,[l/2]\}$. In addition, we define the product spaces

$$\mathcal{R}_1 := H_0^{\alpha,\frac{\alpha}{2}}(\overline{Q_T}) \times H_0^{1+\alpha,\frac{1+\alpha}{2}}(S_T) \times H_0^{1+\alpha,\frac{1+\alpha}{2}}(S_T)\,, \qquad \mathcal{R}_2 := H_0^{2+\alpha,\frac{2+\alpha}{2}}(\overline{Q_T}) \times H_0^{2+\alpha,\frac{2+\alpha}{2}}(S_T)$$

with norms

$$\|(F_1,F_2,F_3)\|_{\mathcal{R}_1} := \|F_1\|_{Q_T}^{(\alpha)} + \|F_2\|_{S_T}^{(1+\alpha)} + \|F_3\|_{S_T}^{(1+\alpha)}, \quad \|(\xi,\sigma)\|_{\mathcal{R}_2} := \|\xi\|_{Q_T}^{(2+\alpha)} + \|\sigma\|_{S_T}^{(2+\alpha)}.$$

Here, we finally introduced the Hölder spaces of functions on the boundary S_T. By switching to local coordinates (given that the boundary is sufficiently smooth), these spaces are defined similarly to the above defined ones.

5.1.3 Assumptions and main theorem

We assume that $0<\alpha'<1$ and that Ω_0 is a given domain in $\mathbb{R}^3$ whose boundary $\partial\Omega_0$ belongs to $H^{3+\alpha'}$ in the sense of [52, pp. 9–10]. For points of the surface $\partial\Omega_0$ we introduce local coordinates $\omega=(\omega_1,\omega_2)$; we also denote by $x(\omega)\in\partial\Omega_0$ or ω the corresponding points in $\mathbb{R}^3$. Let $n(\omega)$ be the unit normal to $\partial\Omega_0$ at ω directed into Ω_0. We assume a positive number γ_0 to be chosen so small that the mapping

$$\begin{aligned} \partial\Omega_0 \times [-\gamma_0,\gamma_0] &\to N \\ (\omega,\lambda) &\mapsto x(\omega,\lambda) := \omega + \lambda n(\omega) \end{aligned}$$

into a neighborhood $N\subset\mathbb{R}^3$ of $\partial\Omega_0$ is regular, one to one, and onto. By $(\omega(x),\lambda(x))$ we denote the inverse mapping of x from N to $\partial\Omega_0\times[-\gamma_0,\gamma_0]$.

We suppose that the moving boundary Γ_t permits the representation

$$\Gamma_t = \{x = \omega + \tilde{h}(\omega,t)n(\omega),\ \omega\in\Gamma_0\}\,, \quad t\in[0,T]\,,$$

with a function

$$\tilde{h} : \Gamma_0 \times [0,T] \to \mathbb{R}\,, \quad \tilde{h}(\omega,0) = 0\,.$$

We further assume that $0 < \alpha < \alpha'$, $u_0 \in H^{2+\alpha}(\overline{\Omega_0})$, $w_0 \in H^{3+\alpha}(\overline{\Omega_0})$, $f \in H^{\alpha,\alpha/2}(\mathbb{R}^3_T)$, $k \in H^{1+\alpha',\frac{1+\alpha'}{2}}(\overline{S_T})$, and $l \in H^{1+\alpha',\frac{1+\alpha'}{2}}(\overline{S_T})$. The extension of k and l into the interior of the domain is chosen similarly to that of $\tilde{h}$, which is defined in (5.3). Furthermore, the compatibility conditions of order zero shall be fulfilled (cf. [52, p. 319]). Then the following theorem holds, which will be proven in the sections below:

Theorem 5.1.1 (Classical solvability of (5.1)-(5.2))**.** *Let $0 < \beta < \alpha$. Under the assumptions made above and provided that T and $\|w_0\|^{(3+\alpha)}_{\Omega_0}$ are sufficiently small, problem* (5.1)-(5.2) *has a solution*

$$\tilde{h} \in H^{2+\alpha,\frac{2+\alpha}{2}}(\overline{\Gamma_0} \times [0,T])\,, \quad u \in H^{2+\beta,\frac{2+\beta}{2}}(\overline{\Omega_T})\,, \quad \nabla p \in H^{\beta,\frac{\beta}{2}}(\overline{\Omega_T})\,, \quad w \in H^{2+\alpha,\frac{2+\alpha}{2}}(\overline{\Omega_T}).$$

5.2 Transformation to fixed domain

Let $N_{\Gamma_0} := \{x \in N :\ \omega(x) \in \Gamma_0\}$. We define

$$h(x,t) := \tilde{h}(\omega(x),t) \quad \text{and} \quad \phi(x,t) := \lambda(x) - h(x,t)\,, \quad (x,t) \in N_{\Gamma_0} \times [0,T]\,. \tag{5.3}$$

Using the level set function ϕ, the moving boundary fulfills

$$\bigcup_{0\le t\le T} \Gamma_t \times \{t\} = \{(x,t) \in N_{\Gamma_0} \times [0,T] :\ \phi(x,t) = 0\}.$$

The evolution of Γ_t is determined by the transport equation

$$\partial_t h - \nabla w \nabla \phi = 0 \ \text{ on } \Gamma_T\,, \quad h(x,0) = 0 \ \text{ on } \Gamma_0\,. \tag{5.4}$$

At this stage, the formulation of the problem contains two different parts of the boundary: the reactive (moving) wall Γ_t and the non-reactive (fixed) material Σ. However, unification to a formulation with a single boundary is straightforward, since $\partial_n w = 0$ on Σ_T and because $\nabla\phi$ is perpendicular to $\partial\Omega_t$. Hence, equation (5.4) holds on the whole boundary $\Gamma_T \cup \Sigma_T$, that is

$$\partial_t h - \nabla w \nabla \phi = 0 \ \text{ on } \Gamma_T \cup \Sigma_T\,, \quad h(x,0) = 0 \ \text{ on } \partial\Omega_0\,. \tag{5.5}$$

In the following, the moving boundary problem is reformulated on the fixed original domain Ω_0, that is the coordinate system is changed from $x(\omega,\lambda)$ to $y(\omega,\eta)$. For this purpose, we choose a smooth cutoff function χ with

$$\chi(\eta) := \begin{cases} 1 & \text{if } |\eta| \le \gamma_0/4 \\ 0 & \text{if } |\eta| \ge 3\gamma_0/4 \end{cases}\,, \quad |\chi'(\eta)| \le \frac{4}{3\gamma_0}\,. \tag{5.6}$$

An appropriate transformation $\Psi_h : Q_T \to \Omega_T$ can be defined as

$$\Psi_h(y,t) := (y + h(y,t)\beta(y),\, t) =: (\Psi_h^{(1)}(y,t), \Psi_h^{(2)}(t))\,, \quad \beta(y) := \chi(\eta(y))\, n(\omega(y))\,. \tag{5.7}$$

Its inverse is denoted by $\Phi_h(x,t) = \big(\Phi_h^{(1)}(x,t), \Phi_h^{(2)}(t)\big)$. The Jacobian $D\Psi_h$ of Ψ_h with respect to space and time variables fulfills

$$D\Psi_h(y,t) = \begin{pmatrix} M_h(y,t) & N_h(y,t) \\ 0 & 1 \end{pmatrix}, \quad M_h := \mathrm{Id} + \beta \nabla_y h^T + h D_y \beta\,, \quad N_h := \partial_t h\, \beta\,. \tag{5.8}$$

We define

$$\underline{f}(y,t) := f(\Psi_h(y,t)) \qquad A_h(y,t) := (M_h^{-1})^T \tag{5.9}$$

$$q_h(y,t) := (\partial_t \Phi_h^{(1)})(\Psi_h(y,t)) \qquad \nabla_{A_h} := A_h(y,t)\nabla_y \tag{5.10}$$

and observe that the differential operators transform as

$$\nabla_x f(x,t) = \nabla_{A_h} \underline{f}(y,t) \qquad \partial_t f(x,t) = \partial_t \underline{f}(y,t) + (q_h \cdot \nabla_y)\underline{f}(y,t) \tag{5.11}$$

$$\nabla \cdot f(x,t) = \nabla_{A_h} \cdot \underline{f}(y,t) \qquad \Delta f(x,t) = \nabla_{A_h}^2 \underline{f}(y,t)\,. \tag{5.12}$$

The inward normal $n = |\nabla\eta|^{-1}\nabla\eta$ transforms into $n_{A_h} := |\nabla_{A_h}\eta|^{-1}\nabla_{A_h}\eta$. For the sake of brevity, the subfix h and the underscores are sometimes omitted.

Using (5.11) and (5.12), the equations (5.2) and (5.5) transform into

$$\begin{cases} \partial_t w - D\nabla_A^2 w + (u\cdot\nabla_A)w + (q\cdot\nabla)w = 0 & \text{in } Q_T \\ D n_A \nabla_A w = kw + l & \text{on } S_T \\ w(t=0) = w_0 & \text{in } \Omega_0 \\ \partial_t h - \nabla_A \eta \nabla_A w = 0 & \text{on } S_T \\ h(t=0) = 0 & \text{on } \partial\Omega_0\,. \end{cases} \tag{5.13}$$

The penultimate equation follows from (5.5) by the observations that (5.3), (5.7), and (5.6) yield

$$\underline{\phi}(y,t) = \eta(y) + h(y,t)\chi(\eta(y)) - \tilde{h}(w(x),t) = \eta(y) + h(y,t) - \tilde{h}(w(y),t) = \eta(y) \quad \forall (y,t) \in S_T\,,$$

and that $q \equiv 0$ on S_T. We note that for fixed u the problem is to determine (w,h) from (5.13).

As second step, we appropriately reduce (5.13) to zero initial conditions. For this purpose, let

$$w^{(1)} := D\Delta w_0 - u_0 \nabla w_0 + (\nabla\eta\nabla w_0)\beta\nabla w_0\,, \qquad h^{(1)} := \nabla\eta\nabla w_0 \tag{5.14}$$

be the functions arising from the compatibility conditions on the equations and the data (cf. [52, p. 319]). By means of [52], Section 4.4 Theorem 4.3., we can construct two functions $\hat{w}$ and $\hat{h}$ that satisfy

$$\hat{w}(y,0) = w_0(y)\,, \quad \partial_t \hat{w}(y,0) = w^{(1)}(y)\,, \quad \hat{h}(y,0) = 0\,, \quad \partial_t \hat{h}(y,0) = h^{(1)}(y)\,, \tag{5.15}$$

and

$$\begin{aligned} \|\hat{w}\|_{Q_T}^{(3+\alpha)} + \|\hat{h}\|_{S_T}^{(3+\alpha')} &\le C(T)\Big(\|w_0\|_{\Omega_0}^{(3+\alpha)} + \|w^{(1)}\|_{\Omega_0}^{(1+\alpha)} + \|h^{(1)}\|_{\partial\Omega_0}^{(1+\alpha')}\Big) \\ &\le g\Big(\|w_0\|_{\Omega_0}^{(3+\alpha)}, \|u_0\|_{\Omega_0}^{(1+\alpha)}, T\Big) \to 0 \end{aligned} \tag{5.16}$$

as $\|w_0\|_{\Omega_0}^{(3+\alpha)} \to 0$, provided that T and $\|u_0\|_{\Omega_0}^{(1+\alpha)}$ are bounded. Finally, we define

$$\sigma := h - \hat{h}\,, \quad \xi := w - \hat{w} - \chi\sigma\partial_n\hat{w}$$

and observe that σ and ξ fulfill

$$\sigma(t=0) = 0\,, \quad \partial_t\sigma(t=0) = 0\,, \quad \xi(t=0) = 0\,, \quad \partial_t\xi(t=0) = 0\,,$$

as well as

$$\begin{cases} \partial_t\xi - D\Delta\xi = -\partial_t(\hat{w} + \chi\sigma\partial_n\hat{w}) + D\nabla_A^2(\xi + \hat{w} + \chi\sigma\partial_n\hat{w}) - D\Delta\xi \\ \qquad\qquad - (u\nabla_A)(\xi + \hat{w} + \chi\sigma\partial_n\hat{w}) - (q\nabla)(\xi + \hat{w} + \chi\sigma\partial_n\hat{w}) \\ \qquad\qquad =: F_1(u,\xi,\sigma) \quad \text{in } Q_T \\ D\partial_n\xi = \ k\xi + (k\chi\partial_n\hat{w})\sigma - Dn_A\nabla_A(\xi + \hat{w} + \chi\sigma\partial_n\hat{w}) + D\partial_n\xi + k\hat{w} + l \\ \qquad\qquad =: k\xi + (k\chi\partial_n\hat{w})\sigma + F_2(\xi,\sigma) \quad \text{on } S_T \\ \xi(t=0) = 0 \quad \text{in } \Omega_0 \\ \partial_t\sigma - \nabla\xi\nabla\eta = -\partial_t\hat{h} + \nabla_A(\xi + \hat{w} + \chi\sigma\partial_n\hat{w})\nabla_A\eta - \nabla\xi\nabla\eta \\ \qquad\qquad =: F_3(\xi,\sigma) \quad \text{on } S_T \\ \sigma(t=0) = 0 \quad \text{on } \partial\Omega_0\,. \end{cases} \tag{5.17}$$

5.3 The linear problem for the platelets; fixed flow

The aim is to solve the linear problem which corresponds to (5.17), that is

$$\begin{cases} \partial_t\xi - D\Delta\xi = F_1 & \text{in } Q_T \\ \partial_n\xi = k\xi + c\sigma + F_2 & \text{on } S_T \\ \xi(t=0) = 0 & \text{in } \Omega_0 \\ \partial_t\sigma - d\partial_n\xi = F_3 & \text{on } S_T \\ \sigma(t=0) = 0 & \text{on } \partial\Omega_0\,. \end{cases} \tag{5.18}$$

ξ can be decomposed into $\xi = \xi_1 + \xi_2$, with the solutions ξ_1 and (ξ_2, σ) of, respectively,

$$\begin{cases} \partial_t\xi_1 - D\Delta\xi_1 = F_1 & \text{in } Q_T \\ \partial_n\xi_1 = k\xi_1 + F_2 & \text{on } S_T \\ \xi_1(t=0) = 0 & \text{in } \Omega_0 \end{cases} \tag{5.19}$$

and

$$\begin{cases} \partial_t\xi_2 - D\Delta\xi_2 = 0 & \text{in } Q_T \\ \partial_n\xi_2 = k\xi_2 + c\sigma & \text{on } S_T \\ \xi_2(t=0) = 0 & \text{in } \Omega_0 \\ \partial_t\sigma - d\partial_n\xi_2 = F_3 + d\partial_n\xi_1 & \text{on } S_T \\ \sigma(t=0) = 0 & \text{on } \partial\Omega_0\,. \end{cases} \tag{5.20}$$

Solvability of (5.19)-(5.20) follows from the solvability of both (5.19) and

$$\begin{cases} \partial_t \xi_2 - D\Delta \xi_2 = 0 & \text{in } Q_T \\ \partial_n \xi_2 = k\xi_2 + c\sigma & \text{on } S_T \\ \xi_2(t=0) = 0 & \text{in } \Omega_0 \\ \partial_t \sigma - d\partial_n \xi_2 = F & \text{on } S_T \\ \sigma(t=0) = 0 & \text{on } \partial\Omega_0\,. \end{cases} \tag{5.21}$$

The solution of (5.19) and (5.21) presupposes their investigation in half space, where Fourier-Laplace transform techniques can be employed. After that, on the basis of these results, the original problem (5.18) is solved in the domain Q_T.

5.3.1 Investigation of auxiliary problems in half space

Throughout this subsection, k, c, and d are assumed to be positive constants. We define

$$\mathbb{R}^3_+ := \mathbb{R}^3 \cap \{z \geq 0\}\,, \quad D^3_T := \mathbb{R}^3_+ \times [0,T]\,, \quad D^2_T := \mathbb{R}^2 \times \{0\} \times [0,T]\,, \quad \mathbb{R}^2_T := \mathbb{R}^2 \times [0,T]\,.$$

The Fourier transform and the inverse Fourier transform of a function $f \in L^1(\mathbb{R}^d)$ are defined by

$$\mathcal{F}(f)(\rho) := \hat{f}(\rho) := \frac{1}{(2\pi)^{\frac{d}{2}}} \int_{\mathbb{R}^d} e^{-i\rho x} f(x)dx\,, \quad \mathcal{F}^{-1}(f)(\rho) := \check{f}(\rho) := \frac{1}{(2\pi)^{\frac{d}{2}}} \int_{\mathbb{R}^d} e^{i\rho x} f(x)dx\,,$$

with $\rho \in \mathbb{R}^d$; the Laplace transform of a real-valued function g is given as

$$\mathcal{L}(g)(p) := \int_0^\infty e^{-pt} g(t)dt \quad (\mathrm{Re}(p) > 0)\,,$$

provided that the integral is convergent.

Solution of (5.21) in half space

Let χ be a smooth cutoff function, that is $\chi \in C_0^\infty(\mathbb{R}^2)$. To solve (5.21), we consider the three coupled problems (5.22)–(5.24) and thereby benefit from the theory that has been developed for (5.23) by Bazalii and Degtyarev [7] and by Kusaka and Tani [51] (see Proposition 5.3.2 on page 71):

$$\begin{cases} \partial_t \zeta_1 - D\Delta \zeta_1 = 0 & \text{in } D^3_T \\ \partial_t \sigma_1 = dk\zeta_1 & \text{on } D^2_T \\ \zeta_1(t=0) = 0 & \text{in } \mathbb{R}^3_+ \\ \partial_t \sigma_1 - d\partial_z \zeta_1 = 2d\chi\partial_z \zeta_3 & \text{on } D^2_T \\ \sigma_1(t=0) = 0 & \text{on } \mathbb{R}^2, \end{cases} \tag{5.22}$$

$$\begin{cases} \partial_t \zeta_2 - D\Delta\zeta_2 = 0 & \text{in } D_T^3 \\ k\zeta_2 = c\sigma_2 & \text{on } D_T^2 \\ \zeta_2(t=0) = 0 & \text{in } \mathbb{R}^3_+ \\ \partial_t \sigma_2 - d\partial_z \zeta_2 = F & \text{on } D_T^2 \\ \sigma_2(t=0) = 0 & \text{on } \mathbb{R}^2, \end{cases} \tag{5.23}$$

$$\begin{cases} \partial_t \zeta_3 - D\Delta\zeta_3 = 0 & \text{in } D_T^3 \\ \partial_z \zeta_3 = -k\zeta_3 + \chi(\partial_z\zeta_2 - 2c\sigma_2 - c\sigma_1) & \text{on } D_T^2 \\ \zeta_3(t=0) = 0 & \text{in } \mathbb{R}^3_+ . \end{cases} \tag{5.24}$$

The solutions ζ_i must belong to $H_0^{2+\alpha,\frac{2+\alpha}{2}}(D_T^3)$; the σ_i must belong to $H_0^{2+\alpha,\frac{2+\alpha}{2}}(\mathbb{R}^2_T)$.

First, the corresponding uncoupled problems are treated. Then, using a smallness assumption on T, the coupled system is solved by application of Banach's theorem. We observe that on $\{(x,y) : \chi(x,y) = 1\}$ the functions $\xi_2 := \zeta_1 + \zeta_2 + \zeta_3$ and $\sigma := \sigma_1 + \sigma_2$ solve the original equations of (5.21), with the exception of the third one. Instead, $\partial_t\sigma - d\partial_z\xi_2 = F + d\partial_z\zeta_3$ is fulfilled. Thus, in a third step, the "defect" $d\partial_z\zeta_3$ has to be corrected.

Investigation of (5.22) and (5.24) This paragraph treats systems of equations which are similar to, respectively, the uncoupled problems (5.22) and (5.24). First, we consider (5.22), that is

$$\begin{cases} \partial_t \zeta - D\Delta\zeta = 0 & \text{in } D_T^3 \\ \partial_t \sigma = k\zeta & \text{on } D_T^2 \\ \zeta(t=0) = 0 & \text{in } \mathbb{R}^3_+ \\ \partial_t \sigma - d\partial_z \zeta = F & \text{on } D_T^2 \\ \sigma(t=0) = 0 & \text{on } \mathbb{R}^2, \end{cases} \tag{5.25}$$

where $F \in H_0^{1+\alpha,\frac{1+\alpha}{2}}(\mathbb{R}^2_T)$ is a compactly supported function. Assuming small time intervals, solvability of (5.24) can then be deduced from the solvability of (5.25) by a fixed point argument (see the proof of Proposition 5.3.1 on page 71).

Lemma 5.3.1. *Take the Fourier transform with respect to the spatial variables (x,y) and the Laplace transform with respect to t. The so transformed functions—denoted by $\tilde\zeta(\rho,z,p)$, $\tilde\sigma(\rho,p)$, and $\tilde F(\rho,p)$—fulfill*

$$\tilde\zeta(\rho,z,p) = \frac{p}{k}\,\tilde\sigma(\rho,p)\,\exp\left[-\left(\frac{p+D|\rho|^2}{D}\right)^{1/2} z\right] \tag{5.26}$$

$$\tilde\sigma(\rho,p) = \frac{\tilde F(\rho,p)}{p(1+\frac{d}{k}\sqrt{D^{-1}p+|\rho|^2})} \qquad (\rho\in\mathbb{R}^2,\ Re(p)>0)\,. \tag{5.27}$$

Proof. The zero initial conditions ensure $\widetilde{\partial_t \zeta} = p\tilde{\zeta}$. Furthermore, the relation $\widetilde{\partial^s \zeta} = (i\rho)^s \tilde{\zeta}$ holds. Thus, transforming the first two equations of (5.25) yields an ODE in z:

$$\partial_z^2 \tilde{\zeta}(\rho, z, p) = \left(\frac{p}{D} + |\rho|^2\right) \tilde{\zeta}(\rho, z, p)\,, \qquad \tilde{\zeta}(\rho, 0, p) = \frac{p}{k}\,\tilde{\sigma}(\rho, p)\,. \tag{5.28}$$

Clearly, $\tilde{\zeta}$ as defined in (5.26) solves (5.28). The minus sign in (5.26) arises from the integrability requirement on $\tilde{\zeta}$ (which implies $\tilde{\zeta} \to 0$ as $|\rho| \to \infty$). Formula (5.27) follows by transforming the fourth equation of (5.25) and making use of (5.26). □

The aim is to invert the Laplace transform in order to derive an explicit representation of $\hat{\sigma}$. For this purpose, we consider the following lemma:

Lemma 5.3.2. *Let the Laplace transform of a function $f(t)$ fulfill*

$$\mathcal{L}(f)(p) = \frac{1}{p(1 + a\sqrt{p+b})} \qquad (Re(p) > 0)\,, \tag{5.29}$$

where a and b are positive constants. Then f equals

$$f(t) = -\frac{1}{2}\frac{1}{(1 + a\sqrt{b})} - \frac{a}{\pi}\int_0^\infty \frac{e^{-(x+b)t}}{x+b}\,\frac{\sqrt{x}}{1 + a^2 x}\,dx \qquad (t > 0)\,. \tag{5.30}$$

Proof. 1. According to the inversion formula of the Laplace transform (cf. [52, p. 256]),

$$f(t) = \frac{1}{2\pi i}\int_{\gamma - i\infty}^{\gamma + i\infty} \frac{e^{pt}}{p(1 + a\sqrt{p+b}\,)}\,dp\,, \tag{5.31}$$

where $\gamma > 0$ is fixed. Since $\sqrt{z} := \sqrt{|z|}\exp\left(\frac{i\mathrm{Arg}(z)}{2}\right)$ is analytic on $\mathbb{C}_-$, $\mathcal{L}(f)$ can be extended to this region. We observe that both $\mathrm{Arg}(z)$ and $|z|$ change along the line $[\gamma - i\infty, \gamma + i\infty]$, which makes direct evaluation of (5.31) extremely difficult. Hence, it is necessary to reduce (5.31) to problems with one argument being constant. We achieve this by integrating along the path shown in Figure 5.2 and by following the subsequently presented steps.

According to Cauchy's theorem,

$$\frac{1}{2\pi i}\oint \frac{e^{pt}}{p(1 + a\sqrt{p+b}\,)}\,dp = 0\,. \tag{5.32}$$

The absolute value of the denominator $p(1 + a\sqrt{p+b}\,)$ rises like $aR^{3/2}$ as $R \to \infty$. Thus,

$$\frac{1}{2\pi i}\int_{\Gamma_1 + \Gamma_2} \frac{e^{pt}}{p(1 + a\sqrt{p+b}\,)}\,dp \to 0 \qquad (R \to \infty)\,. \tag{5.33}$$

Hence, (5.31), (5.32), and (5.33) yield

$$f(t) = -\frac{1}{2\pi i}\lim_{R\to\infty}\int_{L_1 + L_2} \frac{e^{pt}}{p(1 + a\sqrt{p+b}\,)}\,dp \; - \frac{1}{2\pi i}\int_B \frac{e^{pt}}{p(1 + a\sqrt{p+b}\,)}\,dp\,.$$

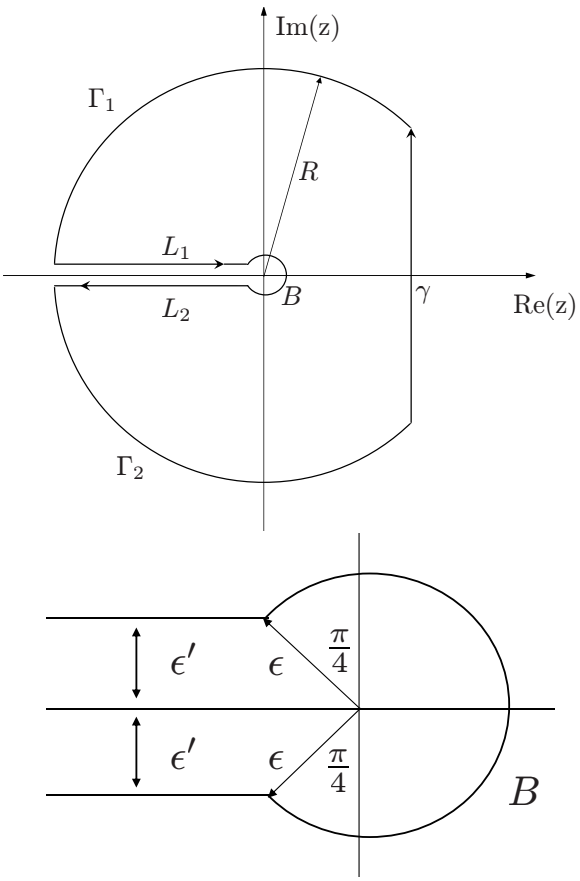

Figure 5.2: Path of integration and its magnification around the origin; $\epsilon' := \epsilon/\sqrt{2} > 0$

Since this equation holds for all $0 < \epsilon < \gamma$, we end up with

$$\begin{aligned} f(t) &= -\frac{1}{2\pi i} \lim_{\epsilon \to 0} \lim_{R \to \infty} \int\limits_{L_1 + L_2} \frac{e^{pt}}{p(1 + a\sqrt{p+b}\,)}\, dp \; - \frac{1}{2\pi i} \lim_{\epsilon \to 0} \int\limits_{B} \frac{e^{pt}}{p(1 + a\sqrt{p+b}\,)}\, dp \\ &=: -I_1 - I_2 \,. \end{aligned} \tag{5.34}$$

2. The second term in (5.34) can be treated with Lebesgue's theorem (cf. [2, p. 52]),

$$I_2 = \frac{1}{2\pi i} \lim_{\epsilon \to 0} \int\limits_{-\frac{3}{4}\pi}^{\frac{3}{4}\pi} \frac{e^{\epsilon e^{i\theta} t} i \epsilon e^{i\theta}}{\epsilon e^{i\theta}(1 + a\sqrt{\epsilon e^{i\theta} + b}\,)}\, d\theta = \frac{3}{4} \frac{1}{(1 + a\sqrt{b})} \,, \tag{5.35}$$

which is applicable since the integrand in (5.35) is bounded. I_1 is split up into three terms:

$$\begin{aligned} I_1 &= \frac{1}{2\pi i}\lim_{\epsilon'\to 0}\left(\int_{-\infty}^{-\epsilon'}\frac{e^{(x+i\epsilon')t}}{(x+i\epsilon')\big(1+a\sqrt{x+i\epsilon'+b}\,\big)}\,dx+\int_{-\epsilon'}^{-\infty}\frac{e^{(x-i\epsilon')t}}{(x-i\epsilon')\big(1+a\sqrt{x-i\epsilon'+b}\,\big)}\,dx\right)\\ &= \frac{1}{2\pi i}\lim_{\epsilon'\to 0}\int_{-\infty}^{0}\frac{e^{(y-b)t}}{a_1a_2}\,\frac{(y-b-i\epsilon')a_1e^{i\epsilon' t}-(y-b+i\epsilon')a_2e^{-i\epsilon' t}}{(y-b)^2+\epsilon'^2}\,dy\\ &\quad+\frac{1}{2\pi i}\lim_{\epsilon'\to 0}\int_{0}^{b/2}\ldots dy\;+\;\frac{1}{2\pi i}\lim_{\epsilon'\to 0}\int_{b/2}^{b-\epsilon'}\ldots dy\\ &=: J_1+J_2+J_3\,, \end{aligned} \tag{5.36}$$

where $a_1 := 1+a\sqrt{y-i\epsilon'}$ and $a_2 := 1+a\sqrt{y+i\epsilon'}$.

3. For all $\epsilon' \geq 0$, the integrands of J_1 and J_2 can be estimated on the respective intervals by the integrable function $Ce^{(y-b)t}$. Hence, Lebesgue's theorem allows once more to interchange integration and limit procedure. We observe that for $y<0$

$$\lim_{\epsilon'\to 0} a_1 = 1-ia\sqrt{-y}\,,\qquad \lim_{\epsilon'\to 0} a_2 = 1+ia\sqrt{-y}\,,$$

whereas for $y>0$

$$\lim_{\epsilon'\to 0} a_1 = 1+a\sqrt{y} = \lim_{\epsilon'\to 0} a_2\,.$$

That is why

$$J_1 = \frac{a}{\pi}\int_0^\infty \frac{e^{-(x+b)t}}{x+b}\,\frac{\sqrt{x}}{1+a^2x}\,dx\,,\qquad J_2 = 0\,. \tag{5.37}$$

In order to treat J_3, we first note that

$$a_1 = 1+a\sqrt{y}-\frac{i\epsilon' a}{2\sqrt{y}}+O(\epsilon'^2)\,,\qquad a_2 = 1+a\sqrt{y}+\frac{i\epsilon' a}{2\sqrt{y}}+O(\epsilon'^2) \tag{5.38}$$

holds uniformly on $[b/2,b]$. Because of this and by expansion of $e^{\pm i\epsilon' t}$, J_3 can be rewritten as

$$\begin{aligned} J_3 &= \frac{1}{2\pi}\lim_{\epsilon'\to 0}\int_{b/2}^{b-\epsilon'}\frac{e^{(y-b)t}}{a_1a_2}\left(2t\big(1+a\sqrt{y}\big)-\frac{a}{\sqrt{y}}\right)\frac{(y-b)\epsilon'}{(y-b)^2+\epsilon'^2}\,dy\\ &\quad+\frac{1}{2\pi i}\lim_{\epsilon'\to 0}O(\epsilon'^2)\int_{b/2}^{b-\epsilon'}\frac{1}{(y-b)^2+\epsilon'^2}\,dy-\frac{1}{\pi}\lim_{\epsilon'\to 0}\int_{b/2}^{b-\epsilon'}\frac{e^{(y-b)t}}{a_1a_2}\,\frac{\epsilon'\big(1+a\sqrt{y}\big)}{(y-b)^2+\epsilon'^2}\,dy\\ &=: J_4+J_5-J_6\,. \end{aligned} \tag{5.39}$$

4. J_4 and J_5 vanish, because

$$|J_4| \le \lim_{\epsilon'\to 0} O(\epsilon') \int_{b/2}^{b-\epsilon'} \frac{(b-y)}{(y-b)^2+\epsilon'^2}\,dy = \lim_{\epsilon'\to 0} \frac{O(\epsilon')}{2}\left(\log\Big(\frac{b^2}{4}+\epsilon'^2\Big) - \log(2\epsilon'^2)\right) = 0\,, \quad (5.40)$$

$$|J_5| \le \lim_{\epsilon'\to 0} O(\epsilon'^2) \int_{b/2}^{b-\epsilon'} \frac{1}{(y-b)^2+\epsilon'^2}\,dy \le \lim_{\epsilon'\to 0} O(\epsilon')\left[\arctan\Big(\frac{y-b}{\epsilon'}\Big)\right]_{b/2}^{b-\epsilon'} = 0\,. \quad (5.41)$$

To evaluate J_6, we observe that (5.38) and (5.41) yield

$$\begin{aligned} J_6 &= \frac{1}{\pi}\lim_{\epsilon'\to 0} \int_{b/2}^{b-\epsilon'} \frac{\epsilon' e^{(y-b)t}}{(1+a\sqrt{y})\big((y-b)^2+\epsilon'^2\big)}\,dy \\ &= \frac{1}{\pi}\lim_{\epsilon'\to 0} \int_{b/2}^{b-\epsilon'} \frac{\epsilon'}{(1+a\sqrt{y})\big((y-b)^2+\epsilon'^2\big)}\,dy - \frac{1}{\pi}\lim_{\epsilon'\to 0}\epsilon' \int_{b/2}^{b-\epsilon'} \frac{O(b-y)}{(1+a\sqrt{y})\big((y-b)^2+\epsilon'^2\big)}\,dy\,, \end{aligned}$$

where the last term vanishes according to (5.40). Thus, integration by parts leads to

$$J_6 = \lim_{\epsilon'\to 0}\frac{1}{\pi}\left[\frac{\arctan\left(\frac{y-b}{\epsilon'}\right)}{1+a\sqrt{y}}\right]_{b/2}^{b-\epsilon'} + \lim_{\epsilon'\to 0}\frac{1}{\pi}\int_{b/2}^{b-\epsilon'} a\frac{\arctan\left(\frac{y-b}{\epsilon'}\right)}{(1+a\sqrt{y})^2 2\sqrt{y}}\,dy\,.$$

The integrand of the second term is bounded, thus allows application of Lebesgue. Hence,

$$J_6 = \frac{1}{\pi}\lim_{\epsilon'\to 0}\left(\frac{\arctan(-1)}{1+a\sqrt{b-\epsilon'}} - \frac{\arctan\left(\frac{-b}{2\epsilon'}\right)}{1+a\sqrt{\frac{b}{2}}}\right) + \frac{1}{2}\int_{b/2}^{b}\frac{d}{dy}\frac{1}{1+a\sqrt{y}}\,dy = \frac{1}{4(1+a\sqrt{b})}\,. \quad (5.42)$$

Finally, the assertion follows from (5.34), (5.35), (5.36), (5.37), (5.39), (5.40), (5.41), and (5.42). □

We define the convolution of $u(t)$ and $w(t)$ as $u * w(t) := \int_0^t u(s)w(t-s)ds$. In addition, we set $a := \frac{d}{k\sqrt{D}}$, $e := \frac{d}{k}$, and

$$\hat{h}(\rho,t) := -\frac{1}{2}\frac{1}{(1+e|\rho|)} - \frac{a}{\pi}\int_0^\infty \frac{e^{-(s+D|\rho|^2)t}}{s+D|\rho|^2}\,\frac{\sqrt{s}}{1+a^2 s}\,ds =: \hat{h}_1(\rho) + \hat{h}_2(\rho,t)\,. \quad (5.43)$$

Then, Lemma 5.3.1, Lemma 5.3.2, and the convolution theorem for the Laplace transform yield

$$\hat{\sigma} = \mathcal{L}^{-1}(\mathcal{L}(\hat{F})\mathcal{L}(\hat{h})) = \mathcal{L}^{-1}(\mathcal{L}(\hat{F}*\hat{h})) = \hat{F}*\hat{h}_1 + \hat{F}*\hat{h}_2 =: \hat{\vartheta}_1 + \hat{\vartheta}_2\,. \quad (5.44)$$

Lemma 5.3.3 (Estimates of ϑ_1)**.** *The following estimate holds:*

$$\|\vartheta_1\|_{\mathbb{R}^2_T}^{(2+\alpha)} \le C\|F\|_{\mathbb{R}^2_T}^{(1+\alpha)}, \quad (5.45)$$

where $C = C(T)$ remains bounded as $T \to 0$.

Proof. 1. According to the proof of Lemma 2 on page 133 in the book of Stein [84], the quotient $-\frac{1}{2}\frac{\left(1+e|\rho|^2\right)^{1/2}}{1+e|\rho|}$ is the Fourier transform of a finite measure μ on $\mathbb{R}^2$. We define the pseudodifferential operator $\mathcal{P}$ acting on a function $u(x,y)$ as

$$\mathcal{P}u := \left(I - e\Delta\right)^{-\frac{1}{2}} u := \mathcal{F}^{-1}\left(\frac{\mathcal{F}(u)}{\left(1+e|\rho|^2\right)^{1/2}}\right).$$

According to [84], Theorem 4 on page 149, $\mathcal{P} : H^{l+\alpha}(\mathbb{R}^2) \to H^{l+1+\alpha}(\mathbb{R}^2)$ $(l \geq 0)$ and

$$\|\mathcal{P}u\|^{(l+1+\alpha)}_{\mathbb{R}^2} \leq C\|u\|^{(l+\alpha)}_{\mathbb{R}^2}. \tag{5.46}$$

We observe that $\hat{\vartheta}_1(\rho,t) = \hat{h}_1(\rho)\int_0^t \hat{F}(\rho,s)ds =: \hat{h}_1(\rho)\hat{F}_1(\rho,t)$. Hence, ϑ_1 can be written as

$$\vartheta_1 = \mathcal{F}^{-1}\left(-\frac{1}{2}\frac{\left(1+e|\rho|^2\right)^{1/2}}{1+e|\rho|}\frac{\mathcal{F}(F_1)}{\left(1+e|\rho|^2\right)^{1/2}}\right) = \mathcal{F}^{-1}\left(\mathcal{F}(\mu)\mathcal{F}(\mathcal{P}(F_1))\right) = \mu * \mathcal{P}F_1\,, \tag{5.47}$$

where the convolution theorem for Fourier transform was used in the last equation. Furthermore,

$$F_1(x,t) = \mathcal{F}^{-1}\left(\int_0^t \hat{F}(.,s)ds\right)(x) = \int_0^t \mathcal{F}^{-1}(\hat{F}(.,s))(x)ds = \int_0^t F(x,s)ds\,, \tag{5.48}$$

and hence

$$G(x,t) := \mathcal{P}F_1(.\,,t)(x) = \int_0^t \mathcal{P}F(.\,,s)(x)ds\,, \qquad \partial_t G(x,t) = \mathcal{P}F(.\,,t)(x)\,. \tag{5.49}$$

2. We show that $G \in H^{2+\alpha}(\mathbb{R}^2_T)$. In doing so, we restrict ourselves to the highest order terms. Using (5.49) and (5.46) we deduce

$$\begin{aligned}
\langle \partial_i\partial_j G\rangle^{(\alpha)}_{x,\mathbb{R}^2_T} &\leq \sup_{\substack{(x,t),\,(y,t)\,\in\,\mathbb{R}^2_T \\ |x-y|\,\leq\,\rho_0}} \int_0^t \frac{\left|\partial_i\partial_j\mathcal{P}F(.\,,s)(x) - \partial_i\partial_j\mathcal{P}F(.\,,s)(y)\right|}{|x-y|^\alpha}\,ds \\
&\leq \sup_t \int_0^t \|\mathcal{P}F(.\,,s)\|^{(2+\alpha)}_{\mathbb{R}^2}\,ds \\
&\leq C\sup_t \int_0^t \|F(.\,,s)\|^{(1+\alpha)}_{\mathbb{R}^2}\,ds \\
&\leq CT\|F\|^{(1+\alpha)}_{\mathbb{R}^2_T}
\end{aligned} \tag{5.50}$$

and, for $t \geq t'$,

$$\begin{aligned}
\langle \partial_i\partial_j G\rangle^{(\alpha/2)}_{t,\mathbb{R}^2_T} &\leq \sup_{\substack{(x,t),\,(x,t')\,\in\,\mathbb{R}^2_T \\ |t-t'|\,\leq\,\rho_0}} \frac{\int_{t'}^t \left|\partial_i\partial_j\mathcal{P}F(.\,,s)(x)\right|ds}{|t-t'|^{\alpha/2}} \\
&\leq C\sup_{t,t'} \frac{\int_{t'}^t \|F(.\,,s)\|^{(1+\alpha)}_{\mathbb{R}^2}}{|t-t'|^{\alpha/2}}\,ds \\
&\leq CT^{1-\alpha/2}\|F\|^{(1+\alpha)}_{\mathbb{R}^2_T}.
\end{aligned} \tag{5.51}$$

Furthermore,

$$\begin{aligned}\langle \partial_t G\rangle^{(\alpha/2)}_{t,\mathbb{R}^2_T} &= \sup_{\substack{(x,\,t),\,(x,\,t')\,\in\,\mathbb{R}^2_T\\ |t-t'|\,\le\,\rho_0}} \left|\mathcal{P}\left(\frac{F(.\,,t)-F(.\,,t')}{|t-t'|^{\alpha/2}}\right)(x)\right| \\ &\le C\sup_{t,t'}\left\|\frac{F(.\,,t)-F(.\,,t')}{|t-t'|^{\alpha/2}}\right\|^{(\alpha)}_{\mathbb{R}^2} \\ &\le C\|F\|^{(1+\alpha)}_{\mathbb{R}^2_T},\end{aligned} \tag{5.52}$$

where the last inequality follows from

$$\begin{aligned}\left\langle\frac{F(.\,,t)-F(.\,,t')}{|t-t'|^{\alpha/2}}\right\rangle^{(\alpha)}_{x,\mathbb{R}^2} &\le \sup_{\substack{x,\,y\,\in\,\mathbb{R}^2\\ |x-y|\,\le\,\rho_0}} \rho_0^{1-\alpha}\int_0^1 \frac{\left|\nabla F(x+s(y-x),t)-\nabla F(x+s(y-x),t')\right|}{|t-t'|^{\alpha/2}}\,ds \\ &\le \rho_0^{1-\alpha}\langle\nabla F\rangle^{(\alpha/2)}_{t,\mathbb{R}^2_T} \\ &\le \rho_0^{1-\alpha}\|F\|^{(1+\alpha)}_{\mathbb{R}^2_T}.\end{aligned}$$

Finally, by the use of (5.49), (5.46), and (5.99) we get

$$\begin{aligned}\langle \partial_t G\rangle^{(\alpha)}_{x,\mathbb{R}^2_T} &\le \sup_{\substack{(x,\,t),\,(y,\,t)\,\in\,\mathbb{R}^2_T\\ |x-y|\,\le\,\rho_0}} \rho_0^{1-\alpha}\int_0^1 \left|\nabla\big(\mathcal{P}F(.\,,t)\big)(x+s(y-x)\right|ds \\ &\le \rho_0^{1-\alpha}\sup_t\|\mathcal{P}F(.\,,t)\|^{(1+\alpha)}_{\mathbb{R}^2} \\ &\le C\|F\|^{(\alpha)}_{\mathbb{R}^2_T} \\ &\le C\sqrt{T}\|F\|^{(1+\alpha)}_{\mathbb{R}^2_T}.\end{aligned} \tag{5.53}$$

Hence, combination of (5.50), (5.51), (5.52), and (5.53) yields

$$\|G\|^{(2+\alpha)}_{\mathbb{R}^2_T} \le C\|F\|^{(1+\alpha)}_{\mathbb{R}^2_T}, \tag{5.54}$$

where C remains bounded as $T\to 0$.

3. To conclude the proof it suffices to note that convolution with a finite measure preserves the H^l-spaces. Thus, assertion (5.45) follows from (5.47), (5.49), and (5.54). □

Lemma 5.3.4 (Estimates of ϑ_2)**.** *Suppose that supp*$\big(F(.\,,\tau)\big)\subset B_R(0)\ \forall\tau\in[0,T]$. *Then*

$$\|\vartheta_2\|^{(2+\alpha)}_{\mathbb{R}^2_T} \le C\|F\|^{(1+\alpha)}_{\mathbb{R}^2_T}, \tag{5.55}$$

where $C=C(T,R,\alpha)$ *remains bounded as* $T\to 0$.

Proof. The assertion is verified for $\langle\partial_i\partial_j\vartheta_2\rangle^{(\alpha)}_{x,\mathbb{R}^2_T}$ and for $\langle\partial_t\vartheta_2\rangle^{(\alpha/2)}_{t,\mathbb{R}^2_T}$. The other terms of $\|\vartheta_2\|^{(2+\alpha)}_{\mathbb{R}^2_T}$ can be treated similarly.

1. To estimate $\langle \partial_i\partial_j\vartheta_2\rangle^{(\alpha)}_{x,\mathbb{R}^2_T}$, we first note the following relations for a function $u(x,y)$:

$$\|u\|_{L^\infty(\mathbb{R}^2)} \le \frac{1}{2\pi}\|\mathcal{F}(u)\|_{L^1(\mathbb{R}^2)}\,, \qquad \mathcal{F}\big(u(.+h)\big)(\rho) = e^{i\rho h}\mathcal{F}(u)(\rho)\,. \tag{5.56}$$

Thus, using the definition (5.44) of $\hat\vartheta_2$,

$$\begin{aligned}
\|\partial_i\partial_j\vartheta_2(\,.+h,t) - \partial_i\partial_j\vartheta_2(.\,,t)\|_{L^\infty(\mathbb{R}^2)} &\le C\|\mathcal{F}\big(\partial_i\partial_j(\vartheta_2(.+h,t)-\vartheta_2(.\,,t))\big)\|_{L^1(\mathbb{R}^2)}\\
&= C\|\rho_i\rho_j(e^{i\rho h}-1)\hat\vartheta_2(.\,,t)\|_{L^1(\mathbb{R}^2)}\\
&\le C\int_0^t \big\|(e^{i\rho h}-1)\mathcal{F}(\partial_i F)(.\,,\tau)\rho_j\hat h_2(.\,,t-\tau)\big\|_{L^1(\mathbb{R}^2)}d\tau\\
&\le C\sup_\tau\big\|\mathcal{F}\big(\partial_i F(.+h,\tau)-\partial_i F(.\,,\tau)\big)\big\|_{L^2(\mathbb{R}^2)}\times\\
&\qquad\times\int_0^t \big\||\rho|\hat h_2(.\,,t-\tau)\big\|_{L^2(\mathbb{R}^2)}d\tau\\
&=: CI_1\times\int_0^t I_2(t-\tau)d\tau\,.
\end{aligned} \tag{5.57}$$

According to Plancherel's theorem (cf. [21, p. 183]),

$$I_1 = \sup_\tau\|\partial_i F(.+h,\tau)-\partial_i F(.\,,\tau)\|_{L^2(\mathbb{R}^2)} \le 2\sqrt{\pi R^2}\,\|F\|^{(1+\alpha)}_{\mathbb{R}^2_T}|h|^\alpha. \tag{5.58}$$

Using polar coordinates and formula (5.43) we estimate I_2 as

$$I_2(t-\tau)^2 = C\int_0^\infty re^{-2Dr^2(t-\tau)}\left(\int_0^\infty \frac{e^{-s(t-\tau)}}{1+a^2s}\,\underbrace{\frac{2\sqrt{s}\sqrt{D}r}{s+Dr^2}}_{\le 1}\,ds\right)^2 dr \le \frac{C}{t-\tau}\left(\int_0^\infty\frac{e^{-s(t-\tau)}}{1+a^2s}\,ds\right)^2.$$

Furthermore,

$$\int_0^\infty\frac{e^{-s(t-\tau)}}{1+a^2s}\,ds \le \int_0^1\frac{1}{1+a^2s}\,ds + \frac{1}{a^2}\int_{t-\tau}^\infty\frac{e^{-s}}{s}\,ds \le C + \frac{1}{a^2}\big(-\log(t-\tau)+e^{-1}\big),$$

where, for the sake of simplicity, we assumed $T\le 1$ in deriving the last inequality. Hence,

$$\int_0^t I_2(t-\tau)d\tau \le C\int_0^t\frac{1-\log(t-\tau)}{\sqrt{t-\tau}}\,d\tau = C\big(6\sqrt{t}-2\log(t)\sqrt{t}\big)\le 6C \quad \forall t\in[0,T]\,. \tag{5.59}$$

Thus, (5.57), (5.58), and (5.59) imply $\langle \partial_i\partial_j\vartheta_2\rangle^{(\alpha)}_{x,\mathbb{R}^2_T} \le C\|F\|^{(1+\alpha)}_{\mathbb{R}^2_T}$.

2. $\langle \partial_t \vartheta_2 \rangle_{t,\mathbb{R}^2_T}^{(\alpha/2)}$ can be treated as follows: By the use of (5.56) and (5.44) we obtain for $h > 0$

$$\begin{aligned}
\|\partial_t\vartheta_2(.\,,t+h) - \partial_t\vartheta_2(.\,,t)\|_{L^\infty(\mathbb{R}^2)} &\le C\big\|\partial_t\Big(\mathcal{F}(\vartheta_2(.\,,t+h)) - \mathcal{F}(\vartheta_2(.\,,t))\Big)\big\|_{L^1(\mathbb{R}^2)} \\
&= C\big\|\partial_t\Big(\int_0^{t+h} \hat{F}(.\,,\tau)\hat{h}_2(.\,,t+h-\tau)d\tau \\
&\qquad - \int_0^t \hat{F}(.\,,\tau)\hat{h}_2(.\,,t-\tau)d\tau\Big)\big\|_{L^1(\mathbb{R}^2)} \\
&\le C\Big(\ \big\|(\hat{F}(.\,,t+h) - \hat{F}(.\,,t))\hat{h}_2(.\,,0)\big\|_{L^1(\mathbb{R}^2)} \\
&\quad + \int_0^t \big\|\hat{F}(.\,,\tau)\partial_t(\hat{h}_2(.\,,t+h-\tau) - \hat{h}_2(.\,,t-\tau))\big\|_{L^1(\mathbb{R}^2)}d\tau \\
&\quad + \int_t^{t+h} \big\|\hat{F}(.\,,\tau)\partial_t\hat{h}_2(.\,,t+h-\tau)\big\|_{L^1(\mathbb{R}^2)}d\tau \ \Big) \\
&=: C(\ J_1 + J_2 + J_3\ ).
\end{aligned} \tag{5.60}$$

3. First, J_1 shall be investigated. We observe from definition (5.43) that

$$|\hat{h}_2(\rho,0)| = \frac{a}{\pi}\int_0^\infty \frac{\sqrt{s}}{(s+D|\rho|^2)(1+a^2s)}\,ds = \frac{1}{1+|\rho|\sqrt{D}a} \le \frac{C}{\sqrt{1+|\rho|^2}}\,.$$

Furthermore, Lemma 7.9.2 in the book of Hörmander [38] states that for a function $u(x,y)$

$$\|u\|_{L^1(\mathbb{R}^2)} \le C\Big(\int_{\mathbb{R}^2} |u|^2(1+|\rho|^2)^{1+\epsilon}d\rho\Big)^{1/2} \qquad (\epsilon > 0).$$

The number ϵ will be specified below. Employing these two estimates we obtain

$$\begin{aligned}
J_1 &\le C\left(\int_{\mathbb{R}^2} |\hat{F}(.\,,t+h) - \hat{F}(.\,,t)|^2(1+|\rho|^2)^\epsilon d\rho\right)^{1/2} \\
&\le C\|F(.\,,t+h) - F(.\,,t)\|_{L^2(\mathbb{R}^2)} \\
&\quad + C\left(\int_{\mathbb{R}^2}\int_{\mathbb{R}^2} \frac{\big|F(\rho,t+h) - F(\rho,t) - F(\tilde{\rho},t+h) + F(\tilde{\rho},t)\big|^2}{|\rho-\tilde{\rho}|^{2+2\epsilon}}\,d\rho\,d\tilde{\rho}\right)^{1/2},
\end{aligned} \tag{5.61}$$

where the last inequality follows from the formulas (7.9.3) and (7.9.4) in [38]. Note that

$$\|F(.\,,t+h) - F(.\,,t)\|_{L^2(\mathbb{R}^2)} \le 2\sqrt{\pi R^2}\,\|F\|^{(1+\alpha)}_{\mathbb{R}^2_T}|h|^{\frac{1+\alpha}{2}}. \tag{5.62}$$

We set $B := B_R(0)$ and split the square of the double integral term in (5.61) into three parts, namely

$$\begin{aligned}
&\int_{\mathcal{C}B}\int_B \frac{\big|F(\rho,t+h) - F(\rho,t)\big|^2}{|\rho-\tilde{\rho}|^{2+2\epsilon}}\,d\rho\,d\tilde{\rho} + \int_B\int_{\mathcal{C}B} \frac{\big|F(\tilde{\rho},t+h) - F(\tilde{\rho},t)\big|^2}{|\rho-\tilde{\rho}|^{2+2\epsilon}}\,d\rho\,d\tilde{\rho} \\
&\quad + \int_B\int_B \frac{\big|F(\rho,t+h) - F(\rho,t) - F(\tilde{\rho},t+h) + F(\tilde{\rho},t)\big|^2}{|\rho-\tilde{\rho}|^{2+2\epsilon}}\,d\rho\,d\tilde{\rho} \\
&=: J_1^{(1)} + J_1^{(2)} + J_1^{(3)}.
\end{aligned} \tag{5.63}$$

4. Estimate of $J_1^{(1)}$ and $J_1^{(2)}$. Let $M := R - |\rho|$, assume $0 < h < 1$, $\epsilon < 1/2$. Proceed as follows:

$$\begin{aligned} J_1^{(1)} &\le C\Big(\|F\|_{\mathbb{R}^2_T}^{(1+\alpha)}\Big)^2 h^{1+\alpha} \int_B \int_{\mathcal{C}B_M(\rho)} |\rho - \tilde\rho|^{-2(1+\epsilon)}\, d\tilde\rho\, d\rho \\ &= C\Big(\|F\|_{\mathbb{R}^2_T}^{(1+\alpha)}\Big)^2 h^{1+\alpha} \int_B \int_M^\infty r^{-2(1+\epsilon)} r\, dr\, d\rho \\ &= C\Big(\|F\|_{\mathbb{R}^2_T}^{(1+\alpha)}\Big)^2 \frac{h^{1+\alpha}}{2\epsilon} \int_0^R (R-r)^{-2\epsilon} r\, dr \\ &\le C \frac{R^{2-2\epsilon}}{2\epsilon(1-2\epsilon)} \Big(\|F\|_{\mathbb{R}^2_T}^{(1+\alpha)} h^{\alpha/2}\Big)^2. \end{aligned} \tag{5.64}$$

$J_1^{(2)}$ can be estimated similarly.

5. Estimate of $J_1^{(3)}$. We set $\epsilon := 1/8$ and calculate as follows:

$$\begin{aligned} J_1^{(3)} &\le \int_B \int_B \frac{\Big(\|\nabla F(.\,,t+h)\|_{L^\infty(\mathbb{R}^2)} |\rho - \tilde\rho| + \|\nabla F(.\,,t)\|_{L^\infty(\mathbb{R}^2)} |\rho - \tilde\rho|\Big)^{1/2}}{|\rho - \tilde\rho|^{9/4}} \times \\ &\qquad \times \Big(|F(\rho, t+h) - F(\rho,t)| + |F(\tilde\rho, t+h) - F(\tilde\rho, t)|\Big)^{3/2} d\rho\, d\tilde\rho \\ &\le C\Big(\|F\|_{\mathbb{R}^2_T}^{(1+\alpha)}\Big)^2 \Big(h^{\frac{1+\alpha}{2}}\Big)^{3/2} \int_B \int_B \frac{1}{|\rho - \tilde\rho|^{7/4}}\, d\rho\, d\tilde\rho \\ &\le C(R)\Big(\|F\|_{\mathbb{R}^2_T}^{(1+\alpha)} h^{\alpha/2}\Big)^2. \end{aligned} \tag{5.65}$$

6. Estimate of J_2. According to [38], Section 7.9., the L^1-norm of the Fourier transform satisfies

$$\|\hat F(.\,,\tau)\|_{L^1(\mathbb{R}^2)} \le C(R,\alpha) \|F(.\,,\tau)\|_{\mathbb{R}^2}^{(1+\alpha)}. \tag{5.66}$$

Hence, from the definitions (5.60) of J_2 and (5.43) of $\hat h_2$ it follows that

$$\begin{aligned} J_2 &\le C \int_0^t \big\|\hat F(.\,,\tau)\big\|_{L^1(\mathbb{R}^2)} \big\|\partial_t \hat h_2(.\,,t+h-\tau) - \partial_t \hat h_2(.\,,t-\tau)\big\|_{L^\infty(\mathbb{R}^2)} d\tau \\ &\le C\|F\|_{\mathbb{R}^2_T}^{(1+\alpha)} \int_0^t \Big\| \int_0^\infty e^{-(s+D|\rho|^2)(t-\tau)} \frac{\sqrt{s}}{1+a^2 s} \Big(1 - e^{-(s+D|\rho|^2)h}\Big)\, ds \Big\|_{L^\infty(\mathbb{R}^2)} d\tau\,. \end{aligned} \tag{5.67}$$

It is not difficult to see that

$$\Big| \int_0^\infty e^{-s(t-\tau)} \frac{\sqrt{s}}{1+a^2 s} \Big(1 - e^{-(s+D|\rho|^2)h}\Big)\, ds \Big| \le C(1 - e^{-D|\rho|^2 h}) + \frac{C}{\sqrt{t-\tau}} \Big(1 - \frac{\sqrt{t-\tau}}{\sqrt{t-\tau+h}} e^{-D|\rho|^2 h}\Big)$$

and that

$$e^{-D|\rho|^2(t-\tau)}\big(1 - e^{-D|\rho|^2 h}\big) \le \frac{h}{t-\tau+h}\ , \quad e^{-D|\rho|^2(t-\tau)} \Big(1 - \frac{\sqrt{t-\tau}}{\sqrt{t-\tau+h}} e^{-D|\rho|^2 h}\Big) \le \frac{\sqrt{h}}{\sqrt{t-\tau+h}}\,.$$

Employing these three estimates in (5.67) yields

$$\begin{aligned} J_2 &\le C\|F\|_{\mathbb{R}^2_T}^{(1+\alpha)} \int_0^t \Big(\frac{\sqrt{h}}{t-\tau+h} + \frac{\sqrt{h}}{\sqrt{t-\tau}\sqrt{t-\tau+h}} \Big) d\tau \\ &= C\|F\|_{\mathbb{R}^2_T}^{(1+\alpha)} \sqrt{h}\Big(-\log(h) + \log(t+h) + \log(h) - 2\log(\sqrt{t+h}-\sqrt{t}) \Big) \\ &\le h^{\alpha/2} C\|F\|_{\mathbb{R}^2_T}^{(1+\alpha)} \underbrace{h^{\frac{1-\alpha}{2}} \log\left(\frac{\sqrt{T+h}}{\sqrt{T+h}-\sqrt{T}} \right)}_{\le C_2(T,\alpha)} . \end{aligned} \tag{5.68}$$

We note that C_2 can be chosen independent of h. Moreover, C_2 remains bounded as $T \to 0$.

7. Estimate of J_3. Equation (5.66) and the definitions (5.60) of J_3 and (5.43) of $\hat{h}_2$ yield

$$\begin{aligned} J_3 &\le C(R)\|F\|_{\mathbb{R}^2_T}^{(1+\alpha)} \int_t^{t+h} \|\partial_t \hat{h}_2(.\,, t+h-\tau)\|_{L^\infty(\mathbb{R}^2)} d\tau \\ &= C(R)\|F\|_{\mathbb{R}^2_T}^{(1+\alpha)} \int_t^{t+h} \int_0^\infty e^{-s(t+h-\tau)} \frac{\sqrt{s}}{1+a^2 s}\, ds\, d\tau \\ &\le C(R)\|F\|_{\mathbb{R}^2_T}^{(1+\alpha)} \int_t^{t+h} \int_0^\infty \frac{e^{-s(t+h-\tau)}}{\sqrt{s}}\, ds\, d\tau \\ &= \sqrt{h}\, C(R)\|F\|_{\mathbb{R}^2_T}^{(1+\alpha)}\, 2\sqrt{\pi}\,. \end{aligned} \tag{5.69}$$

Finally, the equations (5.60)-(5.65), (5.68), and (5.69) yield $\langle \partial_t \vartheta_2 \rangle_{t,\mathbb{R}^2_T}^{(\alpha/2)} \le C\|F\|_{\mathbb{R}^2_T}^{(1+\alpha)}$. □

Proposition 5.3.1 (Solution of problem (5.25) and problem (5.24))**.** *Let F be a compactly supported function in $H_0^{1+\alpha,\frac{1+\alpha}{2}}(\mathbb{R}^2_T)$. Then both problem* (5.25) *and* (5.24) *(the latter with $\chi(\partial_z\zeta_2 - 2c\sigma_2 - c\sigma_1)$ replaced by F) have a unique solution in $H_0^{2+\alpha,\frac{2+\alpha}{2}}(D^3_T) \times H_0^{2+\alpha,\frac{2+\alpha}{2}}(\mathbb{R}^2_T)$. Both solutions fulfill the estimate*

$$\|\zeta\|_{D^3_T}^{(2+\alpha)} + \|\sigma\|_{\mathbb{R}^2_T}^{(2+\alpha)} \le C\|F\|_{\mathbb{R}^2_T}^{(1+\alpha)}, \tag{5.70}$$

where C remains bounded as $T \to 0$.

Proof. 1. Regarding (5.25), the equations (5.44), (5.45), and (5.55) yield $\|\sigma\|_{\mathbb{R}^2_T}^{(2+\alpha)} \le C\|F\|_{\mathbb{R}^2_T}^{(1+\alpha)}$. Using Lemma 5.3.1 we verify that $\|\zeta\|_{\mathbb{R}^3_T}^{(2+\alpha)} \le C\|F\|_{\mathbb{R}^2_T}^{(1+\alpha)}$. A brief sketch of the argument should be sufficient. From (5.26) it follows that for $z > 0$

$$\zeta(x,y,z,t) = \int_0^t \int_{-\infty}^\infty \int_{-\infty}^\infty \sigma(x-\xi_1, y-\xi_2, t-s) g(\xi_1,\xi_2,z,s)\, d\xi_1\, d\xi_2\, ds\,,$$

where $g := \mathcal{F}^{-1}\mathcal{L}^{-1}\left(\frac{p}{k} \exp\left[-\left(\frac{p+D|\rho|^2}{D} \right)^{1/2} z \right] \right)$. Hence, regarding the variables x, y, and t, the function ζ has at least the regularity of σ. Furthermore, g is smooth enough with respect to z.

On the plane $\{z = 0\}$, the equations (5.26) and (5.27) imply

$$\tilde{\zeta}(\rho, 0, p) = \frac{\tilde{F}(\rho, p)}{k + d\sqrt{D^{-1}p + |\rho|^2}}\,.$$

Because of the prefactor $\left(k + d\sqrt{D^{-1}p + |\rho|^2}\right)^{-1}$, the function ζ gains one order of regularity.

2. When the right hand side $\chi(\partial_z\zeta_2 - 2c\sigma_2 - c\sigma_1)$ of (5.24) is replaced by F, the main difference that remains to (5.25) is the sign of k in the boundary condition. However, with regard to (5.70) and (5.99) it is clear that—assuming small time intervals—the solvability of (5.24) follows immediately from the above proven solvability of (5.25) by means of Banach's fixed point theorem. Furthermore, estimate (5.70) carries over to the solution of (5.24).

□

Investigation of (5.23) Problem (5.23) has been investigated by Bazalii and Degtyarev [7] and by Kusaka and Tani [51]. According to their results, the following proposition holds:

Proposition 5.3.2 (Solution of problem (5.23))**.** *Let F be a compactly supported function in $H_0^{1+\alpha,\frac{1+\alpha}{2}}(\mathbb{R}^2_T)$. Then problem (5.23) has a unique solution $(\zeta_2, \sigma_2) \in H_0^{2+\alpha,\frac{2+\alpha}{2}}(D^3_T) \times H_0^{2+\alpha,\frac{2+\alpha}{2}}(\mathbb{R}^2_T)$. This solution fulfills the estimate*

$$\|\zeta_2\|^{(2+\alpha)}_{D^3_T} + \|\sigma_2\|^{(2+\alpha)}_{\mathbb{R}^2_T} \le C\|F\|^{(1+\alpha)}_{\mathbb{R}^2_T}, \tag{5.71}$$

where C remains bounded as $T \to 0$. Furthermore, σ_2 can be represented as ($x' := (x, y)$)

$$\sigma_2(x', t) = \int_0^t \int_{\mathbb{R}^2} K(x' - \xi', t - \tau)F(\xi', \tau)\, d\xi' d\tau \tag{5.72}$$

with

$$K(x', t) := \frac{1}{4\pi^{1/2}} \frac{cd}{kD^{3/2}} \int_0^t (t - \tau)\tau^{-5/2} \exp\left(-\frac{|x'|^2}{4D\tau} - \frac{c^2d^2(t - \tau)^2}{4k^2D\tau}\right) d\tau. \tag{5.73}$$

Solution of the coupled system (5.22)-(5.24) and correction of the defect

Proposition 5.3.3 (Solution of the system (5.22)-(5.24))**.** *Provided that T is sufficiently small and that $F \in H_0^{1+\alpha,\frac{1+\alpha}{2}}(D^2_T)$ is a compactly supported function, the system (5.22)-(5.24) has a unique solution $(\zeta_1, \zeta_2, \zeta_3, \sigma_1, \sigma_2) \in \left(H_0^{2+\alpha,\frac{2+\alpha}{2}}(D^3_T)\right)^3 \times \left(H_0^{2+\alpha,\frac{2+\alpha}{2}}(\mathbb{R}^2_T)\right)^2$.*

Proof. Problem (5.23) can be solved independently of (5.22) and (5.24). To cope with the coupling of (5.22) and (5.24), the right hand side $2d\chi\partial_z\zeta_3$ of (5.22) is replaced by $2d\chi\partial_z h$, with a fixed $h \in H_0^{2+\alpha,\frac{2+\alpha}{2}}(D^3_T)$. The so obtained (ζ_1, σ_1), along with (ζ_2, σ_2), is inserted into (5.24). According to Proposition 5.3.1 and Proposition 5.3.2, the operator

$$\begin{array}{rccc} L_F: & H_0^{2+\alpha,\frac{2+\alpha}{2}}(D^3_T) & \to & H_0^{2+\alpha,\frac{2+\alpha}{2}}(D^3_T) \\ & h & \mapsto & \zeta_3 \end{array}$$

is well defined. Furthermore, we can derive the estimate

$$\|L_F h - L_F \tilde{h}\|_{D_T^3}^{(2+\alpha)} \leq C\|\sigma_1 - \tilde{\sigma_1}\|_{\mathbb{R}_T^2}^{(1+\alpha)} \leq C\sqrt{T}\|\sigma_1 - \tilde{\sigma_1}\|_{\mathbb{R}_T^2}^{(2+\alpha)} \leq C\sqrt{T}\|h - \tilde{h}\|_{D_T^3}^{(2+\alpha)},$$

where (5.99) has been employed to obtain the second inequality. Thus, L_F is a strict contraction for sufficiently small T. □

The aim is to correct the remaining "defect" $d\partial_z\zeta_3$ in a ball $B_R(0) \subset \{(x,y) : \chi(x,y) = 1\}$ (cf. page 60). For this purpose, we examine (5.22)-(5.24), but now with (5.23) containing $F - \chi d\partial_z g$ as right hand side instead of F alone. For small T we consider the operator

$$K_F : \begin{array}{ccc} H_0^{2+\alpha,\frac{2+\alpha}{2}}(D_T^3) & \to & H_0^{2+\alpha,\frac{2+\alpha}{2}}(D_T^3) \\ g & \mapsto & \zeta_3 \end{array} .$$

K_F is well-defined according to Proposition 5.3.3. Furthermore, the functions $\xi_2 := \zeta_1 + \zeta_2 + \zeta_3$ and $\sigma := \sigma_1 + \sigma_2$ fulfill

$$\begin{cases} \partial_t \xi_2 - D\Delta\xi_2 = 0 & \text{in } B_T^3 \\ \partial_z \xi_2 = k\xi_2 + c\sigma & \text{on } B_T^2 \\ \xi_2(t=0) = 0 & \text{in } \mathbb{R}_+^3 \\ \partial_t \sigma - d\partial_z \xi_2 = F - d\partial_z g + d\partial_z \zeta_3 & \text{on } B_T^2 \\ \sigma(t=0) = 0 & \text{on } \mathbb{R}^2 , \end{cases} \tag{5.74}$$

where $B_T^3 := D_T^3 \cap (B_R(0) \times \{z \geq 0\} \times [0,T])$, $B_T^2 := D_T^2 \cap (B_R(0) \times \{0\} \times [0,T])$. Thus, on the indicated sets, a fixed point of K_F fulfills the equations of (5.21). Such a fixed point will be provided by Banach's theorem (cf. the proof of Proposition 5.3.4). To demonstrate K_F to be a strict contraction, we make substantially use of the representation formulas (5.72) and (5.73) of σ_2 (cf. Lemma 5.3.7), combined with a scaling argument (Lemma 5.3.6) and the following estimate:

Lemma 5.3.5 (An estimate of the solution of (5.23))**.** *Suppose that T is sufficiently small. Let $(\zeta_2, \sigma_2) \in H_0^{2+\alpha,\frac{2+\alpha}{2}}(D_T^3) \times H_0^{2+\alpha,\frac{2+\alpha}{2}}(\mathbb{R}_T^2)$ be the unique solution of (5.23) according to Proposition 5.3.2. Then σ_2 can be controlled solely by its second spatial derivatives and $T^{\alpha/2}$ times the norm of F, i.e.*

$$\|\sigma_2\|_{\mathbb{R}_T^2}^{(2+\alpha)} \leq C\left(\sum_{i,j=1}^{2}\left(\|\partial_i\partial_j\sigma_2\|_{\mathbb{R}_T^2}^{(0)} + \langle\partial_i\partial_j\sigma_2\rangle_{x,\mathbb{R}_T^2}^{(\alpha)} + \langle\partial_i\partial_j\sigma_2\rangle_{t,\mathbb{R}_T^2}^{(\alpha/2)}\right) + T^{\alpha/2}\|F\|_{\mathbb{R}_T^2}^{(1+\alpha)}\right),$$

where C remains bounded as $T \to 0$.

Proof. Since ζ_2 solves a Dirichlet problem in half space, it satisfies the estimate

$$\|\zeta_2\|_{D_T^3}^{(2+\alpha)} \leq C\|\sigma_2\|_{\mathbb{R}_T^2}^{(2+\alpha)}, \tag{5.75}$$

where C remains bounded as $T \to 0$ (cf. [52, p. 322]). Observe that

$$\sigma_2(x',t) = \int_0^t d\partial_z\zeta_2(x',0,\tau) + F(x',\tau)\,d\tau .$$

Hence, by the use of (5.75) and (5.99) we obtain

$$\|\sigma_2\|^{(0)}_{\mathbb{R}^2_T} + \|\nabla\sigma_2\|^{(0)}_{\mathbb{R}^2_T} + \|\partial_t\sigma_2\|^{(0)}_{\mathbb{R}^2_T} \le CT^{\frac{1+\alpha}{2}}\Big(\|\sigma_2\|^{(2+\alpha)}_{\mathbb{R}^2_T} + \|F\|^{(1+\alpha)}_{\mathbb{R}^2_T}\Big)\,. \tag{5.76}$$

Furthermore, using (5.75),

$$\begin{aligned}\frac{\big|\partial_t\sigma_2(x',t)-\partial_t\sigma_2(x',s)\big|}{|t-s|^{\alpha/2}} &\le d\frac{\big|\partial_z\zeta_2(x',0,t)-\partial_z\zeta_2(x',0,s)\big|}{|t-s|^{\frac{1+\alpha}{2}}}|t-s|^{1/2} + \frac{\big|F(x',t)-F(x',s)\big|}{|t-s|^{\frac{1+\alpha}{2}}}|t-s|^{1/2}\\ &\le C\sqrt{T}\Big(\langle\partial_z\zeta_2\rangle^{(\frac{1+\alpha}{2})}_{t,D^3_T} + \langle F\rangle^{(\frac{1+\alpha}{2})}_{t,\mathbb{R}^2_T}\Big)\\ &\le C\sqrt{T}\Big(\|\sigma_2\|^{(2+\alpha)}_{\mathbb{R}^2_T} + \|F\|^{(1+\alpha)}_{\mathbb{R}^2_T}\Big)\,.\end{aligned}$$

Once more, we employ (5.99) and obtain

$$\begin{aligned}\frac{\big|\partial_t\sigma_2(x',t)-\partial_t\sigma_2(\tilde{x}',t)\big|}{|x'-\tilde{x}'|^{\alpha}} &\le d\|D^2\zeta_2\|^{(0)}_{D^3_T}\rho_0^{1-\alpha} + \|\nabla F\|^{(0)}_{\mathbb{R}^2_T}\rho_0^{1-\alpha}\\ &\le CT^{\alpha/2}\Big(\|\sigma_2\|^{(2+\alpha)}_{\mathbb{R}^2_T} + \|F\|^{(1+\alpha)}_{\mathbb{R}^2_T}\Big)\,,\end{aligned}$$

and, for $t \ge s$,

$$\begin{aligned}\frac{\big|\partial_i\sigma_2(x',t)-\partial_i\sigma_2(x',s)\big|}{|t-s|^{\frac{1+\alpha}{2}}} &\le C\int_s^t \frac{\big|\partial_i\partial_z\zeta_2(x',0,\tau)+\partial_i F(x',\tau)\big|}{|t-s|^{\frac{1+\alpha}{2}}}\,d\tau\\ &\le CT^{\frac{1-\alpha}{2}}T^{\alpha/2}\Big(\|\sigma_2\|^{(2+\alpha)}_{\mathbb{R}^2_T} + \|F\|^{(1+\alpha)}_{\mathbb{R}^2_T}\Big)\,.\end{aligned}$$

Thus,

$$\langle\partial_t\sigma_2\rangle^{(\alpha/2)}_{t,\mathbb{R}^2_T} + \langle\partial_t\sigma_2\rangle^{(\alpha)}_{x,\mathbb{R}^2_T} + \sum_{i=1}^{2}\langle\partial_i\sigma_2\rangle^{(\frac{1+\alpha}{2})}_{t,\mathbb{R}^2_T} \le CT^{\alpha/2}\Big(\|\sigma_2\|^{(2+\alpha)}_{\mathbb{R}^2_T} + \|F\|^{(1+\alpha)}_{\mathbb{R}^2_T}\Big)\,. \tag{5.77}$$

Now, the assertion of the Lemma follows from (5.76) and (5.77), provided that $CT^{\alpha/2} < 1$. □

Lemma 5.3.6 (Scaling properties)**.** *Let $\tilde{t} := t/T$ and define $\underline{\sigma}(x,y,\tilde{t}) := \sigma(x,y,t)$. Then, according to the chain rule, $\partial_{\tilde{t}}\underline{\sigma}(x,y,\tilde{t}) = T\partial_t\sigma(x,y,t)$ and*

$$\begin{aligned}\|D^r_{\tilde{t}}D^s_x\underline{\sigma}\|^{(0)}_{\mathbb{R}^2_1} &= T^r\|D^r_tD^s_x\sigma\|^{(0)}_{\mathbb{R}^2_T} & \langle\partial_{\tilde{t}}\underline{\sigma}\rangle^{(\alpha)}_{x,\mathbb{R}^2_1} &= T\,\langle\partial_t\sigma\rangle^{(\alpha)}_{x,\mathbb{R}^2_T}\\ \langle\partial_{\tilde{t}}\underline{\sigma}\rangle^{(\alpha/2)}_{\tilde{t},\mathbb{R}^2_1} &= T^{1+\frac{\alpha}{2}}\,\langle\partial_t\sigma\rangle^{(\alpha/2)}_{t,\mathbb{R}^2_T} & \langle\partial_i\underline{\sigma}\rangle^{(\frac{1+\alpha}{2})}_{\tilde{t},\mathbb{R}^2_1} &= T^{\frac{1+\alpha}{2}}\,\langle\partial_i\sigma\rangle^{(\frac{1+\alpha}{2})}_{t,\mathbb{R}^2_T}\\ \langle\partial_i\partial_j\underline{\sigma}\rangle^{(\alpha)}_{x,\mathbb{R}^2_1} &= \langle\partial_i\partial_j\sigma\rangle^{(\alpha)}_{x,\mathbb{R}^2_T} & \langle\partial_i\partial_j\underline{\sigma}\rangle^{(\alpha/2)}_{\tilde{t},\mathbb{R}^2_1} &= T^{\frac{\alpha}{2}}\,\langle\partial_i\partial_j\sigma\rangle^{(\alpha/2)}_{t,\mathbb{R}^2_T}\,.\end{aligned}$$

In addition, $\|\underline{\sigma}\|^{(2+\alpha)}_{\mathbb{R}^2_1} \ge T^{1+\frac{\alpha}{2}}\|\sigma\|^{(2+\alpha)}_{\mathbb{R}^2_T}$ and $\|\underline{\sigma}\|^{(2+\alpha)}_{\mathbb{R}^2_1} \le \|\sigma\|^{(2+\alpha)}_{\mathbb{R}^2_T}$, provided that $0 < T \le 1$.

Proof. This is obvious. □

Proposition 5.3.4. *Provided that T is sufficiently small, K_F has a unique fixed point.*

Proof. The aim is to show that K_F is a strict contraction.

1. According to (5.70), (5.99), and (5.75) we have

$$\begin{aligned}\|\zeta_3-\tilde\zeta_3\|_{D_T^3}^{(2+\alpha)} &\le C\Big(\|\zeta_2-\tilde\zeta_2\|_{D_T^3}^{(2+\alpha)}+\sqrt{T}\|\sigma_2-\tilde\sigma_2\|_{\mathbb{R}_T^2}^{(2+\alpha)}+\sqrt{T}\|\sigma_1-\tilde\sigma_1\|_{\mathbb{R}_T^2}^{(2+\alpha)}\Big)\\ &\le C\Big(\|\sigma_2-\tilde\sigma_2\|_{\mathbb{R}_T^2}^{(2+\alpha)}+\sqrt{T}\|\zeta_3-\tilde\zeta_3\|_{D_T^3}^{(2+\alpha)}\Big)\,.\end{aligned}$$

Using the smallness assumption on T and Lemma 5.3.5 we obtain

$$\begin{aligned}\|\zeta_3-\tilde\zeta_3\|_{D_T^3}^{(2+\alpha)} &\le C\sum_{i,j=1}^{2}\Big(\|\partial_i\partial_j\sigma_2-\partial_i\partial_j\tilde\sigma_2\|_{\mathbb{R}_T^2}^{(0)}+\langle\partial_i\partial_j\sigma_2-\partial_i\partial_j\tilde\sigma_2\rangle_{x,\mathbb{R}_T^2}^{(\alpha)}\Big)\\ &\quad+C\Big(\sum_{i,j=1}^{2}\langle\partial_i\partial_j\sigma_2-\partial_i\partial_j\tilde\sigma_2\rangle_{t,\mathbb{R}_T^2}^{(\alpha/2)}+T^{\alpha/2}\|g-\tilde g\|_{D_T^3}^{(2+\alpha)}\Big)\,.\end{aligned}\tag{5.78}$$

2. The terms on the right hand side of (5.78) shall be estimated by the scaled quantities $(\underline{\zeta_2},\underline{\sigma_2})$, which are defined as in Lemma 5.3.6. For that purpose, we set $a:=DT$, $b:=dT$, and $e:=c/k$. Furthermore, we observe that $(\underline{\zeta_2},\underline{\sigma_2})$ solves

$$\begin{cases}\partial_{\tilde t}\underline{\zeta_2}-a\Delta\underline{\zeta_2}=0 & \text{in } D_1^3\\ \underline{\zeta_2}=e\underline{\sigma_2} & \text{on } D_1^2\\ \underline{\zeta_2}(\tilde t=0)=0 & \text{in } \mathbb{R}_+^3\\ \partial_{\tilde t}\underline{\sigma_2}-b\partial_z\underline{\zeta_2}=T\underline{F}-b\underline{\chi}\partial_z\underline{g} & \text{on } D_1^2\\ \underline{\sigma_2}(\tilde t=0)=0 & \text{on } \mathbb{R}^2\,.\end{cases}$$

Define

$$\underline{K}(x',\tilde t):=\frac{1}{4\pi^{1/2}}\frac{eb}{a^{3/2}}\int_0^{\tilde t}(\tilde t-\tau)\tau^{-5/2}\exp\left(-\frac{|x'|^2}{4a\tau}-\frac{e^2b^2(\tilde t-\tau)^2}{4a\tau}\right)d\tau\,,\tag{5.79}$$

then, according to Proposition 5.3.2,

$$\begin{aligned}\underline{\sigma_2}(x',\tilde t)-\underline{\tilde\sigma_2}(x',\tilde t)&=b\int_0^{\tilde t}\int_{\mathbb{R}^2}\underline{K}(x'-\xi',\tilde t-\tau)(\underline{\chi}\partial_z\underline{\tilde g}-\underline{\chi}\partial_z\underline{g})(\xi',\tau)\,d\xi'd\tau\\ &=:b\underline{K}*(\underline{\chi}\partial_z\underline{\tilde g}-\underline{\chi}\partial_z\underline{g})(x',\tilde t)\,.\end{aligned}$$

Since $\underline{\chi}\partial_z\underline{\tilde g}-\underline{\chi}\partial_z\underline{g}$ has compact support, we deduce

$$\partial_i\partial_j(\underline{\sigma_2}-\underline{\tilde\sigma_2})=b\,\partial_i\underline{K}*\partial_j(\underline{\chi}\partial_z\underline{\tilde g}-\underline{\chi}\partial_z\underline{g})\,.$$

Hence, due to the convolution estimate (cf. [2, p. 94]),

$$\begin{aligned}\|\partial_i\partial_j(\underline{\sigma_2}-\underline{\tilde\sigma_2})\|_{\mathbb{R}_1^2}^{(0)}&\le b\|\partial_i\underline{K}\|_{L^1(\mathbb{R}_1^2)}\|\partial_j(\underline{\chi}\partial_z\underline{\tilde g}-\underline{\chi}\partial_z\underline{g})\|_{\mathbb{R}_1^2}^{(0)}\\ &\le Cb\|\partial_i\underline{K}\|_{L^1(\mathbb{R}_1^2)}\|\underline{g}-\underline{\tilde g}\|_{D_1^3}^{(2+\alpha)}\,.\end{aligned}\tag{5.80}$$

Similar estimates are obtained for the remaining seminorms on the right hand side of (5.78).

3. Using (5.78), Lemma 5.3.6, and the estimate (5.80) we end up with

$$\begin{aligned}
\|\zeta_3 - \tilde{\zeta}_3\|_{D_T^3}^{(2+\alpha)} &\le C \sum_{i,j=1}^{2} \Big(\|\partial_i\partial_j \underline{\sigma_2} - \partial_i\partial_j \tilde{\underline{\sigma}_2}\|_{\mathbb{R}_1^2}^{(0)} + \langle \partial_i\partial_j \underline{\sigma_2} - \partial_i\partial_j \tilde{\underline{\sigma}_2} \rangle_{x,\mathbb{R}_1^2}^{(\alpha)} \Big) \\
&\quad + C\Big(\frac{1}{T^{\alpha/2}} \sum_{i,j=1}^{2} \langle \partial_i\partial_j \underline{\sigma_2} - \partial_i\partial_j \tilde{\underline{\sigma}_2} \rangle_{\tilde{t},\mathbb{R}_1^2}^{(\alpha/2)} + T^{\alpha/2} \|g - \tilde{g}\|_{D_T^3}^{(2+\alpha)} \Big) \\
&\le C\Big(\sum_{i=1}^{2} \frac{b}{T^{\alpha/2}} \|\partial_i \underline{K}\|_{L^1(\mathbb{R}_1^2)} \|\underline{g} - \underline{\tilde{g}}\|_{D_1^3}^{(2+\alpha)} + T^{\alpha/2} \|g - \tilde{g}\|_{D_T^3}^{(2+\alpha)} \Big) \\
&\le \underbrace{C\Big(\sum_{i=1}^{2} \frac{b}{T^{\alpha/2}} \|\partial_i \underline{K}\|_{L^1(\mathbb{R}_1^2)} + T^{\alpha/2} \Big)}_{=:\Theta} \|g - \tilde{g}\|_{D_T^3}^{(2+\alpha)} .
\end{aligned}$$

The factor Θ becomes small for sufficiently small T, according to Lemma 5.3.7. □

Lemma 5.3.7. *Let $\underline{K}$ be defined according to* (5.79)*. Then*

$$\frac{b}{T^{\alpha/2}} \|\partial_i \underline{K}\|_{L^1(\mathbb{R}_1^2)} \to 0 \quad \text{as} \quad T \to 0 \qquad (i = 1, 2) . \tag{5.81}$$

Proof. 1. From (5.79) and the definition of a, b, and e on page 74 it follows that

$$\begin{aligned}
\frac{b}{T^{\alpha/2}} \|\partial_i \underline{K}\|_{L^1(\mathbb{R}_1^2)} &= \frac{CT^2}{T^{\frac{\alpha}{2}+\frac{3}{2}}} \int_0^1 \int_{\mathbb{R}^2} \Big| \int_0^{\tilde{t}} \frac{\tilde{t}-\tau}{T\tau^{\frac{5}{2}+1}} x_i \exp\left(-\frac{C|x'|^2}{T\tau} - \frac{CT^2(\tilde{t}-\tau)^2}{T\tau} \right) d\tau \Big| dx' d\tilde{t} \\
&\le CT^{-\frac{1+\alpha}{2}} \int_0^1 \int_0^{\infty} \int_0^{\tilde{t}} \frac{\tilde{t}-\tau}{\tau^{7/2}} r^2 \exp\left(-\frac{Cr^2}{T\tau} - \frac{CT(\tilde{t}-\tau)^2}{\tau} \right) d\tau dr d\tilde{t} \\
&= CT^{-\frac{1+\alpha}{2}} \int_0^1 \int_0^{\tilde{t}} \frac{\tilde{t}-\tau}{\tau^{7/2}} \exp\left(-\frac{CT(\tilde{t}-\tau)^2}{\tau} \right) \underbrace{\int_0^{\infty} r^2 \exp\left(-\frac{Cr^2}{T\tau} \right) dr}_{=CT^{3/2}\tau^{3/2}} d\tau d\tilde{t} \\
&= CT^{-\frac{\alpha}{2}} \int_0^1 \int_0^{\tilde{t}} \frac{1}{\tilde{t}+\tau} \frac{d}{d\tau} \exp\left(-\frac{CT(\tilde{t}-\tau)^2}{\tau} \right) d\tau d\tilde{t} ,
\end{aligned}$$

where $\frac{d}{d\tau} \exp\left(-\frac{CT(\tilde{t}-\tau)^2}{\tau} \right) = \frac{CT(\tilde{t}-\tau)(\tilde{t}+\tau)}{\tau^2} \exp\left(-\frac{CT(\tilde{t}-\tau)^2}{\tau} \right)$ was used in the last equation.

Hence,

$$\begin{aligned}
\frac{b}{T^{\alpha/2}}\|\partial_i \underline{K}\|_{L^1(\mathbb{R}^2_1)} &\le CT^{-\frac{\alpha}{2}} \int_0^1 \int_0^{\tilde{t}} \frac{d}{d\tilde{t}} \log(\tilde{t}+\tau) \frac{d}{d\tau} \exp\left(-\frac{CT(\tilde{t}-\tau)^2}{\tau}\right) d\tau d\tilde{t} \\
&= CT^{-\frac{\alpha}{2}} \int_0^1 \frac{d}{d\tilde{t}} \int_0^{\tilde{t}} \log(\tilde{t}+\tau) \frac{d}{d\tau} \exp\left(-\frac{CT(\tilde{t}-\tau)^2}{\tau}\right) d\tau d\tilde{t} \\
&\quad - CT^{-\frac{\alpha}{2}} \int_0^1 \int_0^{\tilde{t}} \log(\tilde{t}+\tau) \frac{d}{d\tau}\frac{d}{d\tilde{t}} \exp\left(-\frac{CT(\tilde{t}-\tau)^2}{\tau}\right) d\tau d\tilde{t} \\
&\quad - CT^{-\frac{\alpha}{2}} \int_0^1 \log(2\tilde{t}) \underbrace{\left(\frac{d}{d\tau} \exp\left(-\frac{CT(\tilde{t}-\tau)^2}{\tau}\right)\right)_{|\tau=\tilde{t}}}_{=0} d\tilde{t} \\
&=: J_1(T) + J_2(T)\,.
\end{aligned} \tag{5.82}$$

2. Estimate of J_1. We note that the expansion

$$\log(1+\tau) = \sum_{k=1}^{\infty} (-1)^{k+1} \frac{\tau^k}{k} \qquad (0 \le \tau \le 1)$$

implies

$$\log(1+\tau)\frac{1-\tau^2}{\tau^2} = \frac{1}{\tau} + O(1) \le \frac{C}{\tau} \qquad (0 \le \tau \le 1)\,.$$

In addition,

$$\exp\left(\frac{-CT(1-\tau)^2}{\tau}\right) \le C \exp\left(\frac{-CT}{\tau}\right) \qquad (0 \le \tau \le 1)\,.$$

We define $\mathrm{erf}(x) := C\int_0^x e^{-\tau^2} d\tau$, where C is a suitable constant. Using these relations and $\alpha < 1$ we obtain

$$\begin{aligned}
J_1(T) &= CT^{1-\frac{\alpha}{2}} \int_0^1 \log(1+\tau) \frac{1-\tau^2}{\tau^2} \exp\left(-\frac{CT(1-\tau)^2}{\tau}\right) d\tau \\
&\le CT^{1-\frac{\alpha}{2}} \int_0^1 \frac{\exp\left(-\frac{CT}{\tau}\right)}{\tau} d\tau \\
&\le CT^{1-\frac{\alpha}{2}} \int_1^{\infty} \frac{\exp(-CT\tau)}{\sqrt{\tau}} d\tau \\
&= CT^{1-\frac{\alpha}{2}} \frac{\sqrt{\pi}}{\sqrt{CT}} \left(1 - \mathrm{erf}\left(\sqrt{CT}\right)\right) \\
&\le CT^{\frac{1-\alpha}{2}} \to 0 \qquad (T \to 0)\,.
\end{aligned} \tag{5.83}$$

3. Estimate of J_2. By partial integration, we obtain

$$\begin{aligned} J_2(T) &= -CT^{-\frac{\alpha}{2}} \int_0^1 \int_0^{\tilde{t}} \log(\tilde{t}+\tau) \frac{d}{d\tau} \left(-2CT \frac{\tilde{t}-\tau}{\tau} \exp\left(-\frac{CT(\tilde{t}-\tau)^2}{\tau} \right) \right) d\tau d\tilde{t} \\ &\leq CT^{1-\frac{\alpha}{2}} \int_0^1 \int_0^{\tilde{t}} \frac{\tilde{t}-\tau}{(\tilde{t}+\tau)\tau} \exp\left(-\frac{CT(\tilde{t}-\tau)^2}{\tau} \right) d\tau d\tilde{t} \\ &\leq CT^{1-\frac{\alpha}{2}} \int_0^1 \frac{1}{\tau} \int_0^1 \exp\left(-\frac{CT\tilde{t}^2}{\tau} \right) d\tilde{t} d\tau \\ &\leq CT^{1-\frac{\alpha}{2}} \int_0^1 \left(\tau \sqrt{\frac{CT}{\tau}} \right)^{-1} \operatorname{erf}\left(\sqrt{\frac{CT}{\tau}} \right) d\tau \\ &\leq CT^{1-\frac{\alpha}{2}} \int_0^1 (T\tau)^{-\frac{1}{2}} d\tau \\ &\leq CT^{\frac{1-\alpha}{2}} \to 0 \quad (T \to 0)\,. \end{aligned} \tag{5.84}$$

Hence, (5.81) follows from (5.82), (5.83), and (5.84). □

Lemma 5.3.8. *Assume that T is sufficiently small. Let $\xi_2 := \zeta_1 + \zeta_2 + \zeta_3$, $\sigma := \sigma_1 + \sigma_2$. Here, ζ_i and σ_i solve the system* (5.22)-(5.24)*, where, according to Proposition 5.3.4,* (5.23) *is taken with right hand side $F - d\chi\partial_z\zeta_3$ instead of F. Then*

$$\|\xi_2\|_{D_T^3}^{(2+\alpha)} + \|\sigma\|_{\mathbb{R}_T^2}^{(2+\alpha)} \leq C\|F\|_{\mathbb{R}_T^2}^{(1+\alpha)}, \tag{5.85}$$

and C remains bounded as $T \to 0$.

Proof. First, we observe that, according to (5.70) and (5.99),

$$\|\sigma_1\|_{\mathbb{R}_T^2}^{(2+\alpha)} \leq C\|\zeta_3\|_{D_T^3}^{(2+\alpha)} \leq C\left(\|\zeta_2\|_{D_T^3}^{(2+\alpha)} + \sqrt{T}\|\sigma_2\|_{\mathbb{R}_T^2}^{(2+\alpha)} + \sqrt{T}\|\sigma_1\|_{\mathbb{R}_T^2}^{(2+\alpha)} \right). \tag{5.86}$$

Because of (5.75), we obtain for sufficiently small T

$$\|\sigma_1\|_{\mathbb{R}_T^2}^{(2+\alpha)} \leq C\|\sigma_2\|_{\mathbb{R}_T^2}^{(2+\alpha)}. \tag{5.87}$$

In addition, due to (5.71),

$$\|\sigma_2\|_{\mathbb{R}_T^2}^{(2+\alpha)} \leq C\left(\|F\|_{\mathbb{R}_T^2}^{(1+\alpha)} + \|\zeta_3\|_{D_T^3}^{(2+\alpha)} \right). \tag{5.88}$$

By calculations similar to those of the proof of Proposition 5.3.4 we deduce

$$\|\zeta_3\|_{D_T^3}^{(2+\alpha)} \leq C\Big(\sum_{i=1}^{2} \frac{T}{T^{\alpha/2}} \|\partial_i \underline{K}\|_{L^1(\mathbb{R}_1^2)} + T^{\alpha/2} \Big) \Big(\|\zeta_3\|_{D_T^3}^{(2+\alpha)} + \|F\|_{\mathbb{R}_T^2}^{(1+\alpha)} \Big)\,.$$

Hence, using Lemma 5.3.7, we conclude that for small T

$$\|\zeta_3\|_{D_T^3}^{(2+\alpha)} \leq C\|F\|_{\mathbb{R}_T^2}^{(1+\alpha)}. \tag{5.89}$$

Inserting (5.89) into estimate (5.88) yields

$$\|\sigma_2\|^{(2+\alpha)}_{\mathbb{R}^2_T} \leq C\|F\|^{(1+\alpha)}_{\mathbb{R}^2_T}. \tag{5.90}$$

By combination of (5.87) and (5.90) we obtain

$$\|\sigma_1 + \sigma_2\|^{(2+\alpha)}_{\mathbb{R}^2_T} \leq C\|F\|^{(1+\alpha)}_{\mathbb{R}^2_T}. \tag{5.91}$$

From (5.70) and (5.89) it follows that

$$\|\zeta_1\|^{(2+\alpha)}_{D^3_T} \leq C\|\zeta_3\|^{(2+\alpha)}_{D^3_T} \leq C\|F\|^{(1+\alpha)}_{\mathbb{R}^2_T},$$

and, by the use of (5.75) and (5.90),

$$\|\zeta_2\|^{(2+\alpha)}_{D^3_T} \leq C\|F\|^{(1+\alpha)}_{\mathbb{R}^2_T}.$$

Thus,

$$\|\zeta_1 + \zeta_2 + \zeta_3\|^{(2+\alpha)}_{D^3_T} \leq C\|F\|^{(1+\alpha)}_{\mathbb{R}^2_T}. \tag{5.92}$$

□

Solution of (5.19) in half space

Observe that on $\{(x, y) : \chi(x, y) = 1\}$ the solution ξ_1 of the half space problem corresponding to (5.19) can be written as $\xi_1 = \xi_1^{(1)} + \xi_1^{(2)}$, where $\xi_1^{(1)}$ solves the Dirichlet problem

$$\begin{cases} \partial_t \xi_1^{(1)} - D\Delta\xi_1^{(1)} = F_1 & \text{in } D^3_T \\ \xi_1^{(1)} = 0 & \text{on } D^2_T \\ \xi_1^{(1)}(t=0) = 0 & \text{in } \mathbb{R}^3_+ \end{cases} \tag{5.93}$$

and $\xi_1^{(2)}$ is solution to

$$\begin{cases} \partial_t \xi_1^{(2)} - D\Delta\xi_1^{(2)} = 0 & \text{in } D^3_T \\ \partial_z \xi_1^{(2)} = k\xi_1^{(2)} - \chi(\partial_z \xi_1^{(1)} - F_2) & \text{on } D^2_T \\ \xi_1^{(2)}(t=0) = 0 & \text{in } \mathbb{R}^3_+ \,. \end{cases} \tag{5.94}$$

Problem (5.93) is treated in [52], Section 4.6 Theorem 6.1., and problem (5.94) is covered by Proposition 5.3.1 solving (5.25). The so obtained $\xi_1 = \xi_1^{(1)} + \xi_1^{(2)}$ satisfies the estimate

$$\|\xi_1\|^{(2+\alpha)}_{D^3_T} \leq C\Big(\|F_1\|^{(\alpha)}_{D^3_T} + \|F_2\|^{(1+\alpha)}_{\mathbb{R}^2_T}\Big), \tag{5.95}$$

where C remains bounded as $T \to 0$.

5.3.2 Solution of the linear problem in Q_T

Now, the results obtained for the half space in the case of constant coefficients k, c, and d are used to solve the original problem (5.18) that is posed in Q_T with (x,t)-dependent coefficients.

Theorem 5.3.1 (Local existence in time)**.** *Provided that T is sufficiently small, for each right hand side $(F_1,F_2,F_3)\in\mathcal{R}_1$ the linear problem* (5.18) *has a unique solution $(\xi,\sigma)\in\mathcal{R}_2$. Furthermore,*

$$\|\xi\|_{Q_T}^{(2+\alpha)}+\|\sigma\|_{S_T}^{(2+\alpha)}\le C\Big(\|F_1\|_{Q_T}^{(\alpha)}+\|F_2\|_{S_T}^{(1+\alpha)}+\|F_3\|_{S_T}^{(1+\alpha)}\Big)\,, \tag{5.96}$$

where $C=C(D,k,c,d,T)$ remains bounded as $T\to 0$.

Proof. 1. First, we assume that k, c, and d are positive constants: $k\equiv k_0$, $c\equiv c_0$, and $d\equiv d_0$.

Let $\{\Omega^{(j)}\}$ and $\{\omega^{(j)}\}$ $(j\in M_1\cup M_2)$ be two systems of coverings of $\overline{\Omega_0}$ constructed in the same way as in [52], Section 4.4., and let λ be a positive constant to be specified later. For $j\in M_1$, $\Omega^{(j)}$ and $\omega^{(j)}$ are cubes with common centers which are contained in the interior of Ω_0. Their edges are assumed to be parallel to the coordinate axes, with length λ and $\lambda/2$ $(0<\lambda<1)$, respectively. For $j\in M_2$, $\Omega^{(j)}$ and $\omega^{(j)}$ have common parts with $\partial\Omega_0$, which are defined in local coordinates $\{z\}$ in the neighborhood of $\partial\Omega_0$ as

$$\begin{aligned}\Omega^{(j)}&=\Pi_x^z\big(\{|z_i|\le\lambda\quad(i=1,2),\quad 0\le z_3-q(z_1,z_2)\le 2\lambda\}\big)\,,\\ \omega^{(j)}&=\Pi_x^z\big(\{|z_i|\le\frac{\lambda}{2}\quad(i=1,2),\quad 0\le z_3-q(z_1,z_2)\le \lambda\}\big)\,.\end{aligned}$$

Here, $z_3=q(z_1,z_2)$ represents part of $\partial\Omega_0$. Π_x^z denotes the transformation from the local coordinates z to the coordinates x. Let Π_z^x denote the inverse transformation from x to z. For a function $f(z)$ set $(\Pi_x^z f)(x):=f\big(\Pi_z^x(x)\big)$. Similarly, let $(\Pi_z^x g)(z):=g\big(\Pi_x^z(z)\big)$ for a function $g(x)$. The vector $e_3^{(j)}$ shall be given by $(0,0,1)^T$ in the local coordinates of $\Omega^{(j)}$, $j\in M_2$. Of course, Π_x^z and Π_z^x also depend on j. However, this is omitted in their notation for the sake of brevity.

We define a partition of unity subordinate to $\{\Omega^{(j)}\}$ and $\{\omega^{(j)}\}$ as follows: We choose smooth cutoff functions $\varphi^{(j)}(x)$ such that

$$\varphi^{(j)}(x)=\begin{cases}1 & x\in\omega^{(j)}\\ 0 & x\in\Omega\backslash\Omega^{(j)}\end{cases}\,,\qquad 0\le\varphi^{(j)}(x)\le 1\,,\qquad |D_x^s\varphi^{(j)}(x)|\le C\lambda^{-|s|}\,, \tag{5.97}$$

and define $\eta^{(j)}(x):=\frac{\varphi^{(j)}(x)}{\sum_l\varphi^{(l)}(x)^2}$. Finally, let $H:=\big(F_1,F_2,F_3\big)$ and define a regularizer $\mathcal{R}$ as

$$\mathcal{R}H:=\sum_{j\in M_1}\eta^{(j)}(\xi^{(j)},0)+\sum_{j\in M_2}\eta^{(j)}\Pi_x^z(\xi^{(j)},\sigma^{(j)})\,.$$

If $j\in M_1$, $\xi^{(j)}$ denotes a solution of Cauchy's problem according to [52], Chapter 4 Theorem 6.1:

$$\begin{cases}\partial_t\xi^{(j)}-D\Delta\xi^{(j)}=\varphi^{(j)}F_1 & \text{in }\ \mathbb{R}_T^3\\ \qquad\xi^{(j)}(t=0)=0 & \text{in }\ \mathbb{R}^3.\end{cases} \tag{5.98}$$

If $j \in M_2$, $(\xi^{(j)}, \sigma^{(j)})$ are determined by the procedure described in Section 5.3.1, that is they fulfill

$$\begin{cases} \partial_t \xi^{(j)} - D\Delta \xi^{(j)} = \Pi_z^x(\varphi^{(j)} F_1) & \text{in } B_T^3 \\ \partial_z \xi^{(j)} = k_0 \xi^{(j)} + c_0 \sigma^{(j)} + \Pi_z^x(\varphi^{(j)} F_2) & \text{on } B_T^2 \\ \xi^{(j)}(t=0) = 0 & \text{in } \mathbb{R}_+^3 \\ \partial_t \sigma^{(j)} - d_0 \partial_z \xi^{(j)} = \Pi_z^x(\varphi^{(j)} F_3) & \text{on } B_T^2 \\ \sigma^{(j)}(t=0) = 0 & \text{on } \mathbb{R}^2, \end{cases}$$

where B_T^3 and B_T^2 are defined as in (5.74) and assumed sufficiently large.

2. We define $E(z) := \left(e_{ij}\right)_{ij=1}^3 := \left(D_z \Pi_x^z(z)^{-1}\right)^T$, $\overline{\nabla}(z) := E(z)\nabla_z$, and observe that

$$\partial_t \Pi_x^z \xi^{(k)} = \Pi_x^z \partial_t \xi^{(k)}, \quad \nabla_x \Pi_x^z \xi^{(k)} = \Pi_x^z \overline{\nabla} \xi^{(k)}, \quad \Delta_x \Pi_x^z \xi^{(k)} = \Pi_x^z \overline{\nabla}^2 \xi^{(k)}.$$

Hence, $(\xi, \sigma) := \mathcal{R}H$ satisfies

$$\begin{cases} \partial_t \xi - D\Delta \xi = F_1 - \mathcal{T}_1 H & \text{in } Q_T \\ \partial_n \xi = k_0 \xi + c_0 \sigma + F_2 - \mathcal{T}_2 H & \text{on } S_T \\ \xi(t=0) = 0 & \text{in } \Omega_0 \\ \partial_t \sigma - d_0 \partial_n \xi = F_3 - \mathcal{T}_3 H & \text{on } S_T \\ \sigma(t=0) = 0 & \text{on } \partial\Omega_0\,, \end{cases}$$

where

$$\begin{aligned} \mathcal{T}_1 H &:= D \sum_{j \in M_1} \left(\Delta \eta^{(j)} \xi^{(j)} + 2 \nabla \eta^{(j)} \nabla \xi^{(j)} \right) \\ &\quad + D \sum_{j \in M_2} \left(\eta^{(j)} \Pi_x^z (\overline{\nabla}^2 - \Delta) \xi^{(j)} + 2 \nabla \eta^{(j)} \Pi_x^z \overline{\nabla} \xi^{(j)} + \Delta \eta^{(j)} \Pi_x^z \xi^{(j)} \right), \\ \mathcal{T}_2 H &:= \sum_{j \in M_2} \left(\eta^{(j)} (e_3^{(j)} - n) \Pi_x^z \overline{\nabla} \xi^{(j)} + \eta^{(j)} e_3^{(j)} \Pi_x^z (\nabla - \overline{\nabla}) \xi^{(j)} - \partial_n \eta^{(j)} \Pi_x^z \xi^{(j)} \right), \\ \mathcal{T}_3 H &:= -d_0 \mathcal{T}_2 H. \end{aligned}$$

3. Observe that $\mathcal{T} := (\mathcal{T}_i)_{i=1}^3 : \mathcal{R}_1 \to \mathcal{R}_1$. We will demonstrate below that $\|\mathcal{T}\| < 1$, provided that both λ and T are sufficiently small. Hence, $I - \mathcal{T}$ is invertible and $\mathcal{R}(I - \mathcal{T})^{-1} H$ solves the original equations that contain (F_1, F_2, F_3) as right hand side.

To deduce estimates of the $\mathcal{T}_i H$, we employ the following known inequalities:

$$\begin{aligned} \|u\|_{Q_T}^{(l)} &\le C T^{\frac{l'-l}{2}} \|u\|_{Q_T}^{(l')}, \quad l' > l \ge 0\,, \quad u \in H_0^{l', l'/2}(\overline{Q_T})\,, \\ \|uv\|_{Q_T}^{(l)} &\le C \left(\|u\|_{Q_T}^{(l-1)} \|v\|_{Q_T}^{(l)} + \|u\|_{Q_T}^{(l)} \|v\|_{Q_T}^{(l-1)} \right), \quad l > 1\,, \\ \|uv\|_{Q_T}^{(\alpha)} &\le C \left(\|u\|_{Q_T}^{(0)} \|v\|_{Q_T}^{(\alpha)} + \|u\|_{Q_T}^{(\alpha)} \|v\|_{Q_T}^{(0)} \right), \quad 0 < \alpha < 1\,. \end{aligned} \tag{5.99}$$

Let $Q_T^{(j)} := \Omega^{(j)} \times (0, T]$, $W_T^{(j)} := \Pi_z^x Q_T^{(j)}$. We note that $|\partial^\alpha \eta^{(j)}| \le C\lambda^{-|\alpha|}$ due to (5.97) and that

$$\|\Pi_x^z \xi^{(j)}\|_{Q_T^{(j)}}^{(\alpha)} \le C \|\xi^{(j)}\|_{W_T^{(j)}}^{(\alpha)} \le C T \|\xi^{(j)}\|_{W_T^{(j)}}^{(2+\alpha)},$$

$$\|\Pi_x^z \overline{\nabla}\xi^{(j)}\|_{Q_T^{(j)}}^{(\alpha)} \le C\|\nabla\xi^{(j)}\|_{W_T^{(j)}}^{(\alpha)} \le C\sqrt{T}\|\xi^{(j)}\|_{W_T^{(j)}}^{(2+\alpha)}.$$

The smoothness of the boundary yields $|e_{ik}(z) - \delta_{ik}| \le C\lambda + o(\lambda)$. Thus,

$$\begin{aligned}
\|\Pi_x^z(\overline{\nabla}^2 - \Delta)\xi^{(j)}\|_{Q_T^{(j)}}^{(\alpha)} &\le C\|(\overline{\nabla}^2 - \Delta)\xi^{(j)}\|_{W_T^{(j)}}^{(\alpha)} \\
&\le \|(e_{ik} - \delta_{ik})e_{ir}\partial_k\partial_r\xi^{(j)}\|_{W_T^{(j)}}^{(\alpha)} + \|(e_{kr} - \delta_{kr})\partial_k\partial_r\xi^{(j)}\|_{W_T^{(j)}}^{(\alpha)} \\
&\quad + \|e_{ik}(\partial_k e_{ir})\partial_r\xi^{(j)}\|_{W_T^{(j)}}^{(\alpha)} \\
&\le \|(e_{ik} - \delta_{ik})e_{ir}\|_{W_T^{(j)}}^{(0)}\|\partial_k\partial_r\xi^{(j)}\|_{W_T^{(j)}}^{(\alpha)} + \|(e_{ik} - \delta_{ik})e_{ir}\|_{W_T^{(j)}}^{(\alpha)}\|\partial_k\partial_r\xi^{(j)}\|_{W_T^{(j)}}^{(0)} \\
&\quad + \|(e_{kr} - \delta_{kr})\|_{W_T^{(j)}}^{(0)}\|\partial_k\partial_r\xi^{(j)}\|_{W_T^{(j)}}^{(\alpha)} + \|(e_{kr} - \delta_{kr})\|_{W_T^{(j)}}^{(\alpha)}\|\partial_k\partial_r\xi^{(j)}\|_{W_T^{(j)}}^{(0)} \\
&\quad + \|e_{ik}(\partial_k e_{ir})\|_{W_T^{(j)}}^{(0)}\|\partial_r\xi^{(j)}\|_{W_T^{(j)}}^{(\alpha)} + \|e_{ik}(\partial_k e_{ir})\|_{W_T^{(j)}}^{(\alpha)}\|\partial_r\xi^{(j)}\|_{W_T^{(j)}}^{(0)} \\
&\le C\left(\lambda + T^{\frac{\alpha}{2}} + \lambda + T^{\frac{\alpha}{2}} + \sqrt{T} + T^{\frac{1+\alpha}{2}}\right)\|\xi^{(j)}\|_{W_T^{(j)}}^{(2+\alpha)} \\
&\le C\left(\lambda + T^{\frac{\alpha}{2}}\right)\|\xi^{(j)}\|_{W_T^{(j)}}^{(2+\alpha)},
\end{aligned}$$

where we assumed $T \le 1$ in the last inequality to simplify the result. Furthermore,

$$\|\Pi_z^x(\varphi^{(j)}F_1)\|_{D_T^3}^{(\alpha)} \le C\left(1 + T^{\frac{\alpha}{2}} + \frac{T^{\frac{\alpha}{2}}}{\lambda^\alpha}\right)\|F_1\|_{Q_T^{(j)}}^{(\alpha)}$$

and

$$\|\Pi_z^x(\varphi^{(j)}F_i)\|_{D_T^2}^{(1+\alpha)} \le C\left(1 + T^{\frac{1+\alpha}{2}} + \frac{T^{\frac{\alpha}{2}}}{\lambda^\alpha} + \frac{T^{\frac{1}{2}}}{\lambda} + \frac{T^{\frac{1+\alpha}{2}}}{\lambda^{1+\alpha}}\right)\|F_i\|_{S_T^{(j)}}^{(1+\alpha)} \quad (i = 2, 3)\,,$$

where the extensions $\Pi_z^x(\varphi^{(j)}F_1)(z,t) := 0\ \forall\, z \notin \Pi_z^x\Omega^{(j)}$, etc., have been used. Therefore, using (5.95) and (5.85),

$$\begin{aligned}
\|\xi^{(j)}\|_{W_T^{(j)}}^{(2+\alpha)} &\le C\left(\|\Pi_z^x(\varphi^{(j)}F_1)\|_{D_T^3}^{(\alpha)} + \|\Pi_z^x(\varphi^{(j)}F_2)\|_{D_T^2}^{(1+\alpha)} + \|\Pi_z^x(\varphi^{(j)}F_3)\|_{D_T^2}^{(1+\alpha)}\right) \\
&\le C\left(1 + T^{\frac{\alpha}{2}} + T^{\frac{1+\alpha}{2}} + \frac{T^{\frac{\alpha}{2}}}{\lambda^\alpha} + \frac{T^{\frac{1}{2}}}{\lambda} + \frac{T^{\frac{1+\alpha}{2}}}{\lambda^{1+\alpha}}\right)\|H\|_{\mathcal{R}_1} \\
&\le C\|H\|_{\mathcal{R}_1} \quad \forall j \in M_2\,,
\end{aligned}$$

where $T \le \lambda^2$ was additionally assumed in the last inequality. In addition, the solution of the Cauchy problem (5.98) satisfies

$$\|\xi^{(j)}\|_{Q_T^{(j)}}^{(2+\alpha)} \le C\|\varphi^{(j)}F_1\|_{\mathbb{R}_T^3}^{(\alpha)} \le C\left(1 + T^{\frac{\alpha}{2}} + \frac{T^{\frac{\alpha}{2}}}{\lambda^\alpha}\right)\|F_1\|_{Q_T}^{(\alpha)} \le C\|H\|_{\mathcal{R}_1} \quad \forall j \in M_1.$$

Using these inequalities, we obtain

$$\begin{aligned}
\|\mathcal{T}_1 H\|^{(\alpha)}_{Q_T^{(l)}} &\le C \sup_{j\in M_1}\left(\|\Delta\eta^{(j)}\|^{(0)}_{Q_T^{(j)}}\|\xi^{(j)}\|^{(\alpha)}_{Q_T^{(j)}} + \|\nabla\eta^{(j)}\|^{(0)}_{Q_T^{(j)}}\|\nabla\xi^{(j)}\|^{(\alpha)}_{Q_T^{(j)}}\right)\\
&\quad + C\sup_{j\in M_2}\Big(\|\eta^{(j)}\|^{(0)}_{Q_T^{(j)}}\|\Pi_x^z(\overline{\nabla}^2-\Delta)\xi^{(j)}\|^{(\alpha)}_{Q_T^{(j)}} + \|\nabla\eta^{(j)}\|^{(0)}_{Q_T^{(j)}}\|\Pi_x^z\overline{\nabla}\xi^{(j)}\|^{(\alpha)}_{Q_T^{(j)}}\\
&\qquad + \|\Delta\eta^{(j)}\|^{(0)}_{Q_T^{(j)}}\|\Pi_x^z\xi^{(j)}\|^{(\alpha)}_{Q_T^{(j)}}\Big)\\
&\quad + C\sup_{j\in M_1}\left(\|\Delta\eta^{(j)}\|^{(\alpha)}_{Q_T^{(j)}}\|\xi^{(j)}\|^{(0)}_{Q_T^{(j)}} + \|\nabla\eta^{(j)}\|^{(\alpha)}_{Q_T^{(j)}}\|\nabla\xi^{(j)}\|^{(0)}_{Q_T^{(j)}}\right)\\
&\quad + C\sup_{j\in M_2}\Big(\|\eta^{(j)}\|^{(\alpha)}_{Q_T^{(j)}}\|\Pi_x^z(\overline{\nabla}^2-\Delta)\xi^{(j)}\|^{(0)}_{Q_T^{(j)}} + \|\nabla\eta^{(j)}\|^{(\alpha)}_{Q_T^{(j)}}\|\Pi_x^z\overline{\nabla}\xi^{(j)}\|^{(0)}_{Q_T^{(j)}}\\
&\qquad + \|\Delta\eta^{(j)}\|^{(\alpha)}_{Q_T^{(j)}}\|\Pi_x^z\xi^{(j)}\|^{(0)}_{Q_T^{(j)}}\Big)\\
&\le C\left(\frac{T}{\lambda^2}+\frac{\sqrt{T}}{\lambda}+(\lambda+T^{\frac{\alpha}{2}})+\frac{\sqrt{T}}{\lambda}+\frac{T}{\lambda^2}\right)\left(1+\frac{T^{\frac{\alpha}{2}}}{\lambda^\alpha}\right)\|H\|_{\mathcal{R}_1}\\
&\le C\left(\frac{T}{\lambda^2}+\frac{\sqrt{T}}{\lambda}+\lambda+T^{\frac{\alpha}{2}}\right)\|H\|_{\mathcal{R}_1},
\end{aligned}$$

where the Cs are independent of λ and T. Similarly, with the definition $S_T^{(l)} := (\overline{\Omega^{(l)}}\cap\partial\Omega_0)\times(0,T]$ and using $|e_3^{(j)}-n(x)| \le C|(\partial_{z_1}q,\partial_{z_2}q,0)^T(z')| \le C|D^2q(z_0')(z'-z_0')| + o(|z'-z_0'|) \le C\lambda + o(\lambda)$, we deduce

$$\|\mathcal{T}_2 H\|^{(1+\alpha)}_{S_T^{(l)}} + \|\mathcal{T}_3 H\|^{(1+\alpha)}_{S_T^{(l)}} \le C\left(\frac{T}{\lambda^{2+\alpha}}+\frac{\sqrt{T}}{\lambda^{1+\alpha}}+\lambda^{1-\alpha}\right)\|H\|_{\mathcal{R}_1}.$$

Due to the assumption $T\le\lambda^2$ we have $\|\mathcal{T}_1 H\|^{(\alpha)}_{Q_T} \le C\sup_l \|\mathcal{T}_1 H\|^{(\alpha)}_{Q_T^{(l)}}$, with C being independent of λ and T (see [52, p. 302]). Since analogous relations hold for $\|\mathcal{T}_2 H\|^{(1+\alpha)}_{S_T}$ and $\|\mathcal{T}_3 H\|^{(1+\alpha)}_{S_T}$, we end up with

$$\|\mathcal{T}\| \le C\left(\frac{T}{\lambda^{2+\alpha}}+\frac{\sqrt{T}}{\lambda^{1+\alpha}}+\lambda^{1-\alpha}+T^{\frac{\alpha}{2}}\right)\le\frac{1}{2},$$

provided that λ and $T=T(\lambda)$ are sufficiently small.

4. Now the aim is to get rid of the assumption of k, c, and d being constant coefficients. We define $\mathcal{K}H := \mathcal{R}(I-\mathcal{T})^{-1}H$ and observe that $(\xi,\sigma) := \mathcal{K}H$ solves

$$\begin{cases}
\partial_t\xi - D\Delta\xi = F_1 - \mathcal{S}_1 H & \text{in } Q_T\\
\partial_n\xi = k\xi + c\sigma + F_2 - \mathcal{S}_2 H & \text{on } S_T\\
\xi(t=0) = 0 & \text{in } \Omega_0\\
\partial_t\sigma - d\partial_n\xi = F_3 - \mathcal{S}_3 H & \text{on } S_T\\
\sigma(t=0) = 0 & \text{on } S_0,
\end{cases}$$

where $\mathcal{S}_1 H := 0$, $\mathcal{S}_2 H := (k-k_0)\xi + (c-c_0)\sigma$, $\mathcal{S}_3 H := (d-d_0)\partial_n \xi$; $\mathcal{S} := (\mathcal{S}_1, \mathcal{S}_2, \mathcal{S}_3) : \mathcal{R}_1 \to \mathcal{R}_1$. Thus, $\mathcal{K}H$ solves the original problem with right hand side $(I-\mathcal{S})H$ instead of H. It turns out that $\|\mathcal{S}\| < 1$, provided that $\|d-d_0\|_{S_T}^{(\alpha)}$ and T are sufficiently small, which follows from

$$\begin{aligned}\|\mathcal{S}_2 H\|_{S_T}^{(1+\alpha)} &\le C\left(\|k-k_0\|_{S_T}^{(1+\alpha)}\|\xi\|_{Q_T}^{(1+\alpha)} + \|c-c_0\|_{S_T}^{(1+\alpha)}\|\sigma\|_{S_T}^{(1+\alpha)}\right)\\ &\le C\sqrt{T}\left(\|k-k_0\|_{S_T}^{(1+\alpha)}\|\xi\|_{Q_T}^{(2+\alpha)} + \|c-c_0\|_{S_T}^{(1+\alpha)}\|\sigma\|_{S_T}^{(2+\alpha)}\right)\\ &\le C\sqrt{T}\|H\|_{\mathcal{R}_1}\end{aligned}$$

and from

$$\begin{aligned}\|\mathcal{S}_3 H\|_{S_T}^{(1+\alpha)} &\le C\left(\|d-d_0\|_{S_T}^{(1+\alpha)}\|\xi\|_{Q_T}^{(1+\alpha)} + \|d-d_0\|_{S_T}^{(\alpha)}\|\xi\|_{Q_T}^{(2+\alpha)}\right)\\ &\le C\left(\sqrt{T}\|d-d_0\|_{S_T}^{(1+\alpha)} + \|d-d_0\|_{S_T}^{(\alpha)}\right)\|H\|_{\mathcal{R}_1}.\end{aligned}$$

Since $d(x) = \left|(-\partial_{z_1} q, -\partial_{z_2} q, 1)^T(z')\right|$, the regularity of $\partial\Omega_0$ yields finiteness of $\|d-d_0\|_{S_T}^{(1+\alpha)}$.

5. The last step of this proof is to replace the smallness assumption on $\|d-d_0\|_{S_T}^{(\alpha)}$ made in Step 3 by a smallness assumption on T. For this purpose, in a similar way as in Step 1, we choose another system of coverings $\{\hat\Omega^{(j)}\}$ and $\{\hat\omega^{(j)}\}$ ($j \in \hat M_1 \cup \hat M_2$) of $\overline{\Omega_0}$ with corresponding cutoff functions $\hat\varphi^{(j)}$ and $\hat\eta^{(j)}$, such that for all $j \in \hat M_2$ there exists a constant $d_0^{(j)} > 0$ with $\|d-d_0^{(j)}\|_{\hat S_T^{(j)}}^{(\alpha)} \le \epsilon$, where ϵ is a fixed small positive number determined later and $\hat S_T^{(j)} := (\overline{\hat\Omega^{(j)}} \cap \partial\Omega_0) \times (0,T]$. The existence of such a covering is ensured by the regularity assumption on $\partial\Omega_0$, which implies

$$|\nabla q(z')| = |D^2 q(z_0')(z'-z_0') + o(|z'-z_0'|)| \le C\lambda + o(\lambda)\,, \tag{5.100}$$

and hence, with $d_0^{(j)} \equiv 1$,

$$|d(x) - d_0^{(j)}| = |\sqrt{1+|\nabla q(z')|^2} - 1| = \frac{|\nabla q(z')|^2}{2} + o(|\nabla q(z')|^2) \le C\lambda^2 + o(\lambda^2) \quad \forall x \in \partial\Omega_0\,.$$

Furthermore, $\forall x, \tilde x \in \partial\Omega_0$,

$$\begin{aligned}\frac{|d(x)-d(\tilde x)|}{|x-\tilde x|^\alpha} &= \frac{\left|\sqrt{1+|\nabla q(z')|^2} - \sqrt{1+|\nabla q(\tilde z')|^2}\right|}{\left(|z'-\tilde z'|^2 + |q(z')-q(\tilde z')|^2\right)^{\alpha/2}}\\ &\le \frac{2^{-1}\left(1+|\nabla q(\tilde z')|^2\right)^{-\frac12}\left||\nabla q(z')|^2 - |\nabla q(\tilde z')|^2\right| + o\Big(\big||\nabla q(z')|^2 - |\nabla q(\tilde z')|^2\big|\Big)}{|z'-\tilde z'|^\alpha\left(1+|\nabla q(\tilde z') + o(1)|^2\right)^{\alpha/2}}\\ &\le C\frac{|\nabla q(z') - \nabla q(\tilde z')| + o\left(|\nabla q(z') - \nabla q(\tilde z')|\right)}{|z'-\tilde z'|^\alpha}\\ &\le C\lambda^{1-\alpha} + o(\lambda^{1-\alpha})\,.\end{aligned}$$

Thus, $\|d-d_0^{(j)}\|_{\hat S_T^{(j)}}^{(\alpha)}$ can be made arbitrarily small by refining the covering $\{\hat\Omega^{(j)}, \hat\omega^{(j)}\}$.

Extend $d_{|\hat{S}_T^{(j)}}$ to a function $d^{(j)}$ defined on the whole boundary S_T, such that $\|d^{(j)} - d_0^{(j)}\|_{S_T}^{(\alpha)} \leq C\epsilon$ and C is independent of j, ϵ, and λ. This can be accomplished using the reflection techniques described in [52, p. 297]. For sufficiently small ϵ and $j \in \hat{M}_2$ let $(\hat{\xi}^{(j)}, \hat{\sigma}^{(j)})$ be a solution of

$$\begin{cases} \partial_t \hat{\xi}^{(j)} - D\Delta\hat{\xi}^{(j)} = \hat{\varphi}^{(j)} F_1 & \text{in } Q_T \\ \partial_n \hat{\xi}^{(j)} = k\hat{\xi}^{(j)} + c\hat{\sigma}^{(j)} + \hat{\varphi}^{(j)} F_2 & \text{on } S_T \\ \hat{\xi}^{(j)}(t=0) = 0 & \text{in } \Omega_0 \\ \partial_t \hat{\sigma}^{(j)} - d^{(j)} \partial_n \hat{\xi}^{(j)} = \hat{\varphi}^{(j)} F_3 & \text{on } S_T \\ \hat{\sigma}^{(j)}(t=0) = 0 & \text{on } \partial\Omega_0\,, \end{cases}$$

the existence of which is ensured by Step 3 of this proof. For $j \in \hat{M}_1$ let $\hat{\xi}^{(j)}$ be a solution of

$$\begin{cases} \partial_t \hat{\xi}^{(j)} - D\Delta\hat{\xi}^{(j)} = \hat{\varphi}^{(j)} F_1 & \text{in } \mathbb{R}^3_T \\ \hat{\xi}^{(j)}(t=0) = 0 & \text{in } \mathbb{R}^3. \end{cases}$$

We define $\hat{\mathcal{R}}H := \sum\limits_{j\in\hat{M}_1} \hat{\eta}^{(j)}(\hat{\xi}^{(j)}, 0) + \sum\limits_{j\in\hat{M}_2} \hat{\eta}^{(j)}(\hat{\xi}^{(j)}, \hat{\sigma}^{(j)})$ and observe that $(\hat{\xi}, \hat{\sigma}) := \hat{\mathcal{R}}H$ solves

$$\begin{cases} \partial_t \hat{\xi} - D\Delta\hat{\xi} = F_1 - \hat{\mathcal{T}}_1 H & \text{in } Q_T \\ \partial_n \hat{\xi} = k\hat{\xi} + c\hat{\sigma} + F_2 - \hat{\mathcal{T}}_2 H & \text{on } S_T \\ \hat{\xi}(t=0) = 0 & \text{in } \Omega_0 \\ \partial_t \hat{\sigma} - d\partial_n \hat{\xi} = F_3 - \hat{\mathcal{T}}_3 H & \text{on } S_T \\ \hat{\sigma}(t=0) = 0 & \text{on } \partial\Omega_0\,, \end{cases}$$

where

$$\hat{\mathcal{T}}_1 H := D\sum_j \left(\Delta\eta^{(j)}\xi^{(j)} + 2\nabla\eta^{(j)}\nabla\xi^{(j)}\right),\ \hat{\mathcal{T}}_2 H := -\sum_{j\in M_2} \partial_n\hat{\eta}^{(j)}\hat{\xi}^{(j)},\ \hat{\mathcal{T}}_3 H := d\sum_{j\in M_2} \partial_n\hat{\eta}^{(j)}\hat{\xi}^{(j)}.$$

Clearly, $\hat{\mathcal{T}} := (\hat{\mathcal{T}}_i)_{i=1}^3 : \mathcal{R}_1 \to \mathcal{R}_1$ and $\|\hat{\mathcal{T}}\| \leq C\left(\frac{T}{\lambda^{2+\alpha}} + \frac{\sqrt{T}}{\lambda^{1+\alpha}}\right) \leq \frac{1}{2}$ for sufficiently small T. □

Finally, we prove solvability of the linear problem (5.18) on any finite time interval $[0, T]$, i.e. we cease to assume that time is small.

Corollary 5.3.1 (Global existence in time)**.** *For each $T > 0$ and any right hand side $(F_1, F_2, F_3) \in \mathcal{R}_1$ the linear problem* (5.18) *has a unique solution $(\xi, \sigma) \in \mathcal{R}_2$. Furthermore,*

$$\|\xi\|_{Q_T}^{(2+\alpha)} + \|\sigma\|_{S_T}^{(2+\alpha)} \leq C\Big(\|F_1\|_{Q_T}^{(\alpha)} + \|F_2\|_{S_T}^{(1+\alpha)} + \|F_3\|_{S_T}^{(1+\alpha)}\Big), \tag{5.101}$$

where $C = C(D, k, c, d, T)$ remains bounded as $T \to 0$.

Proof. 1. First, we assume that that $k, c, d \in H^{2+\alpha,\frac{2+\alpha}{2}}(\overline{S_T})$ and that $F_i \in H_0^{1+\alpha,\frac{1+\alpha}{2}}(\overline{S_T}) \cap H^{2+\alpha,\frac{2+\alpha}{2}}(\overline{S_T})$ $(i = 2, 3)$. We define $F_4 := dF_2 + F_3$. By the use of Theorem 5.3.1 we can solve (5.18) on a small time interval $[t_0 = 0, t_0 + \tau]$. We denote this solution by $(\xi^{(1)}, \sigma^{(1)})$ and note

that both the constant C in (5.96) and the length τ of the interval do not depend on the initial time t_0. Using Theorem 4.1. and Theorem 4.3. in [52, p. 298] as well as the remark on page 10 of this book, we can construct two functions $\left(\hat{\xi}^{(2)}, \overline{\sigma}^{(2)}\right) \in H^{2+\alpha,\frac{2+\alpha}{2}}(\overline{Q_T}) \times H^{2+\alpha,\frac{2+\alpha}{2}}(\overline{S_T})$ satisfying

$$\hat{\xi}^{(2)}\left(.,\frac{\tau}{2}\right) = \xi^{(1)}\left(.,\frac{\tau}{2}\right), \quad \partial_t\hat{\xi}^{(2)}\left(.,\frac{\tau}{2}\right) = \partial_t\xi^{(1)}\left(.,\frac{\tau}{2}\right),$$
$$\overline{\sigma}^{(2)}\left(.,\frac{\tau}{2}\right) = \sigma^{(1)}\left(.,\frac{\tau}{2}\right), \quad \partial_t\overline{\sigma}^{(2)}\left(.,\frac{\tau}{2}\right) = \partial_t\sigma^{(1)}\left(.,\frac{\tau}{2}\right),$$

and

$$\|\hat{\xi}^{(2)}\|_{Q_T}^{(2+\alpha)} \leq \|\xi^{(1)}\left(.,\frac{\tau}{2}\right)\|_{\Omega_0}^{(2+\alpha)}, \quad \|\overline{\sigma}^{(2)}\|_{S_T}^{(2+\alpha)} \leq \|\sigma^{(1)}\left(.,\frac{\tau}{2}\right)\|_{\partial\Omega_0}.$$

According to (5.96), the right hand sides of these inequalities can be estimated by the F_i $(i = 1, 2, 3)$. Adding the fourth equation and d times the second equation of (5.18) yields

$$\partial_t\sigma^{(1)} = dk\xi^{(1)} + dc\sigma^{(1)} + F_4 \quad \text{on } S_\tau\,. \tag{5.102}$$

On S_T we define the function $\hat{\sigma}^{(2)}$ as

$$\hat{\sigma}^{(2)}(x,t) := \sigma^{(1)}\left(x,\frac{\tau}{2}\right) + \int_{\frac{\tau}{2}}^{t}\Big(dk\hat{\xi}^{(2)}(x,s) + dc\overline{\sigma}^{(2)}(x,s) + F_4(x,s)\Big)d\tau$$

and observe that $\hat{\sigma}^{(2)} \in H^{2+\alpha,\frac{2+\alpha}{2}}(\overline{S_T})$ and $\partial_t\hat{\sigma}^{(2)} \in H^{2+\alpha,\frac{2+\alpha}{2}}(\overline{S_T})$. Note that we need at least $\partial_t\hat{\sigma}^{(2)} \in H^{1+\alpha,\frac{1+\alpha}{2}}$ to ensure that the below defined $\tilde{F}_3$ is in $H_0^{1+\alpha,\frac{1+\alpha}{2}}$. Furthermore, we observe that $\hat{\sigma}^{(2)}$ and $\partial_t\hat{\sigma}^{(2)}$ fulfill

$$\hat{\sigma}^{(2)}\left(.,\frac{\tau}{2}\right) = \sigma^{(1)}\left(.,\frac{\tau}{2}\right), \quad \partial_t\hat{\sigma}^{(2)}\left(.,\frac{\tau}{2}\right) = \partial_t\sigma^{(1)}\left(.,\frac{\tau}{2}\right),$$

where the latter equation follows from (5.102) and the definitions of $\hat{\xi}^{(2)}$ and $\overline{\sigma}^{(2)}$. We define

$$\tilde{F}_1 := F_1 - \partial_t\hat{\xi}^{(2)} + D\Delta\hat{\xi}^{(2)}$$
$$\tilde{F}_2 := F_2 - \partial_n\hat{\xi}^{(2)} + k\hat{\xi}^{(2)} + c\hat{\sigma}^{(2)}$$
$$\tilde{F}_3 := F_3 - \partial_t\hat{\sigma}^{(2)} + d\partial_n\hat{\xi}^{(2)}$$

and observe that

$$\tilde{F}_1 \in H_0^{\alpha,\frac{\alpha}{2}}(\overline{\Omega_0}\times[\tau/2,T])\,, \quad \tilde{F}_2 \in H_0^{1+\alpha,\frac{1+\alpha}{2}}(\partial\Omega_0\times[\tau/2,T])\,, \quad \tilde{F}_3 \in H_0^{1+\alpha,\frac{1+\alpha}{2}}(\partial\Omega_0\times[\tau/2,T])\,.$$

Hence, using Theorem 5.3.1 we can solve on the interval $[\tau/2, 3\tau/2]$

$$\begin{cases} \partial_t\tilde{\xi}^{(2)} - D\Delta\tilde{\xi}^{(2)} = \tilde{F}_1 \\ \qquad\qquad \partial_n\tilde{\xi}^{(2)} = k\tilde{\xi}^{(2)} + c\tilde{\sigma}^{(2)} + \tilde{F}_2 \\ \qquad \tilde{\xi}^{(2)}(.,\tau/2) = 0 \\ \partial_t\tilde{\sigma}^{(2)} - d\partial_n\tilde{\xi}^{(2)} = \tilde{F}_3 \\ \qquad \sigma^{(2)}(.,\tau/2) = 0\,. \end{cases}$$

Clearly,

$$(\xi,\sigma) := \begin{cases} (\xi^{(1)},\sigma^{(1)}) & t \le \tau \\ (\tilde\xi^{(2)}+\hat\xi^{(2)},\tilde\sigma^{(2)}+\hat\sigma^{(2)}) & \tau \le t \le 3\tau/2 \end{cases}$$

solves (5.18) on $[0,3\tau/2]$ and can be estimated by the F_i $(i=1,2,3)$. Hence, repetition of this argument yields the solution (ξ,σ) of (5.18) on the whole interval $[0,T]$.

2. The general case $F_i \in H_0^{1+\alpha,\frac{1+\alpha}{2}}(\overline{S_T})$ $(i=2,3)$ follows by approximation of the F_i in $H_0^{1+\alpha,\frac{1+\alpha}{2}}(\overline{S_T})$ with smoother functions $F_i^{(n)} \in H_0^{1+\alpha,\frac{1+\alpha}{2}}(\overline{S_T}) \cap H^{2+\alpha,\frac{2+\alpha}{2}}(\overline{S_T})$ $(i=2,3)$. Due to (5.101), the corresponding solutions $\big(\xi^{(n)},\sigma^{(n)}\big)_{n=1}^{\infty}$ form a Cauchy sequence in $\mathcal{R}_2$ and their limit obviously solves the original problem (5.18).

3. The case that the coefficients k,c,d only belong to $H^{1+\alpha,\frac{1+\alpha}{2}}(\overline{S_T})$ can also be treated by approximation. We choose k_1, c_1, and d_1 in $H^{2+\alpha,\frac{2+\alpha}{2}}(\overline{S_T})$ such that

$$C\|k-k_1\|_{S_T}^{(1+\alpha)} \le \frac14, \quad C\|c-c_1\|_{S_T}^{(1+\alpha)} \le \frac14, \quad C\|d-d_1\|_{S_T}^{(1+\alpha)} \le \frac14,$$

where C is a bound of the $C(D,k_1,c_1,d_1,T)$, which are defined as the constants arising in estimate (5.101) of the linear problem (5.18) containing k_1,c_1,d_1 as coefficients instead of k,c,d. The existence of such a bound for all (k_1,c_1,d_1) that are located in a sufficiently small neighborhood of (k,c,d) is not difficult to prove.

Now we observe that a solution of (5.18) can be obtained as fixed point of the operator $K : \mathcal{R}_2 \to \mathcal{R}_2$ mapping $(h,e) \in \mathcal{R}_2$ onto the solution $(\xi,\sigma) \in \mathcal{R}_2$ of

$$\begin{cases} \partial_t\xi - D\Delta\xi = F_1 & \text{in } Q_T \\ \partial_n\xi = k_1\xi + c_1\sigma + \big(F_2 + (k-k_1)h + (c-c_1)e\big) & \text{on } S_T \\ \xi(t=0) = 0 & \text{in } \Omega_0 \\ \partial_t\sigma - d_1\partial_n\xi = F_3 + (d-d_1)\partial_n h & \text{on } S_T \\ \sigma(t=0) = 0 & \text{on } \partial\Omega_0\,. \end{cases}$$

According to Step 1 and 2 of this proof, this operator is well defined and satifies

$$\begin{aligned} \|K(h,e) - K(\tilde h,\tilde e)\|_{\mathcal{R}_2} &\le C\Big(\|k-k_1\|_{S_T}^{(1+\alpha)} + \|c-c_1\|_{S_T}^{(1+\alpha)} + \|d-d_1\|_{S_T}^{(1+\alpha)}\Big)\|(h,e)-(\tilde h,\tilde e)\|_{\mathcal{R}_2} \\ &\le \frac34\|(h,e)-(\tilde h,\tilde e)\|_{\mathcal{R}_2}\,. \end{aligned}$$

Thus, K is a strict contraction. □

5.4 Solution of the nonlinear problem for the platelets; fixed flow

Lemma 5.4.1. *Let r_0 be sufficiently small, $N_T := N \times (0,T]$, and h_i, h be functions of the type $h_i(y,t) = \tilde h_i(\omega(y),t)$ (i=1,2), $h(y,t) = \tilde h(\omega(y),t)$. We assume that $h_i, h \in B_{r_0}(0) \subset$*

$H_0^{2+\alpha,\frac{2+\alpha}{2}}(\overline{N_T})$ *and define* A_h *as in* (5.9) *and* n_{A_h} *as on page 57. Then the following estimates hold:*

$$\|A_{h_1} - A_{h_2}\|_{Q_T}^{(l+\alpha)} \le C\|h_1 - h_2\|_{S_T}^{(l+1+\alpha)} \quad (l = 0, 1)\,, \tag{5.103}$$

$$\|n_{A_{h_1}} - n_{A_{h_2}}\|_{S_T}^{(l+\alpha)} \le C\|h_1 - h_2\|_{S_T}^{(l+1+\alpha)} \quad (l = 0, 1)\,, \tag{5.104}$$

$$\|n_{A_h} - n\|_{S_T}^{(l+\alpha)} \le C\|h\|_{S_T}^{(l+1+\alpha)} \quad (l = 0, 1)\,. \tag{5.105}$$

Proof. 1. From the definition (5.7) of Ψ_h and from $h_i(y,t) = \tilde{h}_i(\omega(y),t)$ we deduce that

$$\|\Psi_{h_1} - \Psi_{h_2}\|_{\mathbb{R}^3_T}^{(l+\alpha)} = \|\beta(h_1 - h_2)\|_{N_T}^{(l+\alpha)} \le C\|h_1 - h_2\|_{S_T}^{(l+\alpha)} \quad (l = 1, 2).$$

Thus,

$$\|M_{h_1} - M_{h_2}\|_{\mathbb{R}^3_T}^{(l+\alpha)} \le C\|h_1 - h_2\|_{S_T}^{(l+1+\alpha)} \quad (l = 0, 1)\,, \tag{5.106}$$

where M_h is defined according to (5.8):

$$M_h = \mathrm{Id} + B_h\,, \quad B_h := \beta\nabla h^T + hD\beta\,.$$

We observe that $\|B_h\|_{Q_T}^{(0)} < 1$ when r_0 is sufficiently small. Therefore, $M_h(x,t)$ has an inverse $A_h(x,t)$ for all $(x,t) \in Q_T$, which fulfills

$$|A_h(x,t)| \le \frac{1}{1 - |B_h(x,t)|}\,. \tag{5.107}$$

Due to its representation

$$A_h(x,t) = \sum_{n=0}^{\infty} B_h(x,t)^n$$

with a uniformly convergent series of continuous functions, the inverse A_h is continuous, too. Hence, we obtain from (5.107)

$$\|A_h\|_{Q_T}^{(0)} \le \frac{1}{1 - \|B_h\|_{Q_T}^{(0)}} \le C(r_0). \tag{5.108}$$

In addition,

$$\begin{aligned} \langle A_h\rangle_{x,Q_T}^{(\alpha)} &= \sup_{\substack{(x,t),\,(y,t)\,\in\,\overline{Q_T} \\ |x-y|\,\le\,\rho_0}} \frac{\big|A_h(x,t)\big(M_h(y,t) - M_h(x,t)\big)A_h(y,t)\big|}{|x-y|^\alpha} \\ &\le \Big(\|A_h\|_{Q_T}^{(0)}\Big)^2 \langle M_h\rangle_{Q_T}^{(\alpha)} \\ &\le C(r_0)\,, \end{aligned} \tag{5.109}$$

where we used the fact that the matrices M_h are bounded in $H^{1+\alpha,\frac{1+\alpha}{2}}(\overline{Q_T})$ for h being bounded in $H^{2+\alpha,\frac{2+\alpha}{2}}(\overline{N_T})$. We note that analogous estimates hold for $\langle A_h\rangle_{t,Q_T}^{(\frac{\alpha}{2})}$ and $\langle A_h\rangle_{t,Q_T}^{(\frac{1+\alpha}{2})}$.

The differentiability of the inverse A_h follows from its above derived continuity, from the differentiability of M_h, and from

$$\begin{aligned}\partial_i A_h(x,t) &= \lim_{s\to 0} \frac{A_h(x+se_i,t)\big(M_h(x,t)-M_h(x+se_i,t)\big)A_h(x,t)}{s} \\ &= -A_h(x,t)\partial_i M_h(x,t)A_h(x,t)\,,\end{aligned} \tag{5.110}$$

where e_i $(i=1,2,3)$ denotes the i-th cartesian coordinate vector. Together with (5.108), formula (5.110) implies

$$\|DA_h\|^{(0)}_{Q_T} \le C(r_0)\,.$$

Next, we observe that two functions p and q satisfy

$$\begin{aligned}\langle pq\rangle^{(\alpha)}_{x,Q_T} &\le \langle p\rangle^{(\alpha)}_{x,Q_T}\,\|q\|^{(0)}_{Q_T} + \|p\|^{(0)}_{Q_T}\,\langle q\rangle^{(\alpha)}_{x,Q_T} \\ \left\langle \frac{p}{q}\right\rangle^{(\alpha)}_{x,Q_T} &\le \inf(q)^{-1}\,\langle p\rangle^{(\alpha)}_{x,Q_T} + \frac{\langle q\rangle^{(\alpha)}_{x,Q_T}}{\inf(q)^2}\,\|p\|^{(0)}_{Q_T}\,.\end{aligned} \tag{5.111}$$

Hence, (5.110), (5.111), (5.108), and (5.109) yield

$$\langle \partial_i A_h\rangle^{(\alpha)}_{Q_T} \le C\left(\|A_h\|^{(\alpha)}_{Q_T}\right)^2 \|M_h\|^{(1+\alpha)}_{Q_T} \le C(r_0)\,. \tag{5.112}$$

In summing up, we have shown that for all $h\in B_{r_0}(0)\subset H_0^{2+\alpha,\frac{2+\alpha}{2}}(\overline{N_T})$ the Matrices A_h are uniformly bounded in $H^{1+\alpha,\frac{1+\alpha}{2}}(\overline{Q_T})$, that is

$$\|A_h\|^{(l+\alpha)}_{Q_T} \le C(r_0) \quad (l=0,1)\,. \tag{5.113}$$

2. To show (5.103), we employ (5.113) and (5.106) as follows:

$$\begin{aligned}\|A_{h_1}-A_{h_2}\|^{(l+\alpha)}_{Q_T} &= \|A_{h_1}(M_{h_2}-M_{h_1})A_{h_2}\|^{(l+\alpha)}_{Q_T} \\ &\le \|A_{h_1}\|^{(l+\alpha)}_{Q_T}\|A_{h_2}\|^{(l+\alpha)}_{Q_T}\|M_{h_2}-M_{h_1}\|^{(l+\alpha)}_{Q_T} \\ &\le C(r_0)\|h_1-h_2\|^{(l+1+\alpha)}_{S_T} \quad (l=0,1)\,.\end{aligned}$$

3. Equation (5.103) yields (5.104). Indeed, we first observe that (5.8) and (5.9) imply

$$A_0 = \mathrm{Id} \tag{5.114}$$

which, together with (5.103), yields

$$|\nabla_{A_{h_i}}\eta| \ge |\nabla\eta| - \|A_{h_i}-\mathrm{Id}\,\|^{(0)}_{Q_T}|\nabla\eta| \ge |\nabla\eta|\Big(1-\|h_i-0\|^{(2+\alpha)}_{S_T}\Big) \ge c(r_0)>0\,. \tag{5.115}$$

From the definition of $n_{A_{h_i}}$ it follows that

$$n_{A_{h_1}} - n_{A_{h_2}} = \frac{|\nabla_{A_{h_2}}\eta|(\nabla_{A_{h_1}}\eta-\nabla_{A_{h_2}}\eta) + \big(|\nabla_{A_{h_2}}\eta|-|\nabla_{A_{h_1}}\eta|\big)\nabla_{A_{h_2}}\eta}{|\nabla_{A_{h_1}}\eta||\nabla_{A_{h_2}}\eta|}\,. \tag{5.116}$$

Using (5.116), (5.115), and (5.103) we obtain

$$\begin{aligned}\|n_{A_{h_1}} - n_{A_{h_2}}\|_{S_T}^{(0)} &\le C(r_0)\Big(\|\nabla_{A_{h_1}}\eta - \nabla_{A_{h_2}}\eta\|_{S_T}^{(0)} + \||\nabla_{A_{h_1}}\eta| - |\nabla_{A_{h_2}}\eta|\|_{S_T}^{(0)}\Big)\\ &\le C(r_0)\|A_{h_1} - A_{h_2}\|_{Q_T}^{(0)}\\ &\le C(r_0)\|h_1 - h_2\|_{S_T}^{(1+\alpha)}.\end{aligned} \tag{5.117}$$

Furthermore, the equations (5.116), (5.111), (5.115), and (5.103) yield

$$\begin{aligned}\langle n_{A_{h_1}} - n_{A_{h_2}}\rangle_{x,S_T}^{(\alpha)} &\le \left\langle \frac{|\nabla_{A_{h_2}}\eta|}{|\nabla_{A_{h_1}}\eta||\nabla_{A_{h_2}}\eta|}\right\rangle_{x,S_T}^{(\alpha)} \|\nabla_{A_{h_1}}\eta - \nabla_{A_{h_2}}\eta\|_{S_T}^{(0)}\\ &\quad + \left\|\frac{|\nabla_{A_{h_2}}\eta|}{|\nabla_{A_{h_1}}\eta||\nabla_{A_{h_2}}\eta|}\right\|_{S_T}^{(0)} \langle\nabla_{A_{h_1}}\eta - \nabla_{A_{h_2}}\eta\rangle_{x,S_T}^{(\alpha)}\\ &\quad + \left\langle \frac{\nabla_{A_{h_2}}\eta}{|\nabla_{A_{h_1}}\eta||\nabla_{A_{h_2}}\eta|}\right\rangle_{x,S_T}^{(\alpha)} \||\nabla_{A_{h_1}}\eta| - |\nabla_{A_{h_2}}\eta|\|_{S_T}^{(0)}\\ &\quad + \left\|\frac{\nabla_{A_{h_2}}\eta}{|\nabla_{A_{h_1}}\eta||\nabla_{A_{h_2}}\eta|}\right\|_{S_T}^{(0)} \langle|\nabla_{A_{h_1}}\eta| - |\nabla_{A_{h_2}}\eta|\rangle_{x,S_T}^{(\alpha)}\\ &\le C(r_0)\Big(\langle\nabla_{A_{h_1}}\eta - \nabla_{A_{h_2}}\eta\rangle_{x,S_T}^{(\alpha)}\\ &\qquad + \langle|\nabla_{A_{h_1}}\eta| - |\nabla_{A_{h_2}}\eta|\rangle_{x,S_T}^{(\alpha)} + \|\nabla_{A_{h_1}}\eta - \nabla_{A_{h_2}}\eta\|_{S_T}^{(0)}\Big).\end{aligned} \tag{5.118}$$

To estimate $\langle|\nabla_{A_{h_1}}\eta| - |\nabla_{A_{h_2}}\eta|\rangle_{x,S_T}^{(\alpha)}$, the expansion

$$|\nabla_{A_{h_1}}\eta| - |\nabla_{A_{h_2}}\eta| \le \frac{\nabla_{A_{h_2}}\eta}{|\nabla_{A_{h_2}}\eta|}(\nabla_{A_{h_1}}\eta - \nabla_{A_{h_2}}\eta) + o\Big(\|\nabla_{A_{h_1}}\eta - \nabla_{A_{h_2}}\eta\|_{Q_T}^{(\alpha)}\Big)$$

is employed, which—together with (5.111), (5.115), and (5.103)—yields

$$\begin{aligned}\langle|\nabla_{A_{h_1}}\eta| - |\nabla_{A_{h_2}}\eta|\rangle_{x,S_T}^{(\alpha)} &\le C(r_0)\Big(\langle\nabla_{A_{h_1}}\eta - \nabla_{A_{h_2}}\eta\rangle_{x,S_T}^{(\alpha)} + \|\nabla_{A_{h_1}}\eta - \nabla_{A_{h_2}}\eta\|_{S_T}^{(0)}\Big)\\ &\le C(r_0)\|A_{h_1} - A_{h_2}\|_{Q_T}^{(\alpha)}\\ &\le C(r_0)\|h_1 - h_2\|_{S_T}^{(1+\alpha)}.\end{aligned} \tag{5.119}$$

Thus, (5.118) and (5.119) yield $\langle n_{A_{h_1}} - n_{A_{h_2}}\rangle_{x,S_T}^{(\alpha)} \le C\|h_1 - h_2\|_{S_T}^{(1+\alpha)}$. We note that $\langle n_{A_{h_1}} - n_{A_{h_2}}\rangle_{t,S_T}^{(\alpha/2)}$ can be treated similarly. These findings and (5.117) imply (5.104) in the case $l = 0$. The case $l = 1$ can be treated by differentiation of (5.116).

4. Because of (5.114), equation (5.105) is a direct consequence of equation (5.104). □

The next step towards existence is to derive estimates of the right hand sides of equations (5.17). For this purpose, we define $\mathcal{B}_d := \{u \in H^{1+\alpha,\frac{1+\alpha}{2}}(\overline{Q_T}) : \|u - u_0\|_{Q_T}^{(1+\alpha)} \le d\}$ and $\mathcal{D}_r := \overline{B_r(0)} \subset \mathcal{R}_2$.

Lemma 5.4.2 (Estimates of the F_i)**.** *Let w_0 fulfill $D\partial_n w_0 = kw_0 + l_0$ along $\partial\Omega_0$ (which follows from the compatibility conditions on the data). Assume that $(\xi,\sigma) \in \mathcal{D}_r$ and $u \in \mathcal{B}_d$. Let F_i $(i = 1,2,3)$ be defined by (5.17). Then the following estimates hold:*

$$\|F_1(u_1,\xi,\sigma) - F_1(u_2,\xi,\sigma)\|_{Q_T}^{(\alpha)} \le C\|u_1 - u_2\|_{Q_T}^{(1+\alpha)} \tag{5.120}$$

$$\|F_1(u,\xi_1,\sigma_1) - F_1(u,\xi_2,\sigma_2)\|_{Q_T}^{(\alpha)} \le C(T^{\alpha/2} + g(r)) \Big(\|\xi_1 - \xi_2\|_{Q_T}^{(2+\alpha)} + \|\sigma_1 - \sigma_2\|_{S_T}^{(2+\alpha)}\Big). \tag{5.121}$$

Furthermore, there exists $\epsilon > 0$ such that

$$\|F_2(\xi_1,\sigma_1) - F_2(\xi_2,\sigma_2)\|_{S_T}^{(1+\alpha)} \le C\Big(T^{\epsilon/2} + \|\hat{w}\|_{S_T}^{(2+\alpha)}\Big) \Big(\|\xi_1 - \xi_2\|_{Q_T}^{(2+\alpha)} + \|\sigma_1 - \sigma_2\|_{S_T}^{(2+\alpha)}\Big) \tag{5.122}$$

$$\|F_3(\xi_1,\sigma_1) - F_3(\xi_2,\sigma_2)\|_{S_T}^{(1+\alpha)} \le C\Big(T^{\epsilon/2} + \|\hat{w}\|_{S_T}^{(2+\alpha)}\Big) \Big(\|\xi_1 - \xi_2\|_{Q_T}^{(2+\alpha)} + \|\sigma_1 - \sigma_2\|_{S_T}^{(2+\alpha)}\Big). \tag{5.123}$$

Finally,

$$\|F_1(u,0,0)\|_{Q_T}^{(\alpha)} + \|F_2(0,0)\|_{S_T}^{(1+\alpha)} + \|F_3(0,0)\|_{S_T}^{(1+\alpha)} \le CT^{\frac{\alpha'-\alpha}{2}} \quad (\alpha' > \alpha > 0)\,. \tag{5.124}$$

All prefactors $C = C(r,d,T)$ remain bounded for bounded r,d, and T. In addition, $g(r) \to 0$ as $r \to 0$.

Proof. 1. The estimates (5.120) and (5.121) were proven in [7], Lemma 2 on page 12.

2. Let $h_i := \sigma_i + \hat{h}$ (i=1,2). Estimate (5.122) can be shown as follows:

$$\begin{aligned}\|F_2(\xi_1,\sigma_1) - F_2(\xi_2,\sigma_2)\|_{S_T}^{(1+\alpha)} &\le \|Dn_{A_{h_1}}\nabla_{A_{h_1}}\xi_1 - Dn\nabla\xi_1 - Dn_{A_{h_2}}\nabla_{A_{h_2}}\xi_2 + Dn\nabla\xi_2\|_{S_T}^{(1+\alpha)} \\ &\quad + \|Dn_{A_{h_1}}\nabla_{A_{h_1}}(\chi\sigma_1\partial_n\hat{w}) - Dn_{A_{h_2}}\nabla_{A_{h_2}}(\chi\sigma_2\partial_n\hat{w})\|_{S_T}^{(1+\alpha)} \\ &\quad + \|Dn_{A_{h_1}}\nabla_{A_{h_1}}\hat{w} - Dn_{A_{h_2}}\nabla_{A_{h_2}}\hat{w}\|_{S_T}^{(1+\alpha)} \\ &=: I_1 + I_2 + I_3\,.\end{aligned}$$

$$\begin{aligned}I_1 &\le \|Dn_{A_{h_1}}\nabla_{A_{h_1}}(\xi_1 - \xi_2) - Dn_{A_{h_1}}\nabla(\xi_1 - \xi_2)\|_{S_T}^{(1+\alpha)} + \|Dn_{A_{h_1}}\nabla(\xi_1 - \xi_2) - Dn\nabla(\xi_1 - \xi_2)\|_{S_T}^{(1+\alpha)} \\ &\quad + \Big(\|Dn_{A_{h_1}}\nabla_{A_{h_1}}\xi_2 - Dn_{A_{h_2}}\nabla_{A_{h_1}}\xi_2\|_{S_T}^{(1+\alpha)} + \|Dn_{A_{h_2}}\nabla_{A_{h_1}}\xi_2 - Dn_{A_{h_2}}\nabla_{A_{h_2}}\xi_2\|_{S_T}^{(1+\alpha)}\Big) \\ &=: J_1 + J_2 + J_3\,.\end{aligned}$$

We define $\epsilon := (1-\alpha)/2$. By the use of (5.114), (5.103), (5.99), and (5.105) we obtain

$$\begin{aligned}J_1 &\le C\|n_{A_{h_1}}\|_{S_T}^{(1+\alpha)}\Big(\|A_{h_1} - \mathrm{Id}\,\|_{Q_T}^{(\alpha)}\|\xi_1 - \xi_2\|_{S_T}^{(2+\alpha)} + \|A_{h_1} - \mathrm{Id}\,\|_{Q_T}^{(1+\alpha)}\|\xi_1 - \xi_2\|_{S_T}^{(1+\alpha)}\Big) \\ &\le C(r)\|n_{A_{h_1}}\|_{S_T}^{(1+\alpha)}\Big(\|h_1\|_{S_T}^{(1+\alpha+\epsilon)}T^{\epsilon/2} + \|h_1\|_{S_T}^{(2+\alpha)}T^{1/2}\Big)\|\xi_1 - \xi_2\|_{Q_T}^{(2+\alpha)} \\ &\le C(r)\Big(\|h_1\|_{S_T}^{(2+\alpha)} + \|n\|_{S_T}^{(1+\alpha)}\Big)\|h_1\|_{S_T}^{(2+\alpha)}T^{\epsilon/2}\|\xi_1 - \xi_2\|_{Q_T}^{(2+\alpha)} \\ &\le C(r)T^{\epsilon/2}\|\xi_1 - \xi_2\|_{Q_T}^{(2+\alpha)}.\end{aligned}$$

From (5.114) and (5.105) it follows that

$$\begin{aligned}
J_2 &\le C\Big(\|n_{A_{h_1}} - n\|_{S_T}^{(\alpha)}\|\xi_1 - \xi_2\|_{S_T}^{(2+\alpha)} + \|n_{A_{h_1}} - n\|_{S_T}^{(1+\alpha)}\|\xi_1 - \xi_2\|_{S_T}^{(1+\alpha)}\Big)\\
&\le C(r)\Big(\|h_1\|_{S_T}^{(1+\alpha+\epsilon)}T^{\epsilon/2} + \|h_1\|_{S_T}^{(2+\alpha)}T^{1/2}\Big)\|\xi_1 - \xi_2\|_{Q_T}^{(2+\alpha)}\\
&\le C(r)T^{\epsilon/2}\|\xi_1 - \xi_2\|_{Q_T}^{(2+\alpha)}.
\end{aligned}$$

Employing (5.114), (5.103), and (5.104) yields

$$\begin{aligned}
J_3 &\le C\|A_{h_1}\|_{Q_T}^{(1+\alpha)}\Big(\|n_{A_{h_1}} - n_{A_{h_2}}\|_{S_T}^{(\alpha)}\|\xi_2\|_{S_T}^{(2+\alpha)} + \|n_{A_{h_1}} - n_{A_{h_2}}\|_{S_T}^{(1+\alpha)}\|\xi_2\|_{S_T}^{(1+\alpha)}\Big)\\
&\quad + C\|n_{A_{h_2}}\|_{S_T}^{(1+\alpha)}\Big(\|A_{h_1} - A_{h_2}\|_{Q_T}^{(\alpha)}\|\xi_2\|_{S_T}^{(2+\alpha)} + \|A_{h_1} - A_{h_2}\|_{Q_T}^{(1+\alpha)}\|\xi_2\|_{S_T}^{(1+\alpha)}\Big)\\
&\le C(r)\Big(\|h_1\|_{S_T}^{(2+\alpha)} + \|h_2\|_{S_T}^{(2+\alpha)} + 1\Big)T^{1/2}\|\sigma_1 - \sigma_2\|_{S_T}^{(2+\alpha)}\|\xi_2\|_{S_T}^{(2+\alpha)}\\
&\le C(r)T^{1/2}\|\sigma_1 - \sigma_2\|_{S_T}^{(2+\alpha)}.
\end{aligned}$$

Hence,

$$I_1 \le C(r)T^{\epsilon/2}\Big(\|\xi_1 - \xi_2\|_{Q_T}^{(2+\alpha)} + \|\sigma_1 - \sigma_2\|_{S_T}^{(2+\alpha)}\Big). \tag{5.125}$$

I_2 is treated as follows:

$$\begin{aligned}
I_2 &\le \|Dn_{A_{h_1}}\nabla_{A_{h_1}}(\chi\sigma_1\partial_n\hat{w}) - Dn_{A_{h_1}}\nabla_{A_{h_2}}(\chi\sigma_1\partial_n\hat{w})\|_{S_T}^{(1+\alpha)}\\
&\quad + \|Dn_{A_{h_1}}\nabla_{A_{h_2}}(\chi\sigma_1\partial_n\hat{w}) - Dn_{A_{h_1}}\nabla_{A_{h_2}}(\chi\sigma_2\partial_n\hat{w})\|_{S_T}^{(1+\alpha)}\\
&\quad + \|Dn_{A_{h_1}}\nabla_{A_{h_2}}(\chi\sigma_2\partial_n\hat{w}) - Dn_{A_{h_2}}\nabla_{A_{h_2}}(\chi\sigma_2\partial_n\hat{w})\|_{S_T}^{(1+\alpha)}\\
&=: J_4 + J_5 + J_6\,.
\end{aligned}$$

J_4 and J_6 can be estimated similarly to J_3:

$$\begin{aligned}
J_4 + J_6 &\le C(r)\Big(\|h_1\|_{S_T}^{(2+\alpha)} + \|h_2\|_{S_T}^{(2+\alpha)} + 1\Big)T^{1/2}\|\sigma_1 - \sigma_2\|_{S_T}^{(2+\alpha)}\Big(\|\chi\sigma_1\partial_n\hat{w}\|_{S_T}^{(2+\alpha)} + \|\chi\sigma_2\partial_n\hat{w}\|_{S_T}^{(2+\alpha)}\Big)\\
&\le C(r)T^{1/2}\|\sigma_1 - \sigma_2\|_{S_T}^{(2+\alpha)}.
\end{aligned}$$

The remaining term is handled as

$$\begin{aligned}
J_5 &\le C(r)\|(\sigma_1 - \sigma_2)\partial_n\hat{w}\|_{S_T}^{(2+\alpha)}\\
&\le C(r)\Big(\|\sigma_1 - \sigma_2\|_{S_T}^{(2+\alpha)}\|\partial_n\hat{w}\|_{S_T}^{(1+\alpha)} + \|\sigma_1 - \sigma_2\|_{S_T}^{(1+\alpha)}\|\partial_n\hat{w}\|_{S_T}^{(2+\alpha)}\Big)\\
&\le C(r)\Big(\|\hat{w}\|_{S_T}^{(2+\alpha)} + T^{1/2}\|\hat{w}\|_{S_T}^{(3+\alpha)}\Big)\|\sigma_1 - \sigma_2\|_{S_T}^{(2+\alpha)}\\
&\le C(r)\Big(\|\hat{w}\|_{S_T}^{(2+\alpha)} + T^{1/2}\Big)\|\sigma_1 - \sigma_2\|_{S_T}^{(2+\alpha)}.
\end{aligned}$$

Thus,

$$I_2 \le C(r)\Big(\|\hat{w}\|_{S_T}^{(2+\alpha)} + T^{1/2}\Big)\|\sigma_1 - \sigma_2\|_{S_T}^{(2+\alpha)}. \tag{5.126}$$

I_3 can also be treated according to J_3:

$$\begin{aligned}
I_3 &\le C(r)\Big(\|h_1\|_{S_T}^{(2+\alpha)} + \|h_2\|_{S_T}^{(2+\alpha)} + 1\Big)T^{1/2}\|\sigma_1 - \sigma_2\|_{S_T}^{(2+\alpha)}\|\hat{w}\|_{S_T}^{(2+\alpha)}\\
&\le C(r)T^{1/2}\|\sigma_1 - \sigma_2\|_{S_T}^{(2+\alpha)}.
\end{aligned} \tag{5.127}$$

Finally, observe that (5.125), (5.126), and (5.127) yield (5.122). Furthermore, the proof of (5.123) is similar to the proof of (5.122).

3. The properties (5.15) and (5.14) of $\hat{w}$ and $\hat{h}$, together with equation (5.114), yield

$$\begin{aligned} F_1(u,0,0)_{|t=0} &= \left(-\partial_t\hat{w} + D\nabla^2_{A_{\hat{h}}}\hat{w} - (u\nabla_{A_{\hat{h}}})\hat{w} - (q_{\hat{h}}\nabla)\hat{w}\right)_{|t=0} \\ &= -D\Delta w_0 + (u_0\nabla)w_0 - (\nabla\eta\nabla w_0)\beta\nabla w_0 + D\Delta w_0 - (u_0\nabla)w_0 - (q_{\hat{h}}(t=0)\nabla)w_0 \\ &= 0\,, \end{aligned}$$

where $q_{\hat{h}}(t=0) = -(\nabla\eta\nabla w_0)\beta$ was employed to derive the last equality. Moreover, there holds

$$F_2(0,0)_{|t=0} = \left(-Dn_{A_{\hat{h}}}\nabla_{A_{\hat{h}}}\hat{w} + k\hat{w} + l\right)_{|t=0} = -D\partial_n w_0 + kw_0 + l_0 = 0$$

and

$$F_3(0,0)_{|t=0} = \left(-\partial_t\hat{h} + \nabla_{A_{\hat{h}}}\hat{w}\nabla_{A_{\hat{h}}}\eta\right)_{|t=0} = -\nabla\eta\nabla w_0 + \nabla w_0\nabla\eta = 0\,.$$

As all functions on the left hand side of (5.124) vanish at $t=0$, this estimate follows from equation (5.99), the three just derived relations, and estimate (5.16).

□

Theorem 5.4.1. *Provided that $\|w_0\|^{(3+\alpha)}_{\Omega_0}$, T, and r are sufficiently small, for each $u \in B_d$ there exists a unique $(\xi,\sigma) \in \mathcal{D}_r$ which solves problem (5.17). Furthermore, the operator*

$$H:\ \begin{array}{ccc} \mathcal{B}_d & \to & \mathcal{D}_r \\ u & \mapsto & (\xi,\sigma) \end{array}$$

is continuous.

Proof. 1. Obviously,

$$F_1:\ \mathcal{B}_d \times \mathcal{R}_2 \to H_0^{\alpha,\frac{\alpha}{2}}(\overline{Q_T})\,, \quad F_2:\ \mathcal{R}_2 \to H_0^{1+\alpha,\frac{1+\alpha}{2}}(\overline{S_T})\,, \quad F_3:\ \mathcal{R}_2 \to H_0^{1+\alpha,\frac{1+\alpha}{2}}(\overline{S_T})\,.$$

Therefore, according to Theorem 5.3.1, the solution of (5.17) can be written as

$$(\xi,\sigma) = B\big(F_1(u,\xi,\sigma), F_2(\xi,\sigma), F_3(\xi,\sigma)\big)$$

with a bounded linear operator $B:\ \mathcal{R}_1 \to \mathcal{R}_2$, or, equivalently, as

$$(\xi,\sigma) = K_u(\xi,\sigma)$$

with a nonlinear operator $K_u:\ \mathcal{R}_2 \to \mathcal{R}_2$.

2. We show that for sufficiently small $\|w_0\|^{(3+\alpha)}_{\Omega_0}$, T, and r the operator K_u maps $\mathcal{D}_r$ into itself and is a strict contraction there. Hence, existence and uniqueness in $\mathcal{D}_r$ follow from Banach's

theorem. By the use of the boundedness of B and (5.121)-(5.123) we obtain

$$\begin{aligned}\|K_u(\xi_1,\sigma_1)-K_u(\xi_2,\sigma_2)\|_{\mathcal{R}_2} &= \|B(F_1(u,\xi_1,\sigma_1),F_2(\xi_1,\sigma_1),F_3(\xi_1,\sigma_1))\\ &\quad - B(F_1(u,\xi_2,\sigma_2),F_2(\xi_2,\sigma_2),F_3(\xi_2,\sigma_2))\|_{\mathcal{R}_2}\\ &\le C\Big(\|F_1(u,\xi_1,\sigma_1)-F_1(u,\xi_2,\sigma_2)\|_{Q_T}^{(\alpha)}\\ &\quad + \|F_2(\xi_1,\sigma_1)-F_2(\xi_2,\sigma_2)\|_{S_T}^{(1+\alpha)}\\ &\quad + \|F_3(\xi_1,\sigma_1)-F_3(\xi_2,\sigma_2)\|_{S_T}^{(1+\alpha)}\Big)\\ &\le C\Big(T^{\delta/2}+g(r)+\|\hat{w}\|_{S_T}^{(2+\alpha)}\Big)\\ &\quad \Big(\|\xi_1-\xi_2\|_{Q_T}^{(2+\alpha)}+\|\sigma_1-\sigma_2\|_{S_T}^{(2+\alpha)}\Big),\end{aligned} \tag{5.128}$$

where $\delta := \min(\alpha,\epsilon)$. Similarly, using (5.124), we obtain

$$\|K_u(0,0)\|_{\mathcal{R}_2} \le CT^{\frac{\alpha'-\alpha}{2}}\,.$$

Now we choose T and r so small that

$$C(T^{\delta/2}+g(r)+\|\hat{w}\|_{S_T}^{(2+\alpha)}) \le \frac{1}{2}\,, \quad CT^{\frac{\alpha'-\alpha}{2}} \le \frac{1}{2}r\,,$$

which is possible since $\hat{w}$ is small due to (5.16) and the given smallness of initial data. Hence,

$$\|K_u(\xi,\sigma)\|_{\mathcal{R}_2} \le \|K_u(0,0)\|_{\mathcal{R}_2} + \|K_u(\xi,\sigma)-K_u(0,0)\|_{\mathcal{R}_2} \le r\,.$$

Thus, K_u maps $\mathcal{D}_r$ into itself and is a strict contraction there because of (5.128).

3. According to part 1 and 2 of this proof, the operator H is well-defined. To demonstrate continuity, let $u_i \in \mathcal{B}_d$ with corresponding (ξ_i,σ_i) $(i=1,2)$. Using once more the boundedness of B and (5.120) it follows that

$$\|K_{u_1}(\xi,\sigma)-K_{u_2}(\xi,\sigma)\|_{\mathcal{R}_2} \le C\|u_1-u_2\|_{Q_T}^{(1+\alpha)}. \tag{5.129}$$

Employing (5.128) and (5.129) we obtain

$$\begin{aligned}\|(\xi_1,\sigma_1)-(\xi_2,\sigma_2)\|_{\mathcal{R}_2} &= \|K_{u_1}(\xi_1,\sigma_1)-K_{u_2}(\xi_2,\sigma_2)\|_{\mathcal{R}_2}\\ &\le \|K_{u_1}(\xi_1,\sigma_1)-K_{u_1}(\xi_2,\sigma_2)\|_{\mathcal{R}_2} + \|K_{u_1}(\xi_2,\sigma_2)-K_{u_2}(\xi_2,\sigma_2)\|_{\mathcal{R}_2}\\ &\le \frac{1}{2}\|(\xi_1,\sigma_1)-(\xi_2,\sigma_2)\|_{\mathcal{R}_2} + C\|u_1-u_2\|_{Q_T}^{(1+\alpha)}.\end{aligned}$$

Hence,

$$\|(\xi_1,\sigma_1)-(\xi_2,\sigma_2)\|_{\mathcal{R}_2} \le C\|u_1-u_2\|_{Q_T}^{(1+\alpha)}. \tag{5.130}$$

□

5.5 Solution of the full nonlinear problem including flow

Application of the transformation (5.7) to the Navier-Stokes system (5.1) yields

$$\begin{cases} \partial_t u - \nu\nabla_A^2 u + \nabla_A p = -(q\nabla)u - (u\cdot\nabla_A)u + f =: F_0(u,\sigma) \quad \text{in } Q_T \\ \nabla_A \cdot u = 0 \quad \text{in } Q_T \\ u = 0 \quad \text{on } S_T \\ u(t=0) = u_0 \quad \text{in } \Omega_0\,. \end{cases} \tag{5.131}$$

Actually, this problem was already studied by Solonnikov [80] (see the proof of Theorem 3). He showed that (5.131) is always uniquely solvable for a given function $F_0(x,t) \in H^{\alpha,\alpha/2}(\overline{Q_T})$, and that the solution fulfills the estimate

$$\|u\|_{Q_T}^{(2+\beta)} + \|\nabla p\|_{Q_T}^{(\beta)} \le C(r)\|F\|_{Q_T}^{(\alpha)} \quad (0<\beta<\alpha)\,. \tag{5.132}$$

In addition, the operator

$$G: \begin{array}{ccc} \mathcal{D}_r \times \mathcal{B}_d & \to & H^{1+\alpha,\frac{1+\alpha}{2}}(\overline{Q_T}) \\ ((\xi,\sigma),v) & \mapsto & u \end{array}$$

is continuous, which maps $((\xi,\sigma),v)$ onto the solution u of the system (5.131) containing $F_0(v,\sigma)$ as right hand side instead of $F_0(u,\sigma)$.

Let H be defined as in Theorem 5.4.1 and consider the operator

$$P: \begin{array}{ccc} \mathcal{B}_d & \to & H^{1+\alpha,\frac{1+\alpha}{2}}(\overline{Q_T}) \\ u & \mapsto & G(H(u),u) \end{array}\,.$$

We note that a fixed point of P solves the full problem (5.1)-(5.2). The existence of such a fixed point will be proven by Schauder's fixed point theorem.

Theorem 5.5.1. *P has at least one fixed point.*

Proof. 1. Let $\epsilon := (\alpha'-\alpha)/2$. The following estimate shows that for sufficiently small T the operator P maps $\mathcal{B}_d$ into itself. Employing (5.99) and (5.132) we obtain

$$\begin{aligned} \|P(u)-u_0\|_{Q_T}^{(1+\alpha)} &\le CT^\epsilon \|P(u)-u_0\|_{Q_T}^{(1+\alpha')} \\ &\le CT^\epsilon \Big(\|P(u)\|_{Q_T}^{(2+\beta)} + \|u_0\|_{Q_T}^{(2+\alpha)} \Big) \\ &\le CT^\epsilon \Big(\|F_0(u,\sigma)\|_{Q_T}^{(\alpha)} + \|u_0\|_{Q_T}^{(2+\alpha)} \Big)\,. \end{aligned}$$

This can be further estimated by the use of Lemma 5.5.1:

$$\begin{aligned} \|P(u)-u_0\|_{Q_T}^{(1+\alpha)} &\le CT^\epsilon \Big(\|u\|_{Q_T}^{(1+\alpha)} + \|f\|_{Q_T}^{(\alpha)} + \|u_0\|_{Q_T}^{(2+\alpha)} \Big) \\ &\le CT^\epsilon \Big(\underbrace{\|u-u_0\|_{Q_T}^{(1+\alpha)}}_{\le d} + \|f\|_{Q_T}^{(\alpha)} + \|u_0\|_{Q_T}^{(2+\alpha)} \Big) \\ &\le CT^\epsilon \to 0 \quad (T\to 0)\,. \end{aligned}$$

2. Since both $H : \mathcal{B}_d \to \mathcal{D}_r$ and $G : \mathcal{D}_r \times \mathcal{B}_d \to H^{1+\alpha,\frac{1+\alpha}{2}}(\overline{Q_T})$ are continuous, their composition $P : \mathcal{B}_d \to H^{1+\alpha,\frac{1+\alpha}{2}}(\overline{Q_T})$ is continuous, too. In addition, P maps bounded sets of $H^{1+\alpha,\frac{1+\alpha}{2}}(\overline{Q_T})$ into bounded sets of $H^{2+\beta,\frac{2+\beta}{2}}(\overline{Q_T})$, according to (5.132) and Lemma 5.5.1. Thus, P is a compact operator and the assertion follows from Schauder's fixed point theorem. □

Lemma 5.5.1. *Let $u \in \mathcal{B}_d$ and $(\xi,\sigma) \in \mathcal{D}_r$. F_0 fulfills the estimate*

$$\|F_0(u,\sigma)\|_{Q_T}^{(\alpha)} \le C\Big(\|u\|_{Q_T}^{(1+\alpha)} + \|f\|_{Q_T}^{(\alpha)}\Big),$$

where $C = C\Big(r, d, T, \|w_0\|_{\Omega_0}^{(3+\alpha)}, \|u_0\|_{\Omega_0}^{(1+\alpha)}\Big)$ remains bounded for bounded arguments.

Proof. From the definition of F_0 it follows that

$$\|F_0(u,\sigma)\|_{Q_T}^{(\alpha)} \le C\Big(\|q_h\|_{Q_T}^{(\alpha)} + \underbrace{\|u\|_{Q_T}^{(\alpha)}}_{\le d + \|u_0\|_{\Omega_0}^{(1+\alpha)}} \|A_h\|_{Q_T}^{(\alpha)}\Big)\|u\|_{Q_T}^{(1+\alpha)} + \|f\|_{Q_T}^{(\alpha)}.$$

The definition (5.10) of q_h and the estimate (5.16) imply that

$$\|q_h\|_{Q_T}^{(\alpha)} \le C\|\partial_t h\|_{S_T}^{(\alpha)} \le C\Big(\|\sigma\|_{S_T}^{(2+\alpha)} + \|\hat{h}\|_{S_T}^{(2+\alpha)}\Big) \le C\Big(r + g\Big(\|w_0\|_{\Omega_0}^{(3+\alpha)}, \|u_0\nabla w_0\|_{\Omega_0}^{(1+\alpha)}, T\Big)\Big).$$

Furthermore, due to (5.103) and (5.114),

$$\|A_h\|_{Q_T}^{(\alpha)} \le C(r)\Big(1 + \|h\|_{S_T}^{(1+\alpha)}\Big) \le C(r)\Big(1 + r + g\Big(\|w_0\|_{\Omega_0}^{(3+\alpha)}, \|u_0\nabla w_0\|_{\Omega_0}^{(1+\alpha)}, T\Big)\Big).$$

□

The proof of Theorem 5.1.1 is completed.

6 Conclusions and outlook

To investigate the influences of shear stress, saturation-dependent changes in surface reactivity, and thrombus growth on primary hemostasis in various vessel geometries, this thesis developed two mathematical models based on the Navier-Stokes equations and on the conservation of particles.

The first model, presented in Chapter 3, describes the initial phase of platelet adhesion, when thrombus growth is negligible. Consequently, this model assumes a fixed domain and was therefore termed "FD-model". It accounts for saturation-dependent changes in surface reactivity by coupling platelet flux conditions to ordinary differential equations describing the evolution of surface-bound platelets. Existence of weak solutions of such ODE-coupled problems was established for generalized parabolic systems using Schauder's fixed point theorem. Uniqueness and positivity of solutions require some tighter conditions which are fulfilled by the presented FD-model. Thus, its mathematical well-posedness is guaranteed. The parameters of the FD-model were optimized to fit experimental data concerning platelet adhesion to glass in stagnation point flow (at Ht= 0%), platelet adhesion to collagen downstream of a tubular expansion (Ht= 20%), and platelet adhesion to polypropylene in a t-junction (Ht= 45%). Moreover, the so obtained parameter values were justified by the observations of Brash et al. [13] studying the effects of various materials, solvents, and hematocrits on platelet deposition. When platelet adhesion was assumed independent of shear stress, the predictions of the FD-model matched none of the experimental data. In contrast to that, when adhesion was taken shear-dependent, good qualitative agreement with the data was achieved. To obtain even good quantitative agreement, it was necessary for the stagnation point flow and for the tubular expansion to additionaly consider saturation-dependent changes in surface reactivity. Furthermore, the so obtained improvement of the model's ability to match the data was observed to be greater in the stagnation point flow than in the tubular expansion. Based on these observations, the first conclusion was that initial platelet deposition is highly determined by shear stress and by changes in surface reactivity. In addition, comparison of the optimized parameter values with the corresponding experimental conditions revealed the impact of changing surface reactivity to likely depend on hematocrit. Consequently, the hypothesis was put forward that the importance of saturation-dependent surface reactivity rises with decreasing hematocrit.

With regard to possible applications in bioengineering and medicine, the FD-model was kept on a rather fundamental level. Hence, due to the biological complexity of hemostasis, some limitations exist. The most striking one is the dependence on surface material and solvent upon changes in inflow velocity, as discussed in Section 3.3.2 for the tubular expansion. Model behavior turned out to be contrary to experimental observations using immobilized fibrinogen as reactive surface or Tyrodes-solution as solvent. However, it matches the behavior observed for the more physiological situation of whole blood as solvent and adhesion to fibrillar collagen,

immobilized vWf, and immobilized platelets. Besides this, the influence of surface pretreatment, of various anticoagulants, and of differences between species (human and animals; see, e.g., [35], [33]) should be carefully analyzed. Another limitation is that the effects of thrombus growth are not satisfyingly captured by the FD-model, as discussed in Section 3.3.1 for the stagnation point. However, the eminent impact of shear stress on platelet deposition calls for consideration of aggregate growth in models intended to capture the long-term behavior of the process: The development of thrombi not only changes the flow field and thus the transport of platelets along the streamlines, it also alters the shear stress. Modeling aggregate growth leads to a free boundary problem with fully coupled fluid dynamic and species conservation equations.

The growth of thrombi is taken into account by the second model, derived in Chapter 4 of this work. It captures the long-term behavior of platelet deposition, when saturation-dependent changes in surface reactivity can be neglected. Regarding mathematical well-posedness of this free boundary problem, a detailed proof of classical solvability in terms of Hölder spaces was presented. This difficult task was subdivided in several steps: First, the moving boundary problem was transformed to an equivalent formulation on the fixed initial domain. Then, the flow field was fixed and the corresponding linear problem for the platelets was addressed in half space by application of Fourier-Laplace transform techniques and pseudodifferential operator theory. After that, the linear problem was solved in the original domain by means of a regularizer and the results derived for the half-space. Next, the linear theory was applied to solve the nonlinear problem for the platelets (the flow field still fixed). This was achieved by Banach's fixed point theorem and required the assumption that the time and the initial data for the platelets are small. Finally, the fully coupled problem was solved by Schauder's theorem, making use of the theory for fixed flow and a result of Solonnikov [80] concerning the solvability of the transformed Navier-Stokes equations. Numerical simulations of the free boundary problem in stagnation point flow and in the tubular expansion were performed by the level set method, which provides a convenient alternative with notably reduced technical complexity compared to present front-tracking approaches. Like the FD-model, the predictions of the free boundary problem showed no agreement with the experimental data when platelet deposition was assumed independent of shear stress. In contrast to that, when adhesion was assumed shear-dependent, good agreement with experimental evidence was obtained. Hence, in addition to the findings obtained by the FD-model, the results for the free boundary problem further confirm the importance of shear stress in the processes of primary hemostasis.

The mathematical models developed in this work provided valuable information on spatial platelet distribution: By comparison with in vitro experimental data, they revealed shear stress, changes in surface reactivity, and thrombus growth to be important factors in the course of primary hemostasis. Due to its rather fundamental character, the FD-model could be used as starting point for an important problem in bioengineering: Given a prescribed inflow, how can the shape and the surface of a vascular prostheses be optimized such that platelet deposition to the vascular surface is minimal? However, due to the influence of shear stress a consideration of the free boundary problem seems unavoidable to derive information about the long-term behavior of platelet deposition. Besides hemostasis and thrombosis, application of the presented approaches to further kinds of adhesion processes under flow is believed to prove beneficial in figuring out how shear stress, surface, and aggregate growth determine their behavior.

Acknowledgments

At first, I would like to express my gratitude to my supervisor Prof. Willi Jäger for introducing me to this very interesting and promising subject, for his guidance to find the key questions and objectives of my work, and for his ongoing advice and support. I enjoyed attending his lectures, where he always pointed out interesting connections between the different mathematical disciplines, and his famous Fehrenbacher Hof and Wallenfels seminars, which, besides the interesting mathematics, offered great possibilities for getting-together. Furthermore, I would like to thank Prof. Rolf Rannacher for his ongoing advice in numerical questions and for kindly offering me the possibility to occupy his compute servers to perform my simulations. I also thank Willi Jäger and Rolf Rannacher for giving me the possibility to attend international conferences at home and abroad, such as the HPSC in Hanoi, the workshops on fluid structure interactions in Prague, the Oberwolfach seminar on Hemodynamical Flows, the "GTH-Intensivkurs für klinische Hämostaseologie" in Hannover, and my two months research visit to Prague.

My special thanks are addressed to my mentor Dr. Maria Neuss-Radu for her enduring support, many fruitful discussions and valuable suggestions concerning my work, as well as for always having time whenever I visited her.

I gratefully acknowledge the funding received during my Ph.D. from the German Research Foundation (DFG) through the *International Research Training Group (IGK) 710 "Complex Processes: modeling, simulation, and optimization"* at the Interdisciplinary Center of Scientific Computing (IWR). I appreciate having been a research fellow of IGK 710 during the past three years and I am grateful for the possibilities the membership of this group has offered.

Many thanks to Thomas Dunne, who guided me during the implementation of the level set method, and to Dominik Meidner, who could give me advice whenever the computer got out of control. All numerical experiments in this work could not have been done without the finite element library Gascoigne. Hence, I would like to thank all people who have contributed to the development of this software package: Roland Becker, Malte Braack, Thomas Dunne, Dominik Meidner, Thomas Richter, Michael Schmich, and Boris Vexler.

I wish to thank the whole Applied Analysis Group and the Numerical Analysis Group at the University of Heidelberg for many discussions, for the exchange of ideas, and for the nice time we spent inside and outside the institute.

I like to thank my parents for their ongoing support in all its forms. Last but by no means least, I thank my wife Daniela for her never-ending encouragement.

List of Figures

2.1 Scanning electron micrographs of resting and activated platelets 5
2.2 The coagulation cascade 8
2.3 The structure of prothrombinase 9
2.4 Cell-based model of coagulation: initiation 10
2.5 Cell-based model of coagulation: priming 11
2.6 Cell-based model of coagulation: propagation 11

3.1 The different parts of the boundary 15
3.2 Stagnation point flow: computational domain and computed streamlines of flow 18
3.3 Stagnation point flow: normalized density of bound platelets and computed normalized wall-shear rate 19
3.4 Stagnation point flow: measured normalized platelet flux and optimized solutions of the various FD-models 20
3.5 Tubular expansion: computational domain and computed streamlines of flow . 21
3.6 Tubular expansion: computed normalized wall-shear rates 22
3.7 Tubular expansion, Re = 40.9: normalized densities of bound platelets; optimized solutions of the various FD-models 23
3.8 Tubular expansion, Re = 56.7: normalized densities of bound platelets; optimized solution of the shear- and surface-dependent FD-model 23
3.9 Tubular expansion, Re = 30.1: normalized densities of bound platelets; optimized solution of the shear- and surface-dependent FD-model 24
3.10 T-junction: computational domain and computed streamlines of flow 25
3.11 T-junction: normalized density of bound platelets, Side (I); optimized solutions of the various FD-models 25
3.12 T-junction: normalized density of bound platelets, Side (II); optimized solutions of the various FD-models 26

4.1 Time-dependent domain 39
4.2 Stagnation point flow with shear-dependent platelet adhesion; coarse grids . . . 45
4.3 Stagnation point flow with shear-dependent platelet adhesion; fine grid 46
4.4 Stagnation point flow with shear-dependent platelet adhesion; finest grid 47
4.5 Thrombus growth affecting radial flow velocity and pressure in stagnation point flow 48
4.6 Thrombus growth affecting the flow field in stagnation point flow 49
4.7 Stagnation point flow with shear-independent platelet adhesion on various grids 50
4.8 Tubular expansion with shear-dependent platelet adhesion on various grids . . 51
4.9 Tubular expansion with shear-independent platelet adhesion on various grids . 52

5.1 Domain of the free boundary model 54
5.2 Path of integration 62

List of Tables

2.1 The main reactions of the coagulation cascade 7

3.1 Optimized parameters for platelet deposition from PRP onto glass in stagnation point flow 20
3.2 Optimized parameters for the deposition of washed platelets to collagen fibers on glass in a tubular expansion 24
3.3 Optimized parameters for platelet deposition from citrated blood onto polypropylene in a t-junction 26

Bibliography

[1] K. Affeld, A. J. Reininger, J. Gadischke, K. Grunert, S. Schmidt, and F. Thiele. Fluid mechanics of the stagnation point flow chamber and its platelet deposition. *Artif. Organs*, 19(7):597–602, 1995.

[2] H. W. Alt. *Lineare Funktionalanalysis*, volume 3. Springer, Berlin Heidelberg, 1999.

[3] I. Babuska. Numerical solution of boundary value problems by the perturbated variational principle. Technical report, University of Maryland, 1969.

[4] R. M. Barstad, P. Kierulf, and K. S. Sakariassen. Collagen induced thrombus formation at the apex of eccentric stenoses—a time course study with non-anticoagulated human blood. *Thromb. Haemostasis*, 75(4):685–692, 1996.

[5] D. Basmadjian, M. V. Sefton, and S. A. Baldwin. Coagulation on biomaterials in flowing blood: some theoretical considerations. *Biomaterials*, 18(23):1511–1522, 1997.

[6] R. J. Baugh, G. J. Broze Jr., and S. Krishnaswamy. Regulation of extrinsic pathway factor Xa formation by tissue factor pathway inhibitor. *J. Biol. Chem.*, 273(8):4378–4386, 1998.

[7] B. V. Bazalii and S. P. Degtyarev. On classical solvability of the multidimensional Stefan problem for convective motion of a viscous incompressible fluid. *Math. USSR Sbornik*, 60(1):1–17, 1988.

[8] R. Becker and M. Braack. Multigrid techniques for finite elements on locally refined meshes. *Numer. Linear Algebra Appl.*, 7(6):363–379, 2000.

[9] R. Becker and M. Braack. A two-level stabilization scheme for the Navier-Stokes equations. In M. Feistauer et al., editors, *ENUMATH 2003*, Numerical Mathematics and Advanced Applications, pages 123–130, Heidelberg, 2004. Springer.

[10] R. Becker, M. Braack, Th. Dunne, D. Meidner, T. Richter, M. Schmich, and B. Vexler. The finite element toolkit GASCOIGNE, 2006. `http://www.gascoigne.uni-hd.de`.

[11] R. Becker and Th. Dunne. VisuSimple: An interactive open source visualization utility for scientific computing. In W. Jäger, R. Rannacher, and J. Warnatz, editors, *Reactive Flows, Diffusion and Transport: From Experiments via Mathematical Modeling to Numerical Simulation and Optimization*. Springer, 2007. `http://visusimple.uni-hd.de`.

[12] M. Braack and E. Burman. Local projection stabilization for the Oseen problem and its interpretation as a variational multiscale method. *SIAM J. Numer. Anal.*, 43(6):2544–2566, 2006.

[13] J. L. Brash, J. M. Brophy, and I. A. Feuerstein. Adhesion of platelets to artificial surfaces: effect of red cells. *J. Biomed. Mater. Res.*, 10:429–443, 1976.

[14] S. Butenas, C. van't Veer, and K. G. Mann. Evaluation of the initiation phase of blood coagulation using ultrasensitive assays for serine proteases. *J. Biol. Chem.*, 272(34):21527–21533, 1997.

[15] J. Chen and X.-Y. Lu. Numerical investigation of the non-newtonian blood flow in a bifurcation model with a non-planar branch. *J. Biomech.*, 37(12):1899–1911, 2004.

[16] S. Chen, B. Merriman, S. Osher, and P. Smereka. A simple level set method for solving Stefan problems. *J. Comput. Phys.*, 135:8–29, 1997.

[17] Y.-J. Chuang, R. Swanson, S. M. Raja, and S. T. Olson. Heparin enhances the specificity of antithrombin for thrombin and factor Xa independent of the reactive center loop sequence. Evidence for an exosite determinant of factor Xa specificity in heparin-activated antithrombin. *J. Biol. Chem.*, 276(18):14961–14971, 2001.

[18] K. J. Clemetson. Primary haemostasis: Sticky fingers cement the relationship. *Curr. Biol.*, 9(3):R110–R112, 1999.

[19] B. Dahlbäck. Blood coagulation. *The Lancet*, 355:1627–1632, 2000.

[20] T. David, S. Thomas, and P. G. Walker. Platelet deposition in stagnation point flow: an analytical and computational simulation. *Med. Eng. Phys.*, 23:299–312, 2001.

[21] L. C. Evans. *Partial Differential Equations.* American Mathematical Society, Providence, 2002.

[22] P. J. Fay, T. L. Beattie, L. M. Regan, L. M. O'Brien, and R. J. Kaufman. Model for the factor VIIIa-dependent decay of the intrinsic factor Xase. *J. Biol. Chem.*, 271(11):6027–6032, 1996.

[23] P. J. Fay and T. M. Smudzin. Characterization of the interaction between the A2 subunit and A1/A3-Cl-C2 dimer in human factor VIIIa. *J. Biol. Chem.*, 267(19):13246–13250, 1992.

[24] A. L. Fogelson and R. D. Guy. Platelet-wall interactions in continuum models of platelet thrombosis: formulation and numerical solution. *Math. Med. Biol.*, 21(4):293–334, 2004.

[25] B. J. Folie and L. V. McIntire. Mathematical analysis of mural thrombogenesis. Concentration profiles of platelet-activating agents and effects of viscous shear flow. *Biophys. J.*, 56(6):1121–1141, 1989.

[26] J. Franssen, I. Salemink, G. M. Willems, T. C. Wun, H. C. Hemker, and T. Lindhout. Prothrombinase is protected from inactivation by tissue factor pathway inhibitor: competition between prothrombin and inhibitor. *Biochem. J.*, 323(1):33–37, 1997.

[27] B. Furie and B. C. Furie. Thrombus formation in vivo. *J. Clin. Invest.*, 115:3355–3362, 2005.

[28] V. Fuster, L. Badimon, J. J. Badimon, and J. H. Chesebro. The pathogenesis of coronary artery disease and the acute coronary syndromes (1). *New Engl. J. Med.*, 326(4):242–250, 1992.

[29] V. Fuster, L. Badimon, J. J. Badimon, and J. H. Chesebro. The pathogenesis of coronary artery disease and the acute coronary syndromes (2). *New Engl. J. Med.*, 326(5):310–318, 1992.

[30] J. N. George. Haemostasis and fibrinolysis. In J. H. Stein et al., editors, *Internal medicine*, pages 534–540. Mosby, St Louis, 5 edition, 1998.

[31] J. N. George. Platelets. *The Lancet*, 355:1531–1539, 2000.

[32] H. L. Goldsmith and V. T. Turitto. Rheological aspects of thrombosis and haemostasis: basic principles and applications. *Thromb. Haemostasis*, 55(3):415–435, 1986.

[33] E. F. Grabowski, P. Didisheim, J. C. Lewis, J. T. Franta, and J. Q. Stropp. Platelet adhesion to foreign surfaces under controlled conditions of whole blood flow: human vs. rabbit, dog, calf, sheep, pig, macaque, and baboon. *Trans. Am. Soc. Artif. Intern. Organs*, 23:141–149, 1977.

[34] E. F. Grabowski, L. I. Friedman, and E. F. Leonard. Effects of shear rate on the diffusion and adhesion of blood platelets to a foreign surface. *Ind. Eng. Chem. Fundam.*, 11(2):224–232, 1972.

[35] E. F. Grabowski, K. K. Herther, and P. Didisheim. Human vs. dog platelet adhesion to cuprophane under controlled conditions of whole blood flow. *J. Lab. Clin. Med.*, 88(3):368–374, 1976.

[36] E. Hanzawa. Classical solutions of the Stefan problem. *Tohoku Math. J.*, 33(3):297–335, 1981.

[37] M. F. Hockin, K. C. Jones, S. J. Everse, and K. G. Mann. A model for the stoichiometric regulation of blood coagulation. *J. Biol. Chem.*, 277(21):18322–18333, 2002.

[38] L. Hörmander. *The Analysis of Linear Partial Differential Operators I.* Springer, Berlin Heidelberg, 1983.

[39] Y. Ikeda, M. Handa, K. Kawano, T. Kamata, M. Murata, Y. Araki, H. Anbo, Y. Kawai, K. Watanabe, I. Itagaki, K. Sakai, and Z. M. Ruggeri. The role of von Willebrand factor and fibrinogen in platelet aggregation under varying shear stress. *J. Clin. Invest.*, 87(4):1234–1240, 1991.

[40] E. Javierre, C. Vuik, F. J. Vermolen, and A. Segal. A level set method for particle dissolution in a binary alloy. Technical report, Delft University of Technology, 2005.

[41] K. C. Jones and K. G. Mann. A model for the tissue factor pathway to thrombin II. A mathematical simulation. *J. Biol. Chem.*, 269(37):23367–23373, 1994.

[42] A. Jordan, T. David, S. Homer-Vanniasinkam, A. Graham, and P. G. Walker. The effects of margination and red cell augmented platelet diffusivity on platelet adhesion in complex flow. *Biorheology*, 41:641–653, 2004.

[43] R. E. Jordan, G. M. Oosta, W. T. Gardner, and R. D. Rosenberg. The kinetics of hemostatic enzyme-antithrombin interactions in the presence of low molecular weight heparin. *J. Biol. Chem.*, 255(21):10081–10090, 1980.

[44] D. Juric and G. Tryggvason. A front-tracking method for dendritic solidification. *J. Comput. Phys.*, 123:127–148, 1996.

[45] T. Karino and H. L. Goldsmith. Adhesion of human platelets to collagen on the walls distal to a tubular expansion. *Microvasc. Res.*, 17(3):238–262, 1979.

[46] B. E. Kehrel. Blutplättchen: Biochemie und Physiologie. *Hämostaseologie*, 23:149–158, 2003.

[47] K. H. Keller. Effect of fluid shear on mass transport in flowing blood. *Fed. Proc.*, 30(5):1591–1599, 1971.

[48] M. H. Kroll, J. D. Hellums, L. V. McIntire, A. I. Schafer, and J. L. Moake. Platelets and shear stress. *Blood*, 88(5):1525–1541, 1996.

[49] A. L. Kuharsky and A. L. Fogelson. Surface-mediated control of blood coagulation: The role of binding site densities and platelet deposition. *Biophys. J.*, 80(3):1050–1074, 2001.

[50] S. Kulkarni, S. M. Dopheide, C. L. Yap, C. Ravanat, M. Freund, P. Mangin, K. A. Heel, A. Street, I. S. Harper, F. Lanza, and S. P. Jackson. A revised model of platelet aggregation. *J. Clin. Invest.*, 105(6):783–791, 2000.

[51] Y. Kusaka and A. Tani. On the classical solvability of the Stefan problem in a viscous incompressible fluid flow. *SIAM J. Math. Anal.*, 30(3):584–602, 1999.

[52] O. A. Ladyzenskaja, V. A. Solonnikov, and N. N. Uralceva. *Linear and Quasilinear Equations of Parabolic Type*. American Mathematical Society, Providence, 1968.

[53] R. D. Langdell, R. H. Wagner, and K. M. Brinkhous. Effect of antihemophilic factor on one-stage clotting tests; a presumptive test for hemophilia and a simple one-stage antihemophilic factor assy procedure. *J. Lab. Clin. Med.*, 41(4):637–647, 1953.

[54] J. H. Lawson, S. Butenas, N. Ribarik, and K. G. Mann. Complex-dependent inhibition of factor VIIa by antithrombin III and heparin. *J. Biol. Chem.*, 268(2):767–770, 1993.

[55] J. H. Lawson, M. Kalafatis, S. Stram, and K. G. Mann. A model for the tissue factor pathway to thrombin I. An empirical study. *J. Biol. Chem.*, 269(37):23357–23366, 1994.

[56] D. Lee, Y.-L. Chiu, and C.-Y. Jen. Wall stresses and platelet adhesion in a t-junction. *Proc. Natl. Sci. Counc. ROC(A)*, 23(2):303–310, 1999.

[57] V. G. Levich. *Physicochemical Hydrodynamics*, pages 112–116. Prentice-Hall, Englewood Cliffs, 1962.

[58] P. Lollar, E. T. Parker, and P. J. Fay. Coagulant properties of hybrid human/porcine factor VIII molecules. *J. Biol. Chem.*, 267(33):23652–23657, 1992.

[59] K. G. Mann. Biochemistry and physiology of blood coagulation. *Thromb. Haemostasis*, 82(2):165–174, 1999.

[60] D. M. Monroe, M. Hoffman, and H. R. Roberts. Platelets and thrombin generation. *Arterioscler. Thromb. Vasc. Biol.*, 22(9):1381–1389, 2002.

[61] M. E. Nesheim, J. B. Taswell, and K. G. Mann. The contribution of bovine factor V and factor Va to the activity of prothrombinase. *J. Biol. Chem.*, 254(21):10952–10962, 1979.

[62] J. Nitsche. Über ein Variationsprinzip zur Lösung von Dirichlet-Problemen bei Verwendung von Teilräumen die keinen Randbedingungen unterworfen sind. *Abh. Math. Univ. Hamburg*, 36:9–15, 1970.

[63] L. Novak, H. Deckmyn, S. Damjanovich, and J. Harsfalvi. Shear-dependent morphology of von Willebrand factor bound to immobilized collagen. *Blood*, 99(6):2070–2076, 2002.

[64] S. Osher and R. P. Fedkiw. *Level Set Methods and Dynamic Implicit Surfaces.* Springer, Berlin Heidelberg, 2003.

[65] D. M. Peterson, N. A. Stathopoulos, T. D. Giorgio, J. D. Hellums, and J. L. Moake. Shear-induced platelet aggregation requires von Willebrand factor and platelet membrane glycoproteins Ib and IIb-IIIa. *Blood*, 69(2):625–628, 1987.

[66] T. B. Pierce, M. A. Razzuk, L. M. Razzuk, and S. J. Hoover. A comprehensive review of the physiology of hemostasis and antithrombotic agents. *BUMC Proceedings*, 12(1):39–49, 1999.

[67] K. T. Preissner. Biochemie und Physiologie der Blutgerinnung und Fibrinolyse. *Hämostaseologie*, 24:84–93, 2004.

[68] A. Quarteroni and A. Valli. *Numerical Approximation of Partial Differential Equations.* Springer, Berlin Heidelberg, 1994.

[69] A. J. Quick. The prothrombin time in haemophilia and obstructive jaundice. *J. Biol. Chem.*, 109:73–74, 1935.

[70] R. Rannacher. Finite element solution of diffusion problems with irregular data. *Numer. Math.*, 43:309–327, 1984.

[71] R. C. Reimers, S. P. Sutera, and J. H. Joist. Potentiation by red blood cells of shear-induced platelet aggregation: Relative importance of chemical and physical mechanisms. *Blood*, 64(6):1200–1206, 1984.

[72] A. R. Rezaie. Prothrombin protects factor Xa in the prothrombinase complex from inhibition by the heparin-antithrombin complex. *Blood*, 97(8):2308–2313, 2001.

[73] Z. M. Ruggeri. Von Willebrand factor, platelets and endothelial cell interactions. *J. Thromb. Haemost.*, 1(7):1335–1342, 2003.

[74] Y. Saad and M. H. Schultz. GMRES: A generalized minimal residual algorithm for solving non-symmetric linear systems. *SIAM J. Sci. Statist. Comput.*, 7:856–869, 1986.

[75] K. S. Sakariassen and H. R. Baumgartner. Axial dependence of platelet-collagen interactions in flowing blood: Upstream thrombus growth impairs downstream platelet adhesion. *Arteriosclerosis*, 9(1):33–42, 1989.

[76] B. Savage, F. Almus-Jacobs, and Z. M. Ruggeri. Specific synergy of multiple substrate-receptor interactions in platelet thrombus formation under flow. *Cell*, 94(5):657–666, 1998.

[77] B. Savage, M. Cattaneo, and Z. M. Ruggeri. Mechanisms of platelet aggregation. *Curr. Opin. Hematol.*, 8(5):270–276, 2001.

[78] B. Savage, E. Saldivar, and Z. M. Ruggeri. Initiation of platelet adhesion by arrest onto fibrinogen or translocation on von Willebrand factor. *Cell*, 84(2):289–297, 1996.

[79] C. A. Siedlecki, B. J. Lestini, K. K. Kottke-Marchant, S. J. Eppell, D. L. Wilson, and R. E. Marchant. Shear-dependent changes in the three-dimensional structure of human von Willebrand factor. *Blood*, 88(8):2939–2950, 1996.

[80] V. A. Solonnikov. Solvability of a problem on the motion of a viscous incompressible fluid bounded by a surface. *Math. USSR Izvestija*, 11(6):1323–58, 1977.

[81] E. N. Sorensen. *Computational Simulation of Platelet Transport, Activation, and Deposition.* PhD thesis, University of Pittsburgh, 2002.

[82] E. N. Sorensen, G. W. Burgreen, W. R. Wagner, and J. F. Antaki. Computational simulation of platelet deposition and activation: I. Model development and properties. *Ann. Biomed. Eng.*, 27(4):436–448, 1999.

[83] E. N. Sorensen, G. W. Burgreen, W. R. Wagner, and J. F. Antaki. Computational simulation of platelet deposition and activation: II. Results for poiseuille flow over collagen. *Ann. Biomed. Eng.*, 27(4):449–458, 1999.

[84] E. M. Stein. *Singular Integrals and Differentiability Properties of Functions.* Princeton University Press, Princeton, 1970.

[85] M. Sussman, P. Smereka, and S. Osher. A level set approach for computing solutions to incompressible two-phase flow. *J. Comput. Phys.*, 114:146–159, 1994.

[86] R. Temam. *Navier-Stokes Equations, Theory and Numerical Analysis.* North-Holland, Amsterdam, 2 edition, 1979.

[87] G. Tryggvason, B. Bunner, A. Esmaeeli, D. Juric, N. Al-Rawahi, W. Tauber, J. Han, S. Nas, and Y.-J. Jan. A front-tracking method for the computations of multiphase flow. *J. Comput. Phys.*, 169:708–759, 2001.

[88] V. T. Turitto and H. R. Baumgartner. Platelet interaction with subendothelium in flowing rabbit blood: effect of blood shear rate. *Microvasc. Res.*, 17(1):38–54, 1979.

[89] V. T. Turitto, A. M. Benis, and E. F. Leonard. Platelet diffusion in flowing blood. *Ind. Eng. Chem. Fundam.*, 11(2):216–223, 1972.

[90] V. T. Turitto and C. L. Hall. Mechanical factors affecting hemostasis and thrombosis. *Thromb. Res.*, 92(6):25–31, 1998.

[91] G. van Dieijen, G. Tans, J. Rosing, and H. C. Hemker. The role of phospholipid and factor VIIIa in the activation of bovine factor X. *J. Biol. Chem.*, 256(7):3433–3442, 1981.

[92] C. van't Veer, N. J. Golden, M. Kalafatis, and K. G. Mann. Inhibitory mechanism of the protein C pathway on tissue factor-induced thrombin generation. Synergistic effect in combination with tissue factor pathway inhibitor. *J. Biol. Chem.*, 272(12):7983–7994, 1997.

[93] C. van't Veer, N. J. Golden, and K. G. Mann. Inhibition of thrombin generation by the zymogen factor VII: implications for the treatment of hemophilia A by factor VIIa. *Blood*, 95(4):1330–1335, 2000.

[94] R. L. Virchow. *Gesammelte Abhandlungen zur wissenschaftlichen Medicin*. Meidinger, Frankfurt a. M., 1856.

[95] H. J. Weiss, V. T. Turitto, and H. R. Baumgartner. Effect of shear rate on platelet interaction with subendothelium in citrated and native blood. I. Shear rate-dependent decrease of adhesion in von Willebrand's disease and the Bernard-Soulier syndrome. *J. Lab. Clin. Med.*, 92(5):750–764, 1978.

[96] H. J. Weiss, V. T. Turitto, and H. R. Baumgartner. Platelet adhesion and thrombus formation on subendothelium in platelets deficient in glycoproteins IIb-IIIa, Ib, and storage granules. *Blood*, 67(2):322–330, 1986.

[97] F. F. Weller. *Anfangs-Randwertprobleme für die Modellierung und Simulation der Hämostase*. Diploma Thesis, University of Heidelberg, 2005.

[98] F. F. Weller. Platelet deposition in non-parallel flow. Influence of shear stress and changes in surface reactivity. *J. Math. Biol.*, 2008. To appear.

[99] J. Wloka. *Partial Differential Equations*. Cambridge University Press, Cambridge, 1992.

[100] K. Yasuda, R. C. Armstrong, and R. E. Cohen. Shear flow properties of concentrated solutions of linear and star branched polystyrenes. *Rheol. Acta*, 20(2):163–178, 1981.

[101] E. Zeidler. *Nonlinear Functional Analysis and its Applications*. Springer, Heidelberg, 1989.

[102] A. L. Zydney and C. K. Colton. Augmented solute transport in the shear flow of a concentrated suspension. *Physicochem. Hydrodyn.*, 10:77–96, 1988.